3.5 Subproject 5: Active deformation determined from GPS and SAR

Contractor:

Freysteinn Sigmundsson
Nordic Volcanological Institute
Grensásvegur 50
108 Reykjavík
Iceland
Tel: +354-525-4494
Fax: +354-562-9767
E-mail: fs@norvol.hi.is

Associated contractor:

Kurt L. Feigl
Centre National de la Recherche Scientifique
UPR 0234 - Dynamique Terrestre et Planétaire
14 Avenue Edouard Belin
FR-31400 Toulouse
France
Tel: +33-5-6133-2940
Fax: +33-5-6125-3205
E-mail: kurt.feigl@cnes.fr

Subcontractor:

Páll Einarsson
Science Institute
University of Iceland
Hofsvallagata 53
107 Reykjavík
Iceland
Tel: +354-525-4816
Fax: +354-552-8801
E-mail: palli@raunvis.hi.is

Researcher:

Sverrir Guðmundsson
Nordic Volcanological Institute
Grensásvegur 50
108 Reykjavík
Iceland
Tel: +354-525-5868
Fax: +354-562-9767
E-mail: sg@raunvis.norvol.hi.is

Researcher:

Amy E. Clifton
Nordic Volcanological Institute
Grensásvegur 50
108 Reykjavík
Iceland
Tel: +354-525-5481
Fax: +354-562-9767
E-mail: amy@norvol.hi.is

The main end results of this Subproject are described in the following. For details of how individual tasks were carried out, we refer to PRENLAB-2 first annual report.

3.5.1 Subpart 5A: SAR interferometry study of the South Iceland seismic zone

The objective was to measure ongoing crustal deformation in the South Iceland seismic zone (SISZ) and relate it to distribution of faults and seismicity there. We have met that objective at the western edge of the SISZ, around the Hengill volcanic center, and published the results in an international, peer-reviewed scientific journal (Feigl et al. 2000).

We have analyzed synthetic aperture radar (SAR) images acquired by the ERS-1 and ERS-2 satellites between July 1993 and September 1998 using interferometry. In spite of our careful image selection, correlation is poor in the relatively flat and wet lowlands of southern Iceland, which unfortunately includes most of the faults in the SISZ. On the other hand, coherence remains good, even after 4 or 5 years, in the mountainous areas around Hengill.

The predominant signature in all the interferograms spanning at least 1 year, is a concentric fringe pattern centered just south of the Hrómundartindur volcanic center (Figure 26). This we interpret as mostly vertical uplift caused by increasing pressure in an underlying magma source. The volume source that best fits the observed interferograms lies at 7±1 km depth and remains in the same horizontal position to within 2 km. It produces 19±2 mm/year of uplift. This deformation accumulates as elastic strain energy at a rate 2.8 times the rate of seismic moment release.

Under our interpretation, magma is injected at 7 km depth, just below the seismogenic zone formed by colder, brittle rock. There, the inflation induces stresses that exceed the Coulomb failure criterion, triggering earthquakes. Accumulated over 5 years, the deformation increases the Coulomb failure stress by >0.6 bar in an area that includes some 84% of the earthquakes recorded between 1993 and 1998 (Figure 27 and Figure 28).

Our model suggests that magmatic inflation can trigger earthquakes, with stress rising slowly to failure and then dropping instantaneously in an earthquake. Thus a plot of stress as a function of time on a given fault forms a sawtooth pattern. Prior to an earthquake, on the leading edge of the sawtooth, the stress increases at a rate of the order of $\sim$ 1 bar/year. After accumulating for a time interval Δt years, the stress then decreases abruptly in an earthquake with stress drop $\delta\tau$. For the magnitude 5.2 earthquake of June 4, 1998, we take a mean stress drop of the order of $\tau \sim 20$ bars, assuming that μ =33 GPa and $\delta\tau = \mu U(LW)^{1/2}$. If this rupture returns the state of its stress to its initial level, then the accumulation interval is of

the order of $\Delta t \sim 20$ years. If this process is cyclical, then this interval is the recurrence time of a characteristic earthquake. It suggests that inflation of a magma chamber can furnish the primary driving force to actually break rocks on a fault in an earthquake.

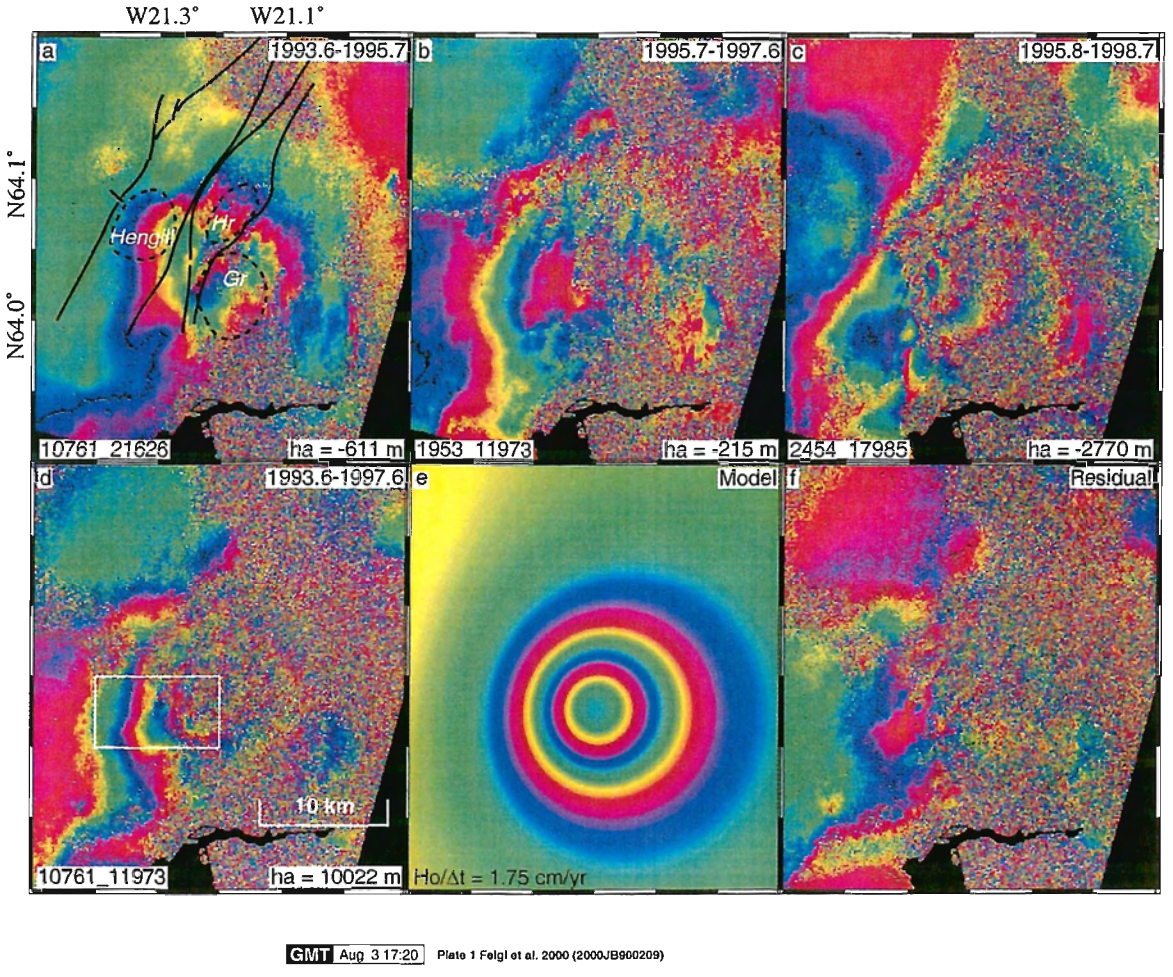

Figure 26. *Observed interferograms of the Hengill area for four different time intervals. The time interval appears in the upper right corner of each panel, the orbit numbers appear at lower left, and the altitude of ambiguity h_a appears at lower right. One fringe represents 28 mm of range change. Two concentric fringes are visible in the 4-year interferogram (d) indicating at least 6 cm of uplift between August 1993 and August 1997. The white box in (d) includes the discontinuity enlarged in (b) and (c).*

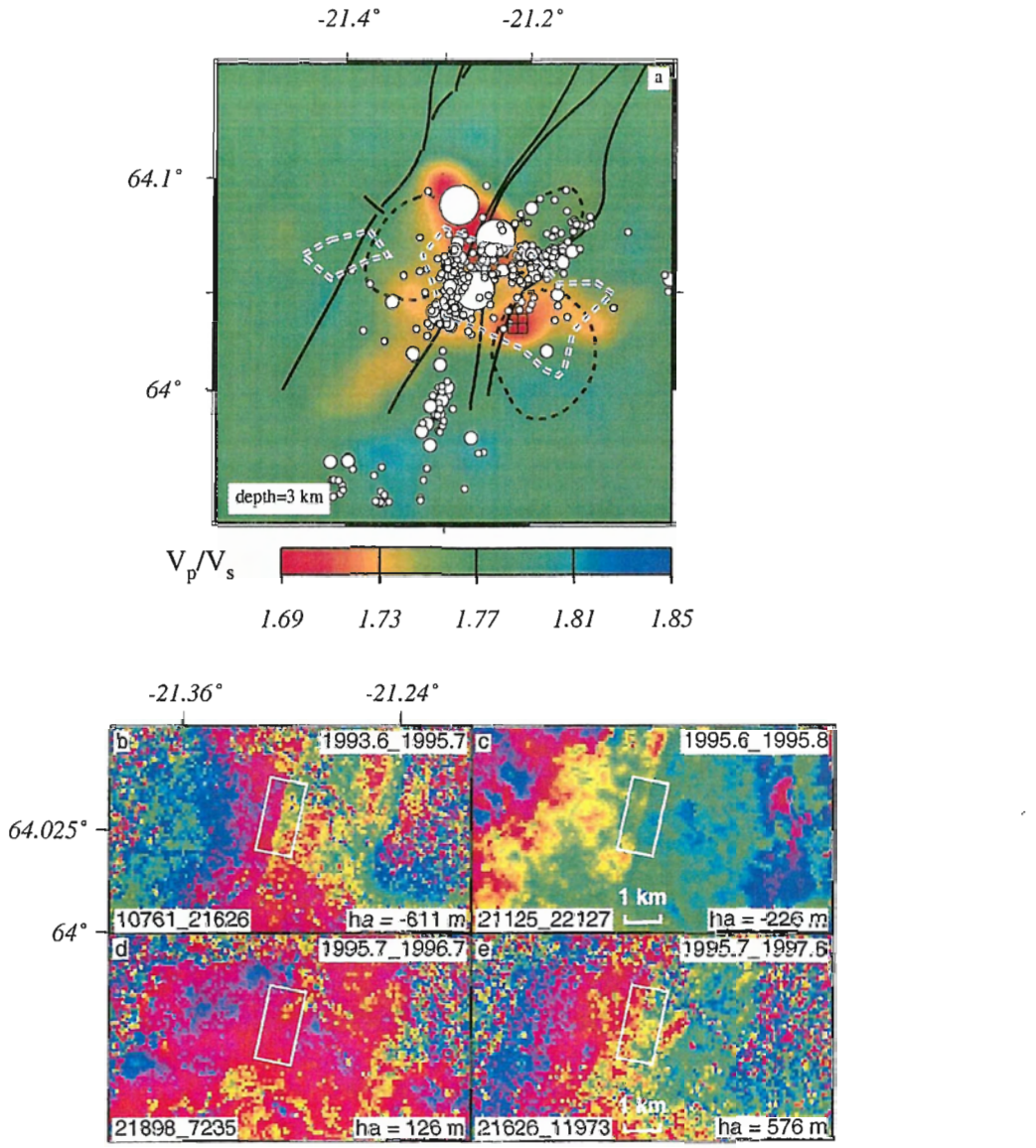

Figure 27. *(a) Structural map showing V_P/V_S wave speed ratio at 4 km depth (Miller et al. 1998); our best fitting volume source (crossed square); contours of P-wave speed velocity anomaly $\delta V_P = +1\%$ at 4 km depth (dashed white lines); contours of Miller et al. (1998); limits of volcanic system (solid black lines); outlines of three central volcanos (dashed black lines). Circles and dots show earthquake hypocenters for events between 1993 and 1998 (Rögnvaldsson et al. 1998a; Rögnvaldsson et al. 1998b). The largest circle is the M_w=5.2 event of June 4, 1998. Events with magnitude smaller than 2.5 plot as dots. (b-e) Enlargement of two interferograms that span August 1995 [b) and c)], and two which do not [d) and e)]. A discontinuity is clearly visible in b) and c) and is interpreted as a fault rupturing. We cannot discern a discontinuity in Figures d) and e).*

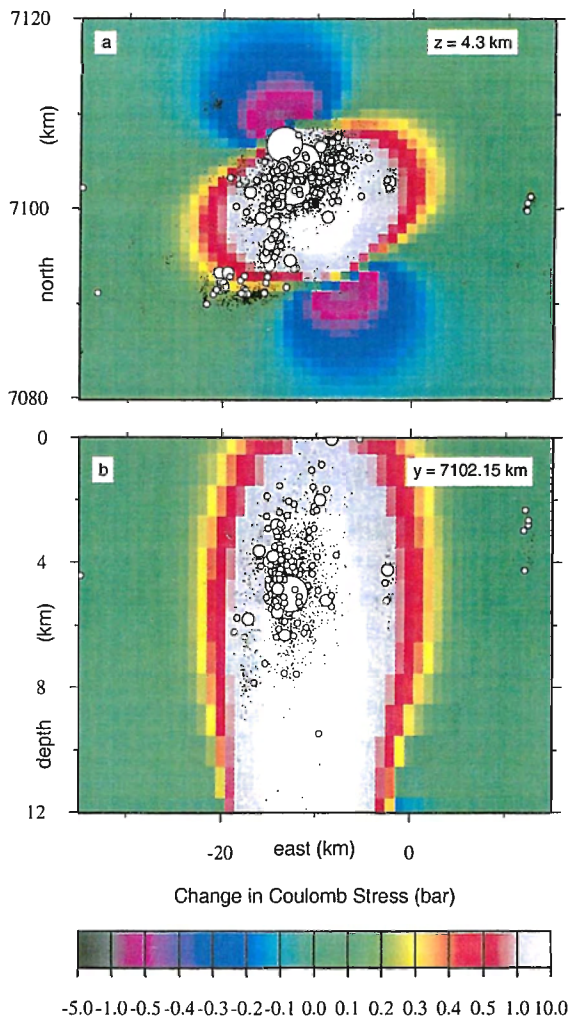

Figure 28. *(a) Coulomb failure stress change on optimally oriented vertical faults shown in a horizontal slice at 4.3 km depth. White color denotes where the stress increase is >1 bar but <10 bar. Source parameters include: latitude* 64.032°*N, longitude* 21.213°*W, depth 7.0 km, tensile opening 12.1 m on each of three dykes with length L=1 km and width W=1 km; the apparent coefficient of friction* μ'_f*=0.4, the azimuth* ϕ*=70° (measured clockwise from north) of the most compressive principal value of the stress tensor, and its magnitude* $|\sigma_1|$*=1 bar, and the two Lame' constants* $\mu=\lambda$*=33 GPa. Hypocenters of the earthquakes (circles and dots) are as in Figure 27. (b) Coulomb failure stress change on optimally oriented vertical faults shown in a vertical cross section passing E-W through the center of the modelled volcanic point source (crossed square). Model parameters and plotting conventions as in Figure 27a.*

3.5.2 Subpart 5B: GPS measurements of absolute displacements

The objective was to measure absolute plate motions near the South Iceland seismic zone (SISZ), in order to help with improved understanding of the mechanism of faulting in the seismic zone. The objective has been met by developing a new technique to combine GPS and satellite radar interferograms into three-dimensional motion maps, that give an unprecedented view of the absolute plate motions (Guðmundsson et al. 2000). The methodology has been applied to the western continuation of the SISZ, the Reykjanes peninsula.

The original plan was to operate one semi-continuous GPS station and interpret data from this station. Rather than doing that, we participated in the installation of network of continuously recording stations in S-Iceland. These results are described in Subproject 1. Additional work was conducted on two topics: Development of a new technique to combine GPS and satellite radar interferometry results (work lead by Sverrir Guðmundsson), and secondly, fault mapping was conducted in the Hengill region in order to advance further the understanding of interferograms collected in Subpart 5A (work lead by Amy Clifton).

The new technique developed to efficiently produce high-resolution three-dimensional surface motion maps, relies on combining information about motion of the earth's surface from interferometric observations of synthetic aperture radar images and repeated Global Positioning System geodetic measurements. Unwrapped interferograms showing pixel-wise change in range from ground to satellite, and sparse values of three-dimensional movements are required as input. The problem of finding the full three-dimensional motion field is separated into two two-dimensional problems. Initially the vertical component of the deformation field, and its horizontal component in the look-direction of the satellite are found. Later the look-direction component is resolved into north and east components. Initial values for the motion fields are assigned to each pixel of interferograms from ordinary kriging of available GPS observations. These values are then updated and optimized by comparison with the interferograms and the GPS observations. Additional constraint is the smoothness of motion field. Markov random field based regularization, and simulated annealing algorithm are used for the optimization. The technique has been applied to create surface motion maps for the Reykjanes peninsula (Figure 29). Although separate interpretation of GPS and InSAR data from the area (Hreinsdóttir et al. 2000; Vadon and Sigmundsson 1997) have shown the main components of deformation, the three-dimensional motion maps provide an unprecedented view of the three-dimensional deformation. The largest signals are plate movements causing large gradients in the east motion field, and circular subsidence centered on the Svartsengi and Eldvörp geothermal area. The north and east motion field images show also clearly that the subsidence is associated with horizontal movements towards the subsidence center, a pattern that is imprinted on the background plate movements. The motion maps form the basis of a future project on conducting a detailed study of strain accumulation in the area and how it correlates with seismicity.

A related effort was the study of faulting and surface rupture that has taken place in the Hengill volcanic area (Clifton and Sigmundsson 2000). It is the same area as studied by satellite radar interferometry under Subpart 5A. The Hengill and Hrómundartindur volcanic systems in SW-Iceland are considered to comprise the Hengill triple junction at which the oblique Reykjanes peninsula rift zone, the western volcanic (rift) zone and the South Iceland seismic (transform) zone meet. It is therefore experiencing both tectonic extension and left-

lateral shear causing seismicity related to both strike-slip and normal faulting. Between 1994 and 1998, the area experienced episodic swarms of enhanced seismicity attributed to magma moving within the system. Activity culminated in a magnitude 5.1 earthquake on June 4, 1998, and a magnitude 5 earthquake on November 13, 1998. Geodetic measurements using GPS, levelling and InSAR detected uplift and expansion of the volcanic edifice above a point source of pressure beneath the Hrómundartindur volcanic system. Magma accumulation elevated the volcanic edifice 2 cm/year and is believed to have triggered motion along strike-slip faults that were near to failure due to tectonic stresses. A number of faults in the area generated small-scale surface breaks. Geographic information system has been used to integrate aerial photographs, field data and geophysical data to determine how the crust breaks in response to deformation along this plate boundary, and to see how much of the recent activity focussed on pre-existing weaknesses in the crust. Our data indicates that all surface rupture has occurred along or adjacent to old faults, several of which were previously unmapped. The most prominent surface breaks occurred along NE- and NNE-trending faults adjacent to the epicenter of the June 4 earthquake. Maximum opening observed along a single fault segment was 1.2 m. Styles of rupture include fresh rockfall into pre-existing fissures and along old scarps, subsidence along and possible widening of old fissures, tears in turf and gashes in soil, shattering of lava blocks and loosening of push-up structures related to strike-slip faulting (Figure 30). Although all geophysical data agree that rupture occurred along a shallow, right-lateral strike-slip fault, no clear evidence of lateral offset was observed at the surface. Foreshocks and aftershocks from the November 13 earthquake define a broad E-W zone that intersects the southern end of the June 4 fault. The only surface rupture observed in this zone was found at that intersection.

In addition to fault mapping in the Hengill area, then Páll Einarsson at UICE.SI worked as a subcontractor on preparing a digitized fault map of the South Iceland seismic zone, as described in the PRENLAB-2 first annual report. That work is still in progress.

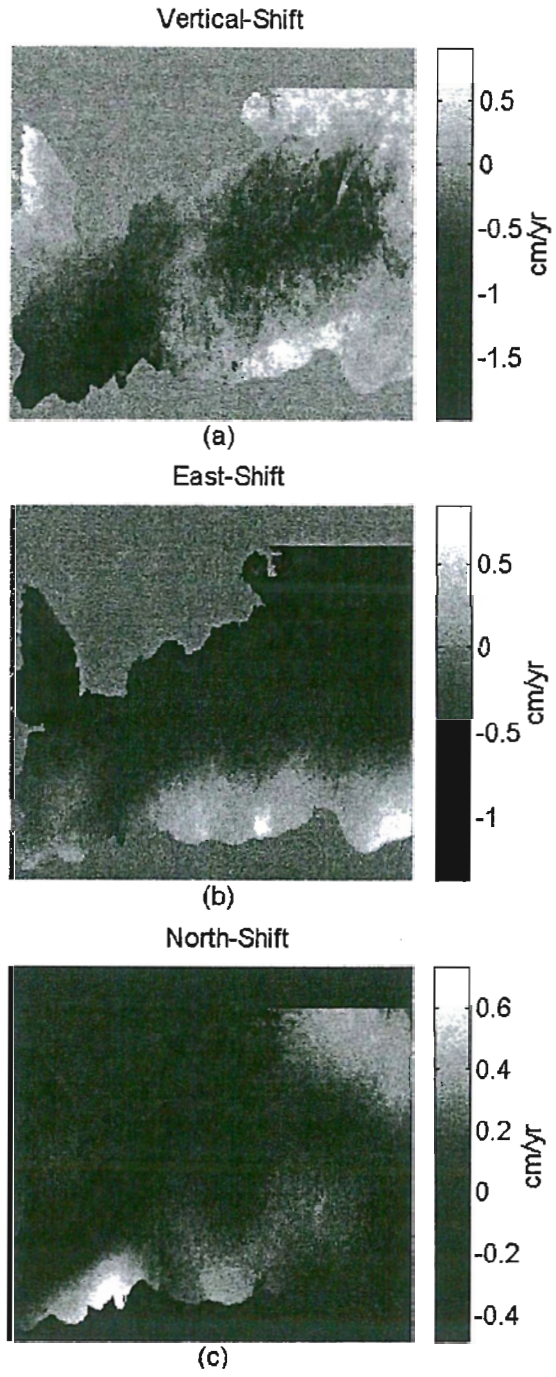

Figure 29. *Estimated one-year average motion field maps at the Reykjanes peninsula. (a), (b) and (c): Average vertical, east and north motion maps, respectively, inferred by the 1992-1993, 1992-1995, 1992-1996 and 1993-1995 InSAR data, and the 1993-1998 GPS data (Guðmundsson et al. 2000).*

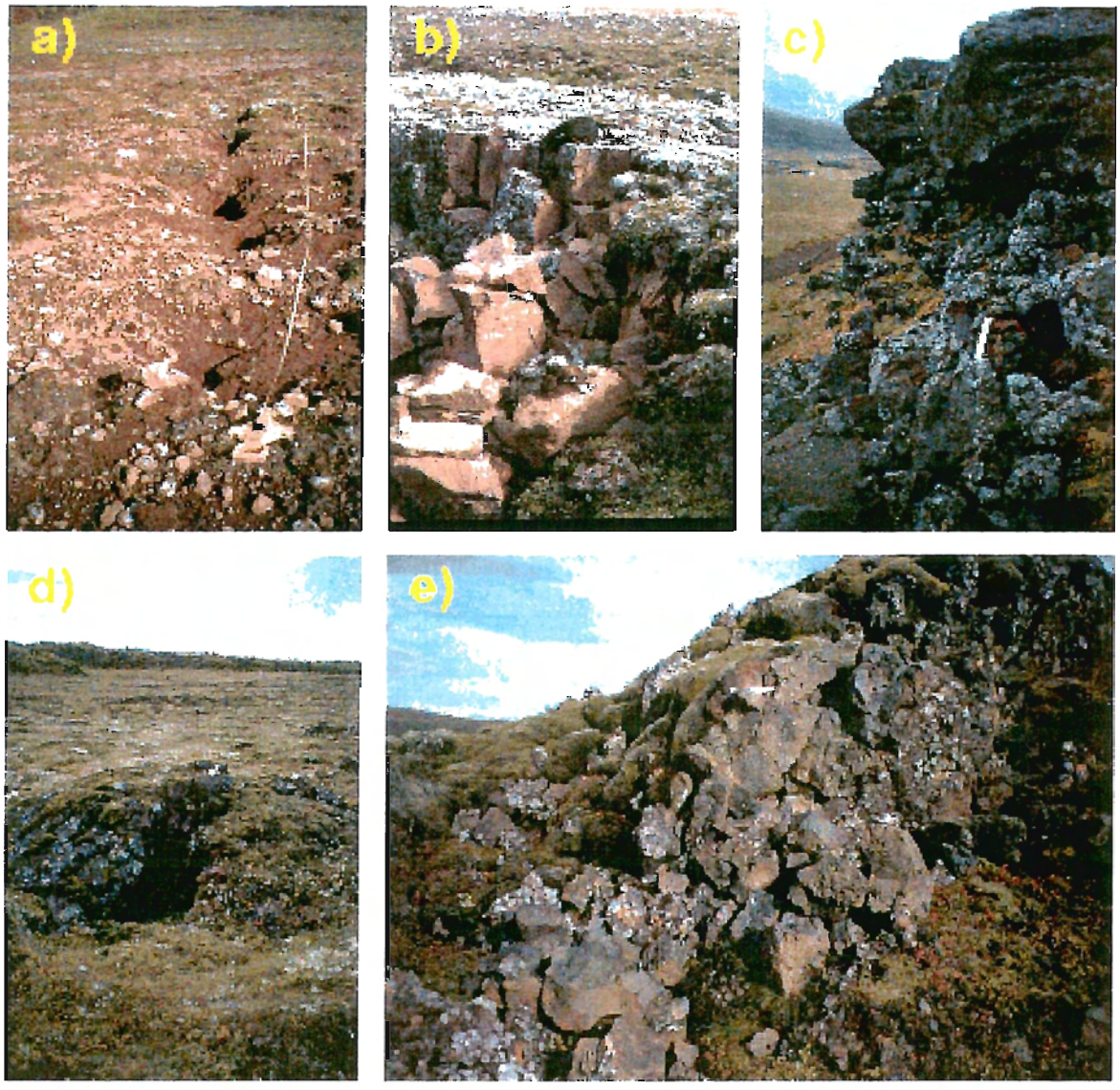

Figure 30. *Different styles of surface rupture observed in the Hengill area in response to uplift, and the June 4, 1998, M=5.1 earthquake. a) Gashes in soil: Ellipital segments up to 1.5 m wide, 2 m long, more than 1 m deep, en-echelon and along-strike arrangement. b) Rock fall along old fissures: Unweathered surfaces of broken rock, free of vegetation, plant roots freshly exposed. c) Rock fall along old fault scarps: Large fallen blocks, exposing freshly torn plant roots and soil, large rocks dislodged from slope leaving gaps between rocks and soil. d) Loosened push-up structures: Piles of rock with gaps of up to several centimeters between rock and soil; individual rocks may show evidence of rotation. e) Shattered aa lava: Broken blocks up to 1 m in diameter, aligned along strike and at flow margins near the June earthquake epicenter (Clifton 2000).*

3.5.3 References

Clifton, A. 2000. Surface deformation related to volcanic uplift and seismicity in SW-Iceland. Poster presented at the Nordvulk-Ridge summer school, Iceland, August 20-30, 2000.

Clifton, A. & F. Sigmundsson 2000. Faulting and deformation resulting from magma accumulation at the Hengill triple junction, SW-Iceland. In: Abstracts from the AGU fall meeting, San Francisco, California, USA, December 15-19, 2000.

Feigl, K.L., J. Gasperi, F. Sigmundsson & A. Rigo 2000. Crustal deformation near Hengill volcano, Iceland, 1993-1998: coupling between magmatic activity and faulting inferred from elastic modeling of satellite radar interferograms, *J. Geophys. Res.* 105, 25655-25670.

Guðmundsson, S., F. Sigmundsson & J.M. Carstensen 2000. Three-dimensional surface motion maps estimated from combined InSAR and GPS data. *J. Geophys. Res.*, submitted.

Hreinsdóttir, S., P. Einarsson, & F. Sigmundsson 2000. Crustal deformation at the oblique spreading Reykjanes peninsula, SW-Iceland: GPS measurements from 1993 to 1998. *J. Geophys. Res.*, submitted.

Miller, A.D., B.R. Julian & G.R. Foulger 1998. Three dimensional seismic structure and moment tensors of non-double-couple earthquakes at Hengill-Grensdalur volcanic complex, Iceland. *Geophys. J. Int.* 133, 309-325.

Rögnvaldsson, S.Th., G.B. Guðmundsson, K. Ágústsson, S.S. Jakobsdóttir, R. Slunga & R. Stefánsson 1998a. Overview of the 1993-1996 seismicity near Hengill. *Rit Veðurstofu Íslands* VÍ-R98006-JA05. Research report, Icelandic Meterological Office, Reykjavík, 16 pp.

Rögnvaldsson, S. Th., Þ. Árnadóttir, K. Ágústsson, Þ. Skaftadóttir, G.B. Guðmundsson, G. Björnsson, K.S. Vogfjörð, R. Stefánsson, R. Böðvarsson, R. Slunga, S.S. Jakobsdóttir, B.S. Þorbjarnardóttir, P. Erlendsson, B.H. Bergsson, S. Ragnarsson, P. Halldórsson, B. Þorkelsson & M. Ásgeirsdóttir 1998b. Skjálftahrina í Ölfusi í nóvember 1998. *Greinargerð Veðurstofu Íslands* VÍ-G98046-JA09. Report, Icelandic Meteorological Office, Reykjavík, 19 pp. In Icelandic.

Vadon, H., & F. Sigmundsson 1997. Crustal deformation from 1992 to 1995 at the mid-Atlantic ridge, Southwest Iceland, mapped by satellite radar interferometry. *Science* 257, 194-197.

3.6 Subproject 6: Effects of stress fields and crustal fluids on the development and sealing of seismogenic faults

Contractor:

Françoise Bergerat
Département de Géotectonique, Boite 129
Université Pierre et Marie Curie
4, place Jussieu
FR-75252 Paris Cedex 05
France
Tel: 33-1-4427-3443
Fax: 33-1-4427-5085
E-mail: bergerat@lgs.jussieu.fr

Subcontractor:

Jacques Angelier
Département de Géotectonique, Boite 129
Université Pierre et Marie Curie
4, place Jussieu
FR-75252 Paris Cedex 05
France
Tel: 33-1-4427-5857
Fax: 33-1-4427-5085
E-mail: jacques.angelier@lgs.jussieu.fr

Subcontractor:

Ágúst Guðmundsson
Geological Institute
University of Bergen
Allégaten 41
N-5007 Bergen
Norway
Tel: 47-5558-3503
Fax: 47-5558-9416
E-mail: agust.gudmundsson@geol.uib.no

Subcontractor:

Thierry Villemin
Laboratoire de Geodynamique des Chaines Alpines
Université de Savoie
Batiment Belledonne
Domaine Universitaire
73376 Le Bourget du Lac Cedex
France
Tel: 33-4-7975-8735
Fax: 33-4-7975-8777

E-mail: Thierry.Villemin@univ-savoie.fr

Subcontractor:

Philip Meredith
Department of Geological Sciences
University College London
Gower Street
London WC1E 6BT
United Kingdom
Tel: 44-171-380-7822
Fax: 44-171-387-1612
E-mail: p.meredith@ucl.ac.uk

3.6.1 Task 1: Determination of the paleostress fields associated with the test areas from fault-slip data

3.6.1.1 Task 1.1: The South Iceland seismic zone (SISZ)

We carried out a structural study in this area, including analysis of aerial photographs, local observation of major faults and collection of minor fault slip data in outcrops, as well as an analysis of the focal mechanisms of earthquakes (Bergerat et al. 1998; Bergerat et al. 1999; Bergerat and Angelier 2000). At the regional scale, the main fault trends are approximately NNE-SSW and NE-SW. ENE-WSW, NW-SE and WNW-ESE trending faults are also detected in aerial photographs and in the field. All these faults are normal or strike-slip in character. Some of the historical major earthquake fractures are observed in the post-glacial lava flows in the SISZ: most are right-lateral and trend roughly N-S. We analyzed more than 700 minor faults at 25 sites. Most sites are located in rocks of Upper Pliocene-Pleistocene age. Inversion of fault-slip datasets enabled us to reconstruct local paleostress tensors, hence to define the major tectonic regimes which have prevailed in the SISZ. Two main groups of faulting mechanisms reveal two distinct stress regimes, with perpendicular directions of extension, NW-SE (primary) and NE-SW (secondary). Both groups, however, display inhomogeneous datasets, related to extensional and to strike-slip faulting. The primary stress regime is in agreement with both the general behaviour of the SISZ as a left-lateral transform zone and the opening of the rift segments. The secondary stress regime, incompatible with the primary stress regime, is interpreted in terms of stress permutations. A population of 231 double-couple focal mechanisms (M>1 and depth>2 km) was also analyzed in terms of stress states. The results show great similarity in terms of stress directions. Figure 31 gives an example of a characteristic fault-slip data site and a comparison with focal mechanisms of earthquakes.

The present-day stress field mainly inferred from analyses of earthquake focal mechanisms is consistent with the present behaviour of the SISZ as a left-lateral transform zone. However, the proportion of strike-slip faulting within the present-day seismic activity (71%) is significantly higher than that revealed by the geological observation of Quaternary faults (50%). This contrast is interpreted in terms of development and evolution of the transform fault zone. Figure 32 schematically presents a comparison between the paleostress results obtained from faulting analysis and the present day activity based on focal mechanisms of

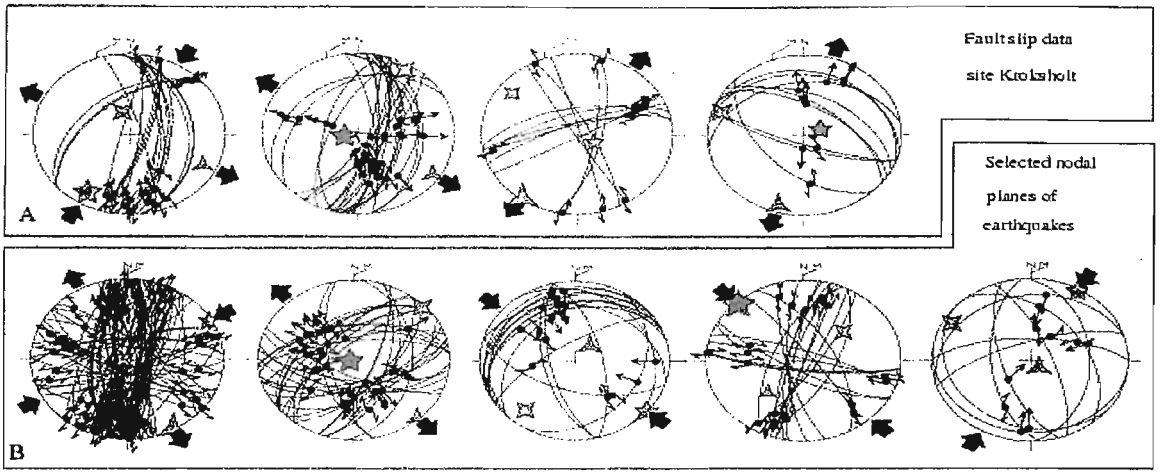

Figure 31. *Comparison between the main stress regimes as indicated by fault–slip datasets and focal mechanisms of earthquakes in the SISZ, based on two case examples (after Bergerat and Angelier 2000). (A) Striated faults at site Króksholt. (B) Selected nodal planes and slip vectors of earthquakes throughout the SISZ for the years 1991-1994 and 1996, at crustal depths larger than 2 km, with magnitudes larger than 1.*

earthquakes analysis. Stress permutations between different regimes are shown as couples of open arrows. The paleostress fields identified in the Upper Pliocene-Pleistocene formations of the SISZ reflect both the previous behaviour of the area, when it was located inside the rift zone, and its present behaviour as a transform zone, thus illustrating the local evolution from rifting to transform motion.

3.6.1.2 Task 1.2: The Tjörnes fracture zone (TFZ)

The inversion of about 1000 fault-slip data collected in 20 sites in the Flateyjarskagi peninsula allows reconstruction of eight normal and strike-slip regimes (Angelier et al. 2000b; Bergerat et al. 2000) related to the general behaviour of the Húsavík-Flatey fault (HFF), a major structure of the Tjörnes fracture zone connecting the Kolbeinsey ridge and the North Icelandic rift. The two most important regimes (E-W and NE-SW extensions), consistent with the right-lateral motion along the Húsavík-Flatey fault, constitute the main tectonic group. The two others (NW-SE and N-S extensions), forming the subordinate tectonic group, are incompatible and result from drastic stress permutations (as a probable result of stress drop, elastic rebound and dyke injection). Figure 33 summarizes the local paleostress determinations made in Flateyjarskagi.

The relationships between these stress regimes imply not only σ_1/σ_2 and σ_2/σ_3 stress permutations, but also σ_1/σ_3 reversals. An important factor controlling the transform mechanism is the variation of coupling along the HFF. The obliquity between the direction of transform motion and the trend of extension for the two main regimes may vary between 25° and 85°, reflecting repeated changes of the coefficient of friction along the HFF (Figure

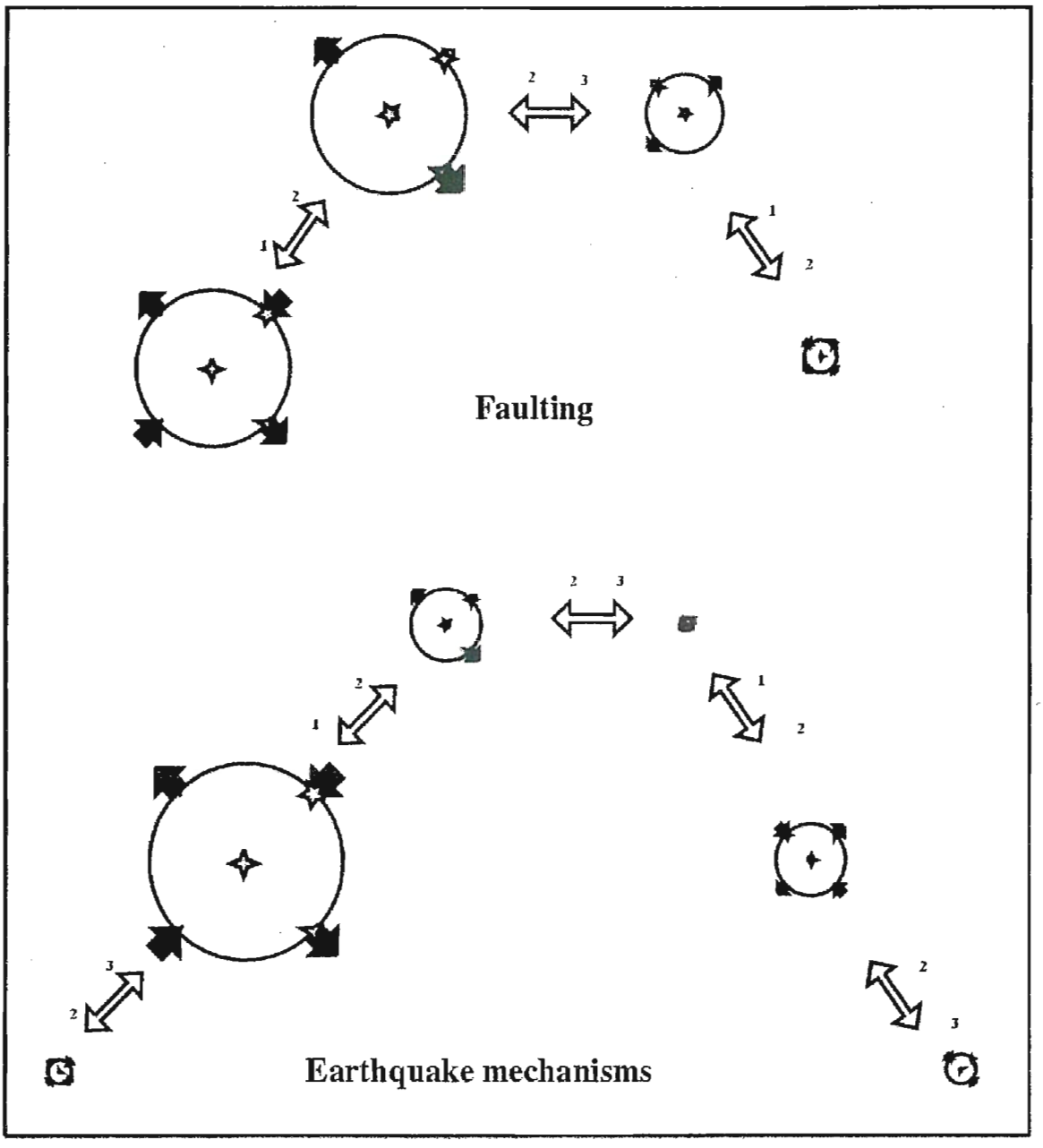

Figure 32. *The different stress tensors obtained from analyses of sets of fault-slip data and earthquake focal mechanisms in the SISZ (after Bergerat et al. 1999). Size of diagrams proportional to numbers of data. Three-, four-, and five-branched stars: regional axes of σ_3, σ_2 and σ_1 respectively (schematic). Couples of black arrows: directions of compression (convergent) or extension (divergent). Couples of open arrows: stress permutations (σ_1/σ_2 or σ_2/σ_3 modes) between the different regimes.*

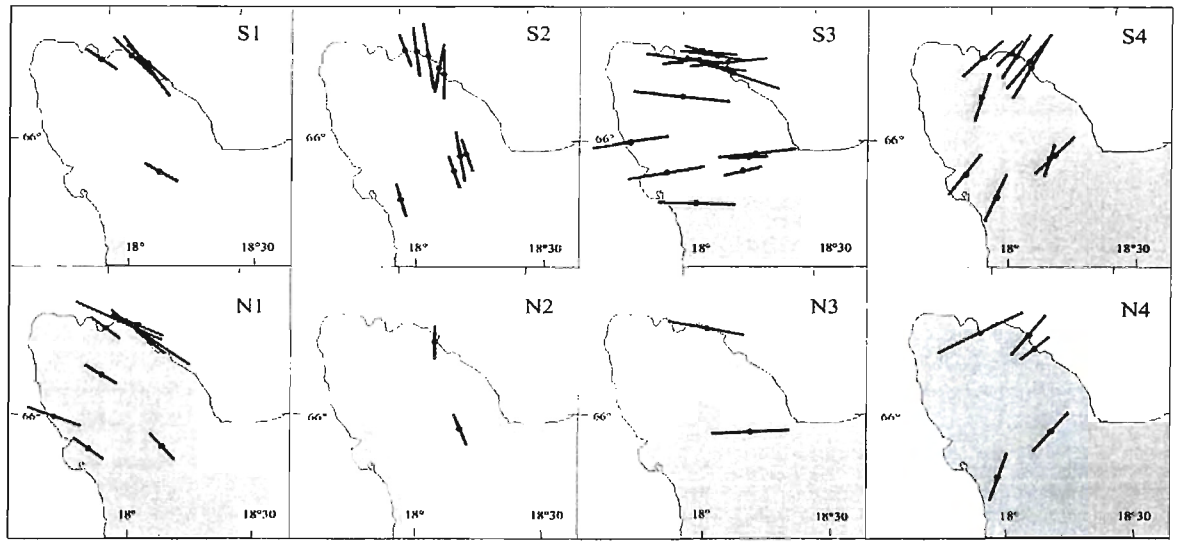

Figure 33. *Summary of local paleostress determinations made in Flateyjarskagi using Angelier's inversion (1990) (after Angelier et al. 2000b). Solid bars: trends of minimum compressive stress, σ_3. Bar size increases with quality of paleostress tensor determination. Nature of brittle tectonic regime: S-type for nearly vertical σ_2, N-type for nearly vertical σ_1.*

34). Such changes from very low mechanical coupling (weak fault) to moderate friction may occur very rapidly since it takes place several times in a few years, as shown by focal mechanisms of earthquakes analysis. Thus, the tectonic regimes need not be interpreted in terms of numerous tectonic episodes, but rather as a consequence of variable coupling across the transform zone.

3.6.2 Task 2: Reconstruction of the current stress field associated with the test areas

3.6.2.1 Task 2.1: Inversion of large sets of focal mechanisms of earthquakes

Using a new inversion technique suitable for focal mechanisms of earthquakes (in that it does not require the choice of a nodal plane as the actual fault plane) was particularly worthwhile in order to process the very large numbers of focal mechanisms of earthquakes determined within the SIL network set-up and monitored by IMOR.DG. This was because of the mathematical aspects which imply analytical resolution so that at the core of the inversion process itself the runtime does not depend on the quantity of data (Angelier 1998).

The inversion was carried out with a total dataset of about 50000 double–couple focal mechanisms of earthquakes (Angelier et al. 2000a). It revealed regional deviations as large as 40° in the direction of extension near the major transform zones (clockwise for the South Iceland seismic zone, counterclockwise for the Tjörnes fracture zone), relative to the N104°E trend of plate separation across the mid-Atlantic ridge. However, the mean axis of minimum stress obtained from these inversions for the whole of Iceland is quite consistent with the

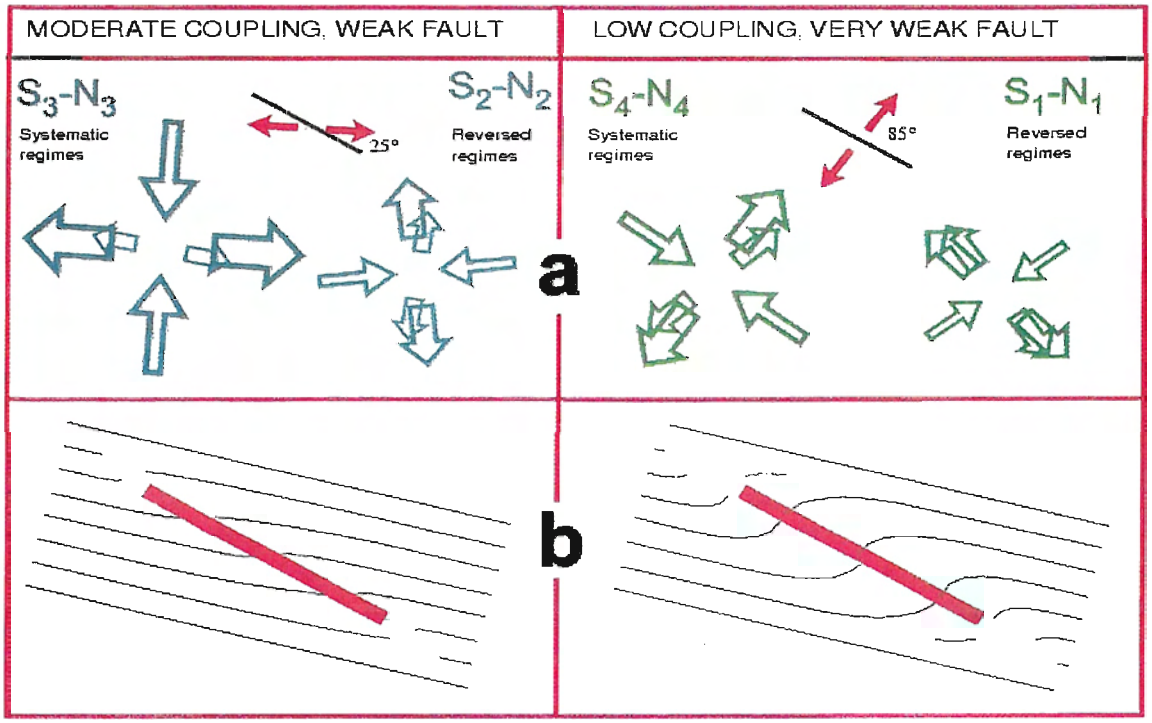

Figure 34. *Interpretation of tectonic regimes in terms of variable coupling near transform zone (after Angelier et al. 2000b). (a) Groups of tectonic regimes. Angles between transform direction (dotted lines) and averaged trends of extension (black arrows) indicated. (b) Schematic pattern of minimum compressive stress trajectories (thin lines) due to tensile loading parallel to spreading vector in North Iceland around oblique dextral transform fault zone (thick line).*

trend of plate separation independently reconstructed by DeMets et al. (1990).

3.6.2.2 Task 2.2: Seismotectonic analysis of individual faults

The Tjörnes fracture zone

The study of the Húsavík–Flatey fault in the Tjörnes fracture zone includes a tectonic analysis (see Subsection 3.6.1.2) and also a seismotectonic analysis in order to obtain a reconstruction of the stress patterns in accordance with the mechanisms of the transform zone since about 7 million years to the present (Garcia 1999; Garcia et al. 2000; Garcia et al., in preparation). We carried out an analysis of 669 double-couple earthquake mechanisms (period 1995-1997, magnitude ranging between 1 and 4.8). Three main sets of stress regimes have been identified, each including three individual stress regimes (Figure 35). The major one corresponds to an ENE-WSW trending right-lateral transtension. The two other regimes, less important, correspond to transform-parallel (WNW-ESE) and transform-perpendicular extensions (NNE-SSW).

Considering the angle between the trends of the rift and of the transform zone involves an extension occurring throughout the transform zone. This extension is accommodated by the transtensional regime, as well as, locally, by the extension sub-perpendicular to the transform direction. The extension sub-parallel to the transform direction may express by pull-apart process or by locking of part of the transform fault. The analysis of focal mechanisms of earthquakes indicates that most of these regimes currently occur, invalidating as well the hypothesis of polyphase tectonism (see Subsection 3.6.1.2). It suggests that transform motion along an oceanic fault zone may induce a variety of tectonic regimes. A major point of the transform mechanism is the variation of coupling along the HFF. These changes may correspond, at least partly, to the necessity of extension in this area because of the obliquity of the transform zone versus the rifts zones of N–Iceland and of Kolbeinsey, but the occurrence of magmatism at depth probably plays an important role also in such a phenomenon.

The Leirubakki fault

The Leirubakki fault is one of the large N-S seismic faults of the South Iceland seismic zone, located in its eastern part, a few kilometers west of the 1912 earthquake major earthquake. The Leirubakki rupture occurred earlier during historical times (maybe before the settlement of Iceland). Our work included the reconnaissance of the fault trace based on aerial photograph analysis and field study, a GPS mapping to reconstruct the morphology of the rupture zone, and some measurements of structures along the fault, including orientations and amplitudes (Bergerat et al. 2000; Bergerat et al., in preparation). We thus identify a pattern of dextral segments that connect typical push-up structures, with specific angular relationships between these features and the general trend of the earthquake fault (Figure 36). The fracturing process involved development of near-surface strike-slip segments, oblique relative to the underlying shear zone (Figure 36). We computed the shortening amounts and rock volumes involved in push-up development and estimated the magnitude of the Leirubakki fault to more than 7.

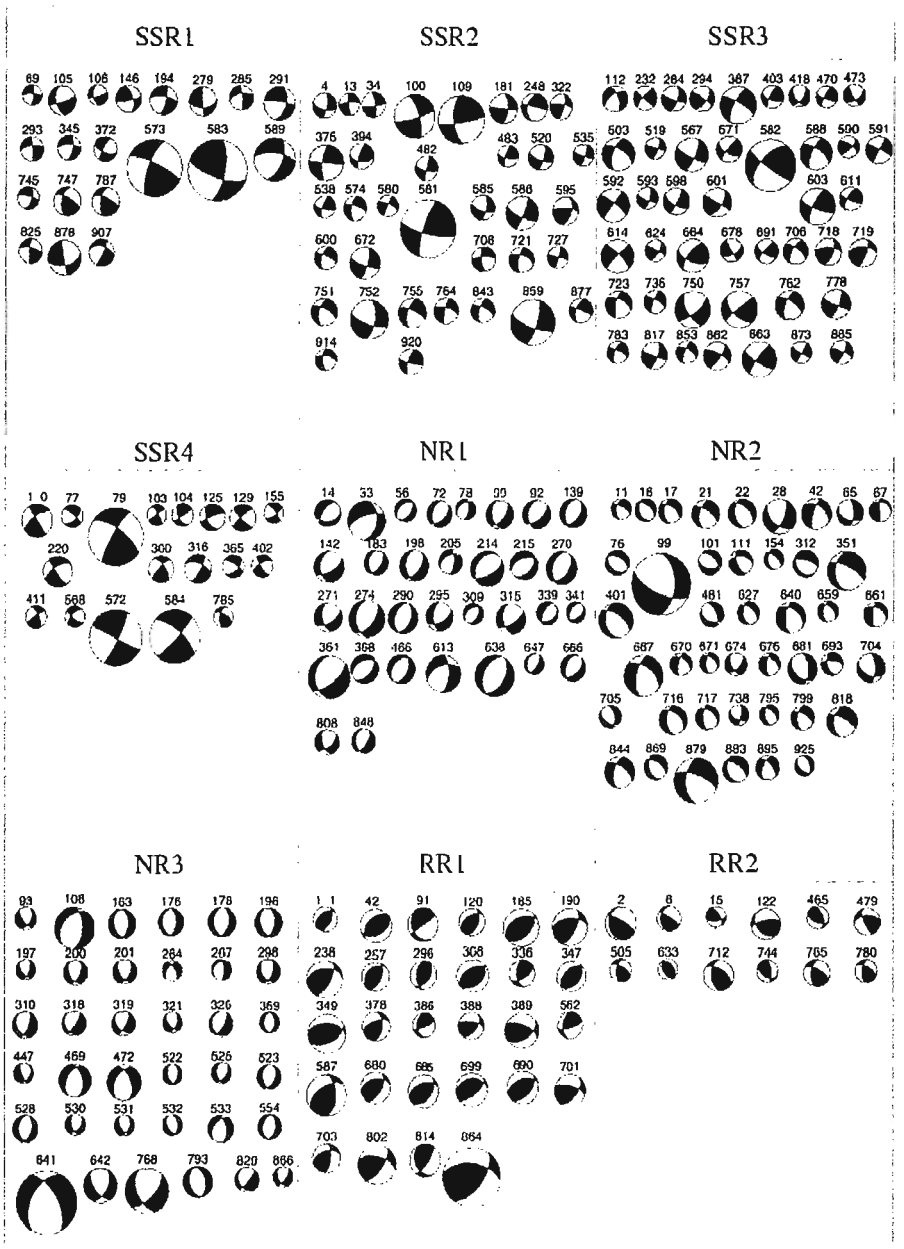

Figure 35. *Focal mechanisms of earthquakes characterizing the nine stress regimes in the Tjörnes fracture zone (SSR: strike-slip regime, NR: normal regime, RR: reverse regime) (after Garcia 1999; Garcia et al., in preparation). For the SSR2, SSR3, NR3 and RR4, only the focal mechanisms with M>1.8 are shown, for the other regimes all the focal mechanisms (M>1) are shown.*

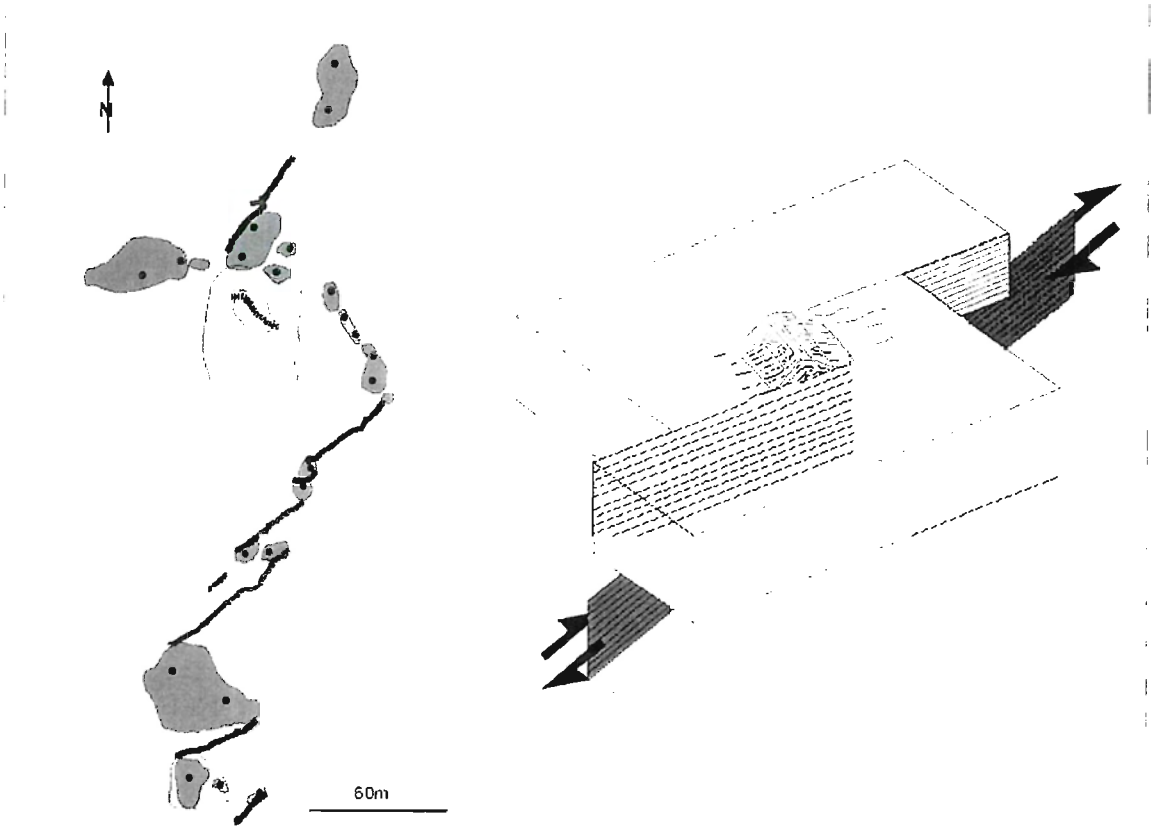

Figure 36. *The Leirubakki fault in the SISZ. On the left: detailed part of the map (drawn after GPS measurements) showing a typical array of individual fractures and individual push-ups. On the right: schematic view of a push-up and en-echelon fractures in the uppermost part of the crust and a single right-lateral strike-slip fault at depth (after Bergerat et al. 2000; Bergerat et al., in preparation).*

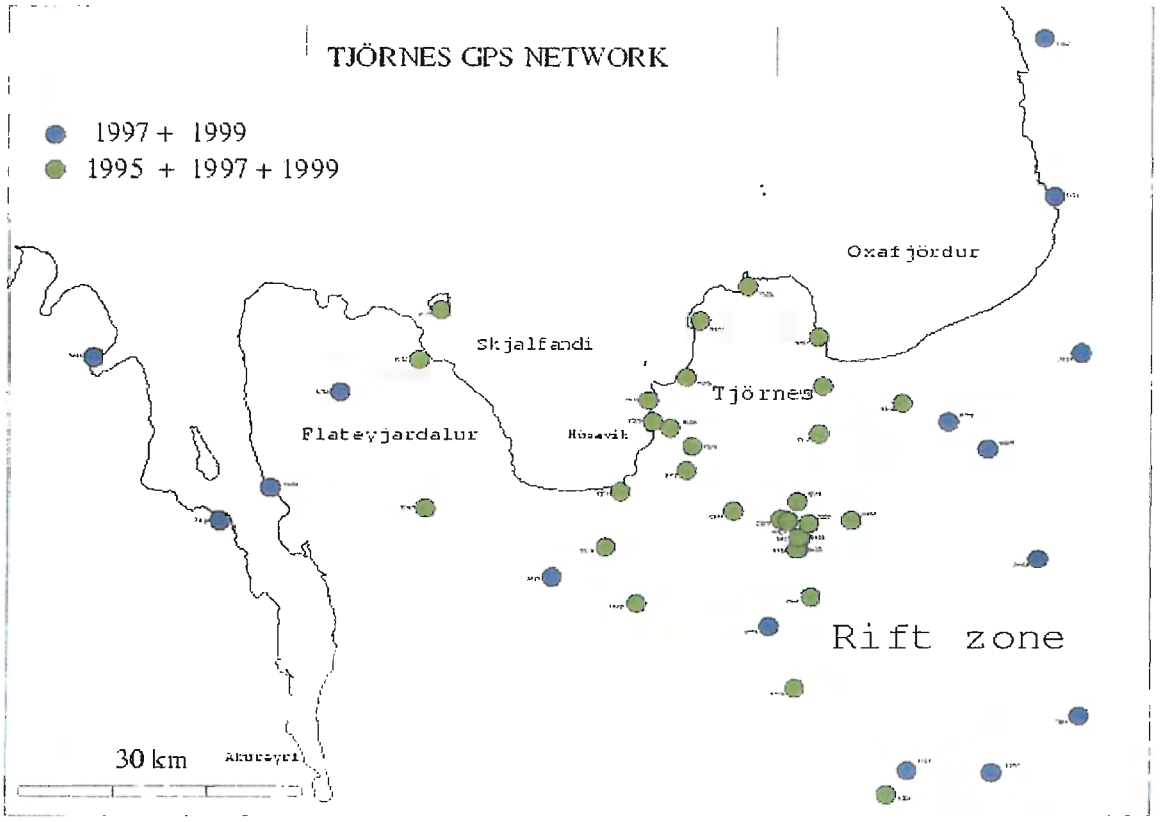

Figure 37. *The Tjörnes GPS network. 32 points have been measured in 1995, 1997 and 1999. The whole network has been measuring both in 1997 and 1999.*

3.6.3 Task 3: Present–day deformation from GPS network and interferograms of ERS-SAR scenes

3.6.3.1 Task 3.1: Measuring the present–day crustal displacements in the Tjörnes fracture zone and adjacent areas

The Tjörnes GPS network

The network consists of about 45 sites distributed in the northern Iceland seismic zone (Figure 37). It completes the geodetic networks already installed over the whole Iceland at a smaller scale. The TGN has been designed to measure the surface displacement field on each side of the Húsavík-Flatey fault (HFF). It has been done in order to estimate if there are locked fault segments in the area and how these segments can contribute to increase the seismic risk.

1995–1997 velocity field

The velocities (Figure 38) have been computed by reference to a point located in the southern part of the network. Two tendencies can be distinguished on the Tjörnes peninsula: eastward velocities reaching 13 mm/year for the most northern points of the peninsula and NNE velocities up to 15 mm/year for the points located on both sides of the HFF. Displacements

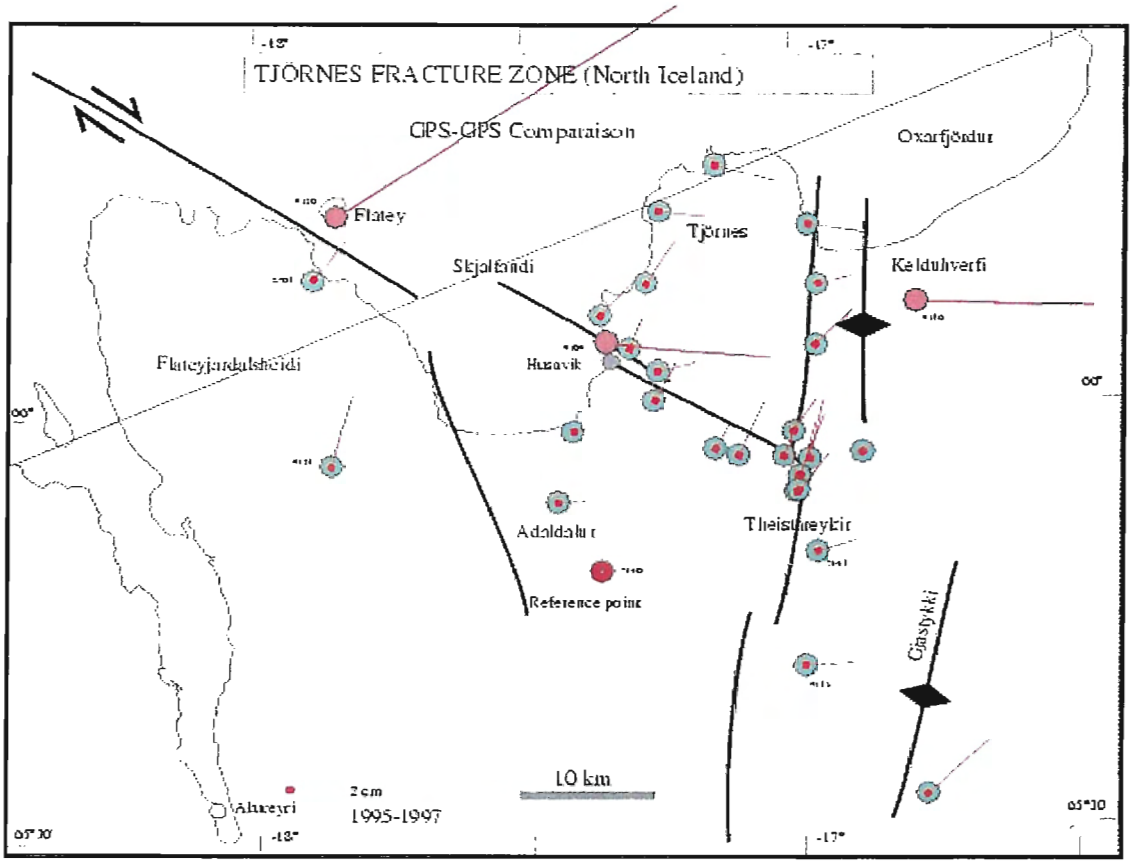

Figure 38. *1995-1997 horizontal displacements on the TGN.*

to the east have been computed for the points located in the fissure swarms. Points on Flateyjardalur move to the north. The point on the Flatey island reveals a large displacement to the NE that could be due to a local instability.

The assumption of an interseismic strain has been tested by using a simple dislocation model. This model assumes that a set of buried planar fault surfaces are locked above a given depth and are affected by uniform aseismic creep below this depth. In order to determine this brittle/ductile transition we used the microseismicity recorded by the SIL network from 1995 to 1997. We assume that most earthquakes are localized in the brittle crust. Thus gives us a limit at a 10 km depth in average. We founded a solution that minimizes the differences between simulated and observed velocities.

The model (Figure 39) assumes: (1) a dyke opening of 20 mm/year affecting all the brittle crust along the Kolbeinsey ridge; (2) two dyke openings of 30 mm/year and 20 mm/year respectively along the Krafla and Þeistareykir fissure swarms; (3) a dextral strike–slip fault striking N100°E between the two previous rift segments with a velocity of 50 mm/year below a depth of 10 km and completely locked above the brittle/ductile transition; (4) a 15 mm/year opening zone striking N140°E south of the HFF; (5) a fault along the Grímsey lineament with both a 15 mm/year opening and 20 mm/year dextral strike–slip movements.

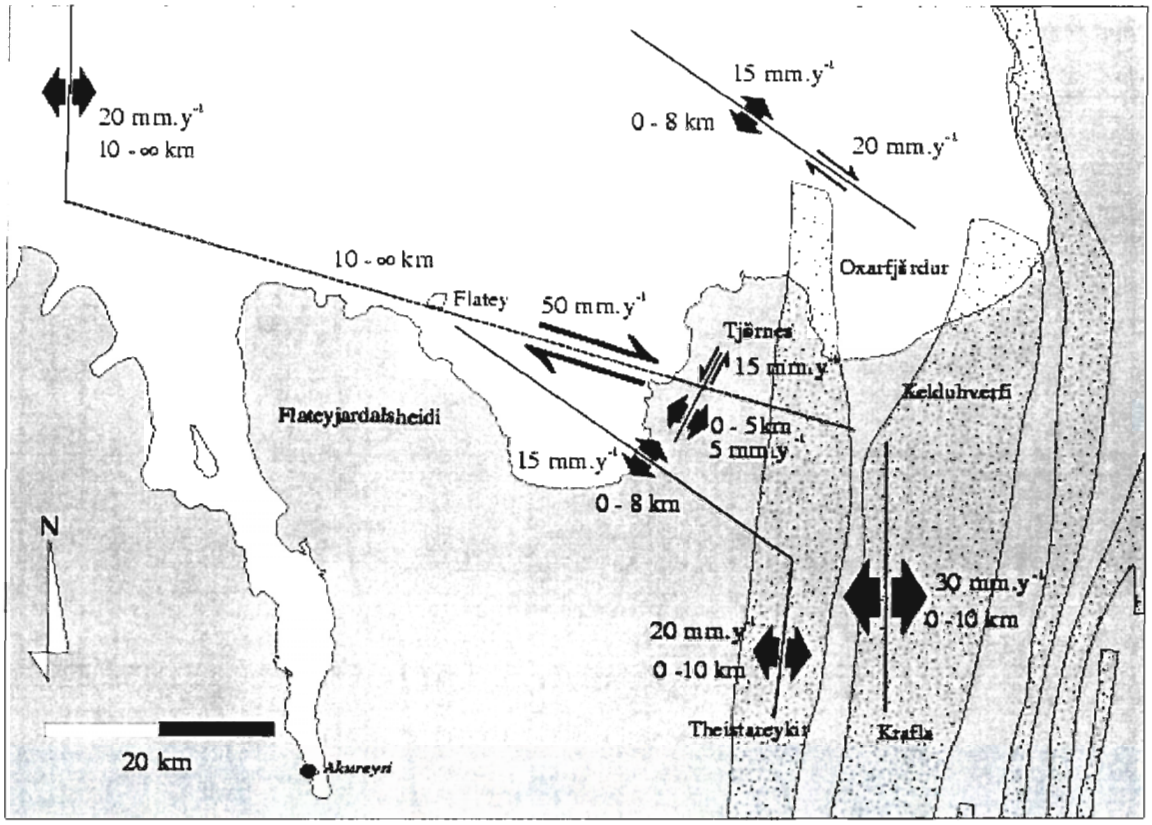

Figure 39. *Dislocations used in the simulation of the 1995-1997 displacement field (after Jouanne et al. 1999). Two main kinds of dislocation can be distinguished: superficial dislocations that affected the upper crust with mainly aseismic opening or strike-slip (Kolbeinsey ridge) and a major dislocation simulating a fault locked at 10 kilometers depth and affected by a constant slip below this limit simulating ductile slip at depth.*

In addition small wavelength tendencies has been adjusted by superficial faults.

This model based on our 1995-1997 TGN comparison revealed extension and strike–slip movements 3 to 4 times larger than the average velocity. The transform motion is locked on a large (150x10 km) fault surface and this represents the main risk for destructive earthquakes in the near future. From a mechanical point of view, the lockage could be due to the increase of normal stress on this surface following the double opening north and south of the fault zone.

1997-1999 velocity field

Comparison with the 1995–1997 velocity field

32 common points have been measured during the 3 campaigns (1995, 1997 and 1999). In comparison with to the first period and using the same reference point located in the southern part of the network, the 1997-1999 velocity field has the following main characteristics:

The eastward tendencies north of Tjörnes are always present but the average velocity

has been divided by 2. We observed less than 1 cm/year of dextral displacement north of Tjörnes. The NNE displacements observed in 1995-1997 on both side of the Húsavík fault are always observed but their component are in the opposite direction of those observed during the first period. These points are now moving to the south also with smaller velocities. Similar conclusions are drawn with the 2 points on Flateyjardalur. The large displacement observed in 1995-1997 for Flatey is no more observed.

From this comparison we can argue that the displacements on Tjörnes have varied significantly in sense and size in less than 2 years. A model compatible with both period is presently being elaborated.

Velocities for the points added to the 1995 network

13 new points have been added to the 1995 network both to the east and to the west to the first study area. All eastern points shows very similar ESE azimuth of displacements. A difference of 1 cm/year has been observed between the points respectively inside and outside the Krafla fissure swarm. This demonstrates the activity of the eastern margin of this swarm. The points added to the west of the network show similar displacements to those located on Flateyjardalur, which mean a general sinistral displacement of the SW area, relatively to a point located in the southern middle part of the network.

3.6.3.2 Task 3.2: 1992-1998 deformation of the Krafla volcano

The Krafla fissure swarm, in the North Iceland rift zone, last underwent rifting between 1975 and 1984. Activity mostly concentrated at the Krafla volcano although it occurred all along the fissure swarm. We formed interferograms of ERS-SAR scenes (Figure 40) covering the area of Krafla with time span values of up to six years (1992–1998). This long period interferograms have been revealed steady rate of deformation at Krafla volcano, N–Iceland. The deformation rate at Krafla and within the fissure swarm, has values reaching +2.1 cm/year in the ground to satellite direction, at the volcano. The area affected by deformation extends 20 km both north and south of the volcano. The best fit dislocation model consists of sills, to the north and south of the volcano, and a magma chamber, located below the volcano, all of them undergoing contraction. The contraction of the magma chamber induced a subsidence that has been constant in rate during all of the studied period (Figure 41).

3.6.4 Task 4: Effects of fluid pressure on faulting

It is well known that seismogenic faulting is normally associated with zones of fluid overpressure (Guðmundsson 1999; Guðmundsson 2000a; Guðmundsson 2000b); in absence of fluids there would be hardly any tectonic earthquakes. The origin and magnitude of the fluid overpressure are, however, uncertain. For example, for the San Andreas fault, there are two models; one assuming the fluids to be of local and shallow origin, the other assuming the fluids to be of deep origin.

In order to throw light on the potential fluid overpressure in a major fault zone, as a part of a general study on the effects of fluid pressure on the probability of fault-slip, field measurements were made of 1717 mineral-filled veins in the damage zone in deeply eroded and

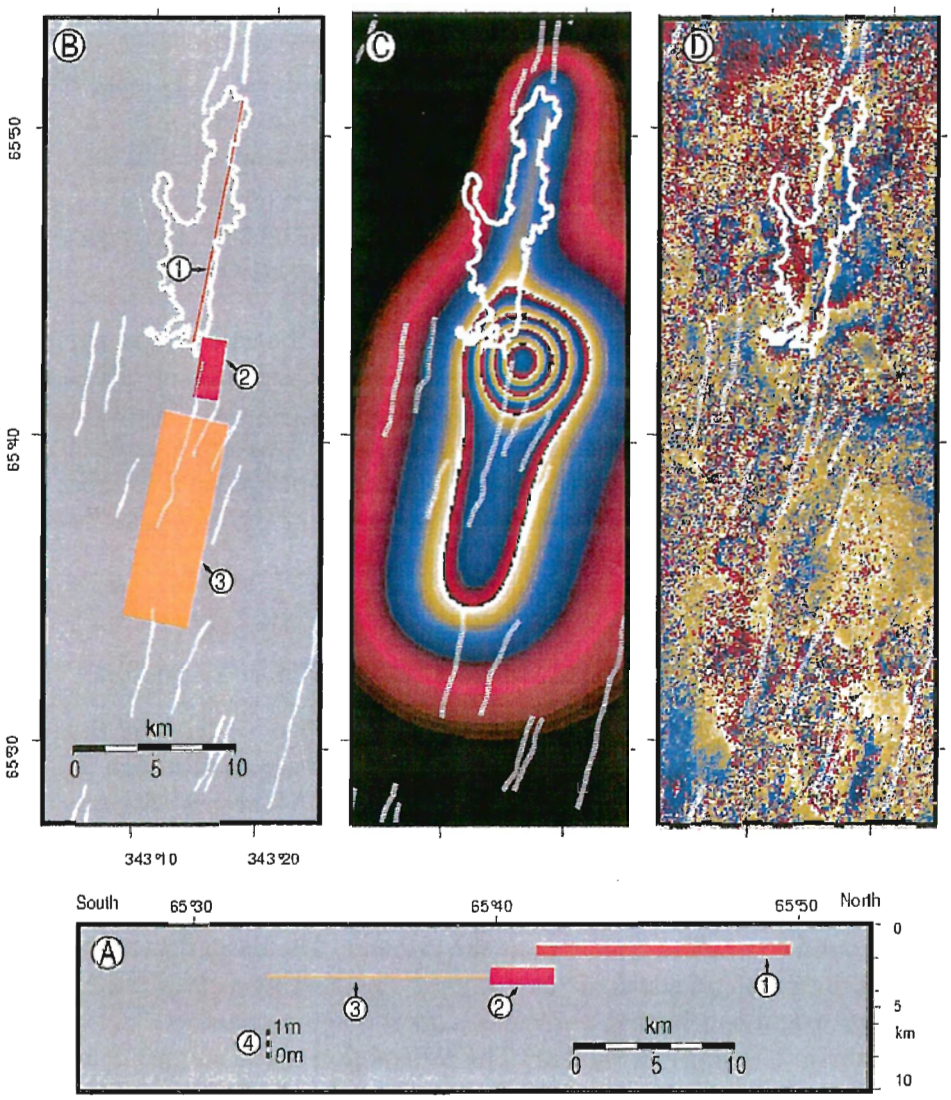

Figure 40. *Model geometry in cross section (A) and plan view (B), best fit model for the 6 year interferogram (C) and residual interferogram, i.e. model minus 6 year interferogram, (D) for the 6 year interferogram (after Henriot et al. 2000). Model elements represented in (A) and (B) are the northern sill (1), the magma chamber (2) and the southern sill (3). The model element dimensions represent their real geometries. The thickness of the lines in the cross-section (A) is proportional to the amount of contraction applied to the discontinuity in the model. The scale for the contraction in the 6 year interferogram model is given in (4).*

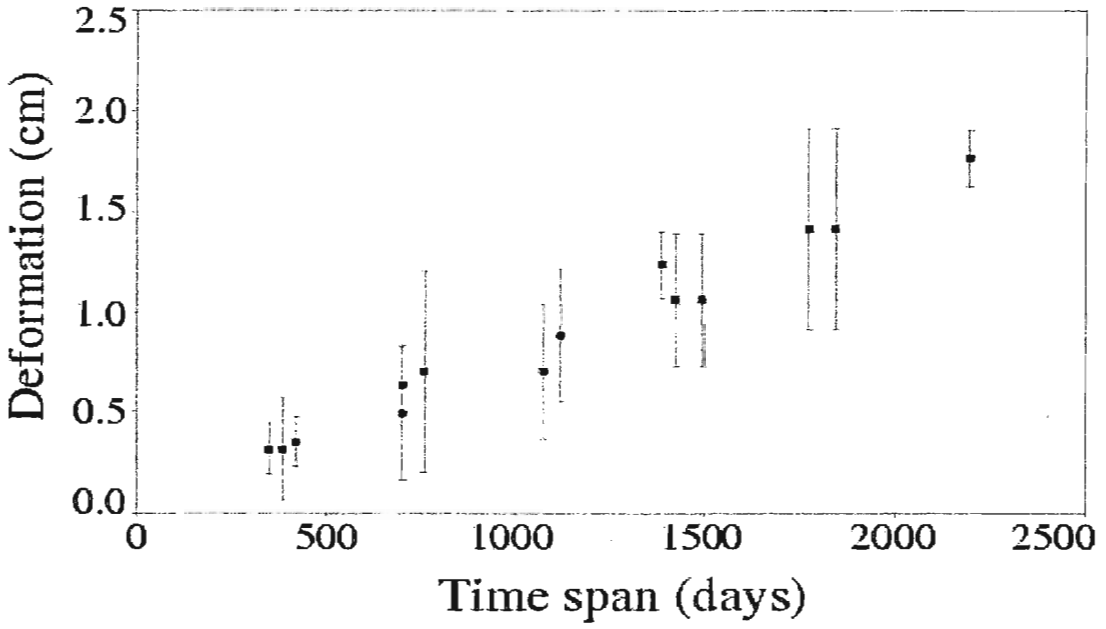

Figure 41. *Deformation at Leirhnjúkur, in the ground to satellite direction, with respect to the time span of the corresponding interferogram (after Henriot et al. 2000). The error is a function of the visual quality (Q) of the interferogram, 0 for no readability, 9 for perfect readability. It has been estimated as 1/Q of a fringe.*

well-exposed parts of the Tjörnes fracture zone, particularly on the Flateyjarskagi peninsula (Guðmundsson 1999; Guðmundsson 2000c; Guðmundsson et al. 2000). Most veins are composed of quartz, chalcedony and zeolites, strike roughly parallel or perpendicular to the fault zone, and are members of dense palaeo–fluid transporting networks. A common vein frequency in these networks is 10 veins per meter. Cross-cutting relationships indicate that 79% of the veins are extension (mode I) cracks; 21% are shear cracks. The apertures of most veins, measured as mineral-fill thicknesses, are from 0.1 mm to 85 mm, and the aperture frequency distribution is a power law. The outcrop trace lengths of 384 veins (of the 1717) could be measured accurately. These 384 veins are mostly small and range in length from 2.5 cm to 400 cm, in aperture from 0.01 cm to 0.9 cm, and have an average length/aperture ratio of about 400. Using simple fracture mechanics models, and the appropriate elastic properties of the host rock, this length/aperture ratio indicates and average fluid overpressure during vein formation of 20 MPa. If this fluid pressure acted on a potential fault plane, the effective normal stress across that plane would be zero or negative and, therefore, reduce the driving shear stress needed to trigger slip on that plane to only 4-6 MPa. This compares well with the most common stress drops, estimated at 3-6 MPa, for earthquakes worldwide.

Another potentially strong effect of fluid pressure on the probability of fault-slip in seismic zones is dyke emplacement in the nearby volcanic zones (Guðmundsson 2000d). In this model, dyke injection (and normal faulting) in the volcanic systems can lock or unlock the Húsavík-Flatey fault and the central parts of the South Iceland seismic zone. Dyke injection in the parts of the North and East volcanic zones between the Húsavík-Flatey fault and the South Iceland seismic zone tends to open (unlock) these zones and trigger seismogenic faulting. By contrast, dyke injection south of the South Iceland seismic zone and north of the Húsavík-Flatey fault tends to lock these faults and suppress their seismogenic faulting. Similarly, dyke injection in the north part of the West volcanic zone tends to lock, but dyke injection in its south part (including the Reykjanes peninsula) to unlock, the South Iceland seismic zone. Locking by dyke injection, however, is always temporary because plate pull gradually relaxes the compressive stresses generated by the dykes.

In terms of this model, the largest historical eruption in Iceland, Laki 1783, may have triggered the largest known earthquake sequence in S-Iceland, that of 1784. Conversely, the Húsavík-Flatey fault has recently experienced locking by dyke injection. There was considerable seismicity associated with the Húsavík-Flatey fault until early 1976. Then dyke injection and normal faulting in the northernmost part of the Krafla volcanic systems generated horizontal compressive stresses encouraging sinistral movement on the otherwise dextral Húsavík-Flatey fault, thereby locking the fault. Renewed seismicity on the Húsavík-Flatey fault, since February 1994, indicates that the Húsavík-Flatey fault is currently being unlocked by normal plate-pull movements which gradually relax the horizontal compressive stresses generated by the 1976 dyke. The unlocking began at the westernmost part of the Húsavík-Flatey fault, at the greatest distance from the 1976 dyke.

3.6.5 Task 5: Numerical models on faults and fault populations

Part of this work has focussed on quantitative field studies and modelling of the linking up of fractures into normal faults (Acocella et al. 2000) and strike-slip faults (Belardinelli et al. 2000). Part of the work, however, has focussed on the general evolution of the seismic

zones, exploring the model of a stress-field homogenization being a necessary condition for the generation of large earthquakes (Guðmundsson and Homberg 1999). The work on the South Iceland seismic zone made in collaboration with Maria Elina Belardinelli and Maurizio Bonafede (Belardinelli et al. 2000) is described in Subproject 7.

Detailed, quantitative field and photogeological studies were made of the interaction and linkage of extension fractures and normal faults (Acocella et al. 2000), a fault type that is common in the South Iceland seismic zone and the Tjörnes fracture zone. 90 zones of interacting fracture segments in Holocene pahoehoe lava flows of the rift zone of Iceland were studied, each zone being located between a pair of extension fractures or a pair of normal faults, with lengths from tens of meters to several kilometers. Of all the zones, only 7% are underlapping, whereas 93% are overlapping and mostly with hook-shaped fracture pairs. The length/width ratios of most overlapping zones are from 2-6, with a mean value of 3.5. In the overlapping zones, most fracture pairs show moderate shear (strike-slip) components which are related to local variations in the extension (opening) directions. Vertical displacements on normal faults decrease as the overstep and length of overlapping zone increase; both, in turn, are proportional to the total lengths of the faults forming the pair. During their evolution, these zones develop from an underlapping stage, through an overlapping stage (the most common configuration) and, finally, to a linkage stage. The geometrical features of overlapping spreading centres at mid-ocean ridges show great similarities to those reported here. These similarities indicate that the architecture and evolution of overlapping zones are scale independent.

It is proposed that on entering crustal parts where the state of stress is unfavourable to any particular type of seismogenic faulting, the fault propagation becomes arrested (Guðmundsson and Homberg 1999). This model is supported by field and numerical studies on the propagation of fractures of various types (Guðmundsson 2000e). It follows that prior to the propagation of an earthquake fracture, the stress conditions in the zone along the whole potential rupture plane must be homogenized. The proposed homogenization of the stress field in a large rock volume as a precursor to large earthquakes implies that by monitoring the state of stress in a seismic zone, its large earthquakes may possibly be forecasted.

3.6.6 Task 6: Analyzing the fracture properties of Icelandic rocks in the laboratory

Our main overall objective has been to determine changes in the strength, deformability and physical properties of rocks subjected to elevated temperatures. In order to achieve this objective, we have designed and constructed an apparatus for the measurement of rock fracture and deformation properties at high temperatures and pressures, and performed a series of experiments to measure these properties.

3.6.6.1 Task 6.1: Apparatus development

We previously reported on the design and manufacture of an environmental cell for the measurement of fracture mechanics parameters under high-temperature/high-pressure conditions (PRENLAB–2 first annual report). We have now extended the range of capabilities of this apparatus so that it can perform four different types of experiment: (1) rock fracture mechan-

ics experiments, (2) confined compression experiments, (3) confined extension experiments, and (4) direct tension experiments. The extended operating conditions are: (i) confining pressure up to 70MPa, (ii) test temperatures up to 500°C with water as the confining/pore fluid, (iii) test temperatures up to 900°C with dry nitrogen as the confining/pore fluid, and (iv) sample diameters from 25 mm to 60 mm. A schematic diagram of the apparatus and its operating modes is given in Figure 42.

3.6.6.2 Task 6.2: Experimental results and discussion

Starting material

The measurements reported here were made on samples of a macroscopically isotropic basalt collected from a roadstone quarry located southeast of Reykjavík, Iceland. Microscopically it has an aphyric texture, comprising euhedral laths of unaltered plagioclase averaging 0.2 mm in length, and anhedral augite microphenocrysts averaging 0.1 mm in diameter, with accessory anhedral oxides up to 0.1 mm in diameter. No free quartz was visible under either optical or SEM microscopy.

Summary of previously reported results

We previously reported results of measurements made at room temperature on samples that have previously been heat-treated to temperatures up to a maximum of 900°C in order to induce thermal crack damage. In a shallow crustal environment where the geothermal gradient is anomalously high, such as in Iceland, thermal stresses may well be large enough to induce such fracturing. Furthermore, where enough fractures propagate and link up to provide an interconnected network, they can provide permeable pathways for fluid flow which can in turn lead to embrittlement and weakening of the rock. The thermal cracking was monitored by measuring the compressional (P) and shear (S) wave velocities through the samples both prior to and following heat-treatment. Both P-wave and S-wave velocities remained essentially constant up to 400°C, with values of about 5.3 km/s and 3.0 km/s respectively. For higher temperatures the velocities decrease rapidly, so that by 800° they decreased to about 3.4 km/s and 2.2 km/s repectively.

We presented results from a series of fracture toughness measurements on heat-treated specimens of Icelandic basalt using the ISRM recommended methodology. Fracture toughness at ambient temperature was 2.71 MPa/m^2, and this remained essentially constant up to 400°C. There was then a very rapid decrease in fracture resistance between 400°C and 600°C, with relatively little change between 600°C and the highest heat-treatment temperature of 900°C. This pattern of behaviour was considered to be entirely consistent with the wave velocity data.

Finally, we presented the results of permeability measurements on heat-treated cores of basalt. The mean permeability of the basalt prior to heat-treatment was 9.4 nanodarcy (9.4 x $10^{-21}m^2$). Similar to the previous results, the permeability remained essentially constant after heat treatment to temperatures up to 300°C, and showed only a slight increase after treatment to 400°C. At higher temperatures, however, the normalized permeability changed dramatically, increasing by an order of magnitude at 700°C and by a factor of 40 by 800°C. We concluded that such a large increase in permeability was unlikely to result merely from the increase in the number or size of thermally-induced cracks, but from crack linkage processes

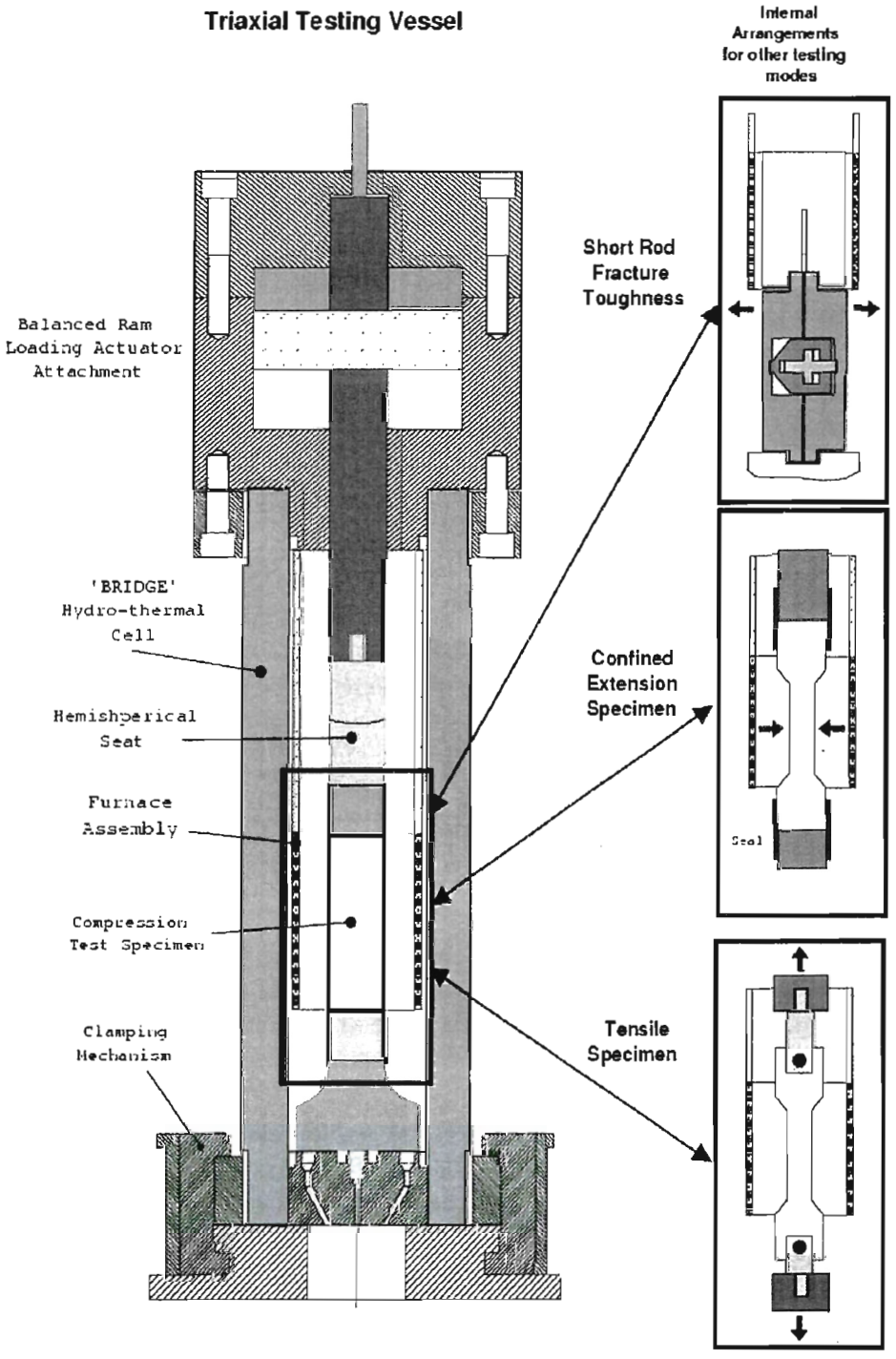

Figure 42. *Schematic diagram of the apparatus and its operating modes.*

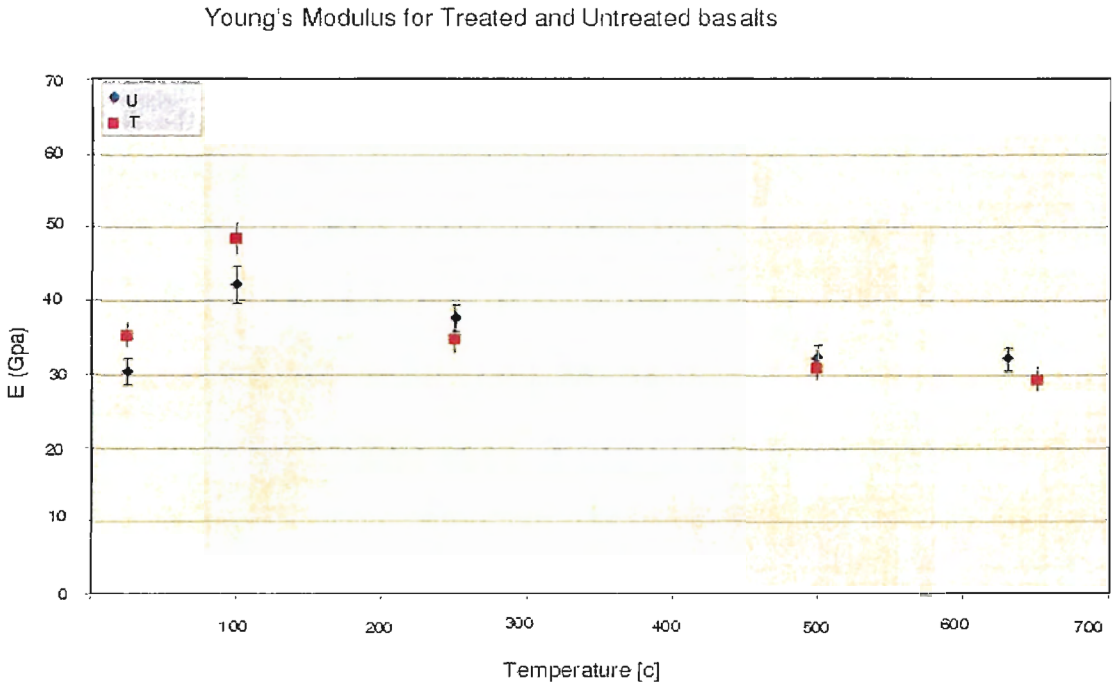

Figure 43. *Results of measurements of Young's modulus of elasticity for both PHT and NHT specimens up to 650° C.*

above some percolation threshold to form extensive sample-spanning permeable pathways for fluid flow.

New experimental results

In our most recent programme, we have performed suites of experiments on both pre-heat treated (PHT) and non-heat-treated (NHT) specimens of basalt. The reason for this is that when a measurement is made at elevated temperature, there are two potential effects on the measurement, which act simultaneously. First, the high temperature can lead to thermal cracking and hence in a change to the microstructure of the material being tested. Second, the temperature can influence the actual deformation mechanism. By performing these two suites of experiments, we hope to be able to discriminate betwen these two effects.

Figure 43 shows the results of measurements of Young's modulus of elasticity for both PHT and NHT specimens up to 650°C (all PHT specimens were pre-heated to 750°C). The two datasets show very similar trends and values, suggesting that the pre–heat treatment has relatively little effect on this parameter. As the temperature is raised from room temperature to 100°C, there is a significant increase in the modulus. This may appear counterintuitive, but is consistent with previously reported data on deformation properties of brittle rocks over this temperature interval (e.g. Meredith and Atkinson 1985). It is considered to be due to thermal expansion leading to microcrack closure and hence higher stiffness and crack resistance. At all higher temperatures, the modulus decreases monotonically with increasing

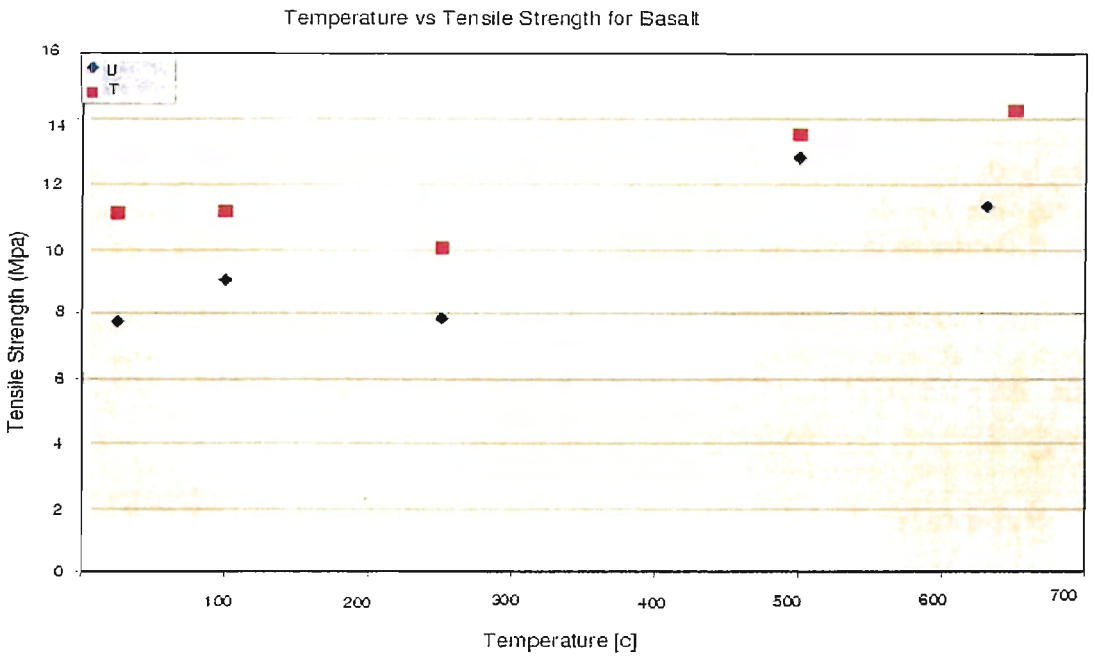

Figure 44. *Results of measurements of tensile strength up to* $650°C$ *for both PHT and NHT specimens.*

temperature.

Figure 44 shows the results of measurements of tensile strength up to 650°C, again for both PHT and NHT specimens. Here, the strength values for both datasets at first decreases for temperatures up to 250°C, and then actually increases for temperatures up to 650°C. Furthermore, tensile strength values for the PHT specimens are consistently higher than for the NHT specimens. The reasons for these variations are not fully understood at present, but we consider that it is likely to be due to local microplasticity at crack tips. Microplasticity is generally enhanced by high stresses, and hence is more likely to occur at crack tips than elsewhere in the rock because of the high stress concentrations at these sites. Microplasticity acts to blunt crack tips and therefore make crack propagation more difficult. If this is the case, then we could expect specimens to be less susceptible to tensile crack growth at higher temperatures. Furthermore, we might also expect the PHT specimens to exhibit higher strength because they have previously been subjected to a higher temperature (750°C) and hence potentially to more microplasticity. This explanation is consistent with the observation of little difference in modulus between PHT and NHT specimens. The modulus is controlled by the mere presence of cracks and not by their growth, and hence crack tip blunting is not likely to affect modulus values.

These are very new results, and we will be investigating this possible explanation microstructurally with a combination of scanning electron and optical microscopy.

3.6.7 Conclusions

Due to the high temperature gradient and low lithostatic stress, thermal cracking may be an important process in controlling fracture in Icelandic crust. In the absence of confining stress, such cracking starts in the temperature range 300° to 400°C in fresh basalt. Thermal cracking leads to increased fluid permeability above about 300°C, with the permeability increasing very non-linearly with temperature. Thermal cracking also appears to lead to significant decreases in mechanical strength and resistance to crack propagation of PHT specimens when tested after cooling at room temperature.

However, a somewhat different picture emerges when both PHT and NHT specimens are actually tested at elevated temperatures. There appears to be an increase in tensile strength with increasing temperature. We attribute this to enhanced microplasticity at highly stressed crack tips effectively blunting cracks.

3.6.8 References

Acocella, V., Á. Guðmundsson & R. Funiciello 2000. Interaction and linkage of extension fractures and normal faults: examples from the rift zone of Iceland. *Journal of Structural Geology* 22, 1233–1246.

Angelier, J. 1998. A new direct inversion of earthquake focal mechanisms to reconstruct the stress tensor. In: *Annales Geophysicae.* Abstracts from the XXIII EGS General Assembly, Nice, France, April 20–24, 1998.

Angelier, J., F. Bergerat, H.-T. Chu, Á. Guðmundsson, J.-C. Hu, J.-C. Lee, C. Homberg, H. Kao & S.Th. Rögnvaldsson 2000a. Active faulting, earthquakes and deformation–stress fields: from mid–Atlantic ridge spreading (Iceland) to collision in Southeast Asia (Taiwan). In: B. Þorkelsson & M. Yeroyanni (editors), *Destructive earthquakes: Understanding crustal processes leading to destructive earthquakes.* Proceedings of the second EU–Japan workshop on seismic risk, Reykjavík, Iceland, June 23–27, 1999. European Commission, 48–61.

Angelier, J., F. Bergerat & C. Homberg 2000b. Variable coupling explains complex tectonic regimes near oceanic transform fault: Flateyjarskagi, Iceland. *Terra Nova*, in press.

Belardinelli, M.E., M. Bonafede & Á. Guðmundsson 2000. Secondary earthquake fractures generated by a strike–slip fault in the South Iceland seismic zone. *J. Geophys. Res.* 105, 13613–13629.

Bergerat, F., Á. Guðmundsson, J. Angelier & S.Th. Rögnvaldsson 1998. Seismotectonics of the central part of the South Iceland seismic zone. *Tectonophysics* 298, 319–335.

Bergerat, F., J. Angelier & S. Verrier 1999. Tectonic stress regimes, rift extension and transform motion: the South Iceland seismic zone. *Geodin. Acta* 12(5), 303–319.

Bergerat, F. & J. Angelier 2000. The South Iceland seismic zone: tectonic and seismotectonic analyses revealing the evolution from rifting to transform motion. *Journ. Geodynamics* 29(3–5), 211–231.

Bergerat, F., J. Angelier & C. Homberg 2000. Tectonic analysis of the Húsavík–Flatey fault (northern Iceland) and mechanisms of an oceanic transform zone, the Tjörnes fracture

zone. *Tectonics*, in press.

Bergerat, F., J. Angelier & Á. Guðmundsson. The Leirubakki earthquake rupture: a large fault of the South Iceland seismic zone. In preparation.

DeMets, C., R.G. Gordon, D.F. Argus & S. Stein 1990. Current plate motions. *Geophys. J. Int.* 101, 425–478.

Garcia, S. 1999. *De sismotectonique d'un segment transformant en domaine océanique: la Zone de Fracture de Tjörnes, Islande.* Unpublished master thesis. Universite Pierre & Marie Curie, Paris.

Garcia, S., J. Angelier, F. Bergerat & C. Homberg 2000. Etude sismotectonique d'un segment transformant: la Zone de Fracture de Tjörnes, Islande. 18^{me} RST, Paris, France, April 2000.

Garcia, S., J. Angelier, F. Bergerat & C. Homberg. Tectonic behaviour of an oceanic transform fault zone from fault–slip data and focal mechanisms of earthquakes analyses: the Tjörnes fracture zone, Iceland. In preparation.

Guðmundsson, Á. 1999. Fluid pressure and stress drop in fault zones. *Geophys. Res. Lett.* 25, 115–118.

Guðmundsson, Á. 2000a. Active fault zones and groundwater flow. *Geophys. Res. Lett.*, in press.

Guðmundsson, Á. 2000b. Fluid overpressure and flow in fault zones: field measurements and models. *Tectonophysics*, in press.

Guðmundsson, Á. 2000c. Fracture dimensions, displacements and fluid transport. *Journal of Structural Geology* 22, 1221–1231.

Guðmundsson, Á. 2000d. Dynamics of volcanic systems in Iceland: Example of tectonism and volcanism at juxtaposed hot spot and mid–ocean ridge system. *Annual Review of Earth and Planetary Sciences* 28, 107–140.

Guðmundsson, Á. 2000e. Displacement and stresses of arrested hydrofractures. *Tectonophysics*, in preparation.

Guðmundsson, Á. & C. Homberg 1999. Evolution of stress fields and faulting in seismic zones. *Pure and Applied Geophysics* 154, 257–280.

Guðmundsson, Á., S.S. Berg, K.B. Lyslo & E. Skurtveit 2000. Fracture networks and fluid transport in active fault zones. *Journal of Structural Geology*, in press.

Henriot, O., T. Villemin & F. Jouanne 2000. Long period interferograms reveal 1992–1998 steady rate of deformation at Krafla volcano (North Iceland). *Geophys. Res. Lett.*, in press.

Jouanne, F., T. Villemin, V. Ferber, C. Maveyraud, J. Ammann, O. Henriot & J.-L. Got 1999. Seismic risk at the rift–transform junction in North Iceland. *Geophys. Res. Lett.* 26(24), 3689.

Meredith, P.G. & B.K. Atkinson 1985. Fracture toughness and subcritical crack growth during high-temperature deformation of Westerly granite and Black gabbro. *Phys. Earth & Planet. Ints.* 39, 33–51.

3.7 Subproject 7: Theoretical analysis of faulting and earthquake processes

Contractor:

Maurizio Bonafede
Department of Physics
University of Bologna
Viale Berti-Pichat 8
40127 Bologna
Italy
Tel: +39-051-630-5001/5017
Fax: +39-051-630-5058
E-mail: bonafede@ibogfs.df.unibo.it

Associated contractor:

Frank Roth
Section: Earthquakes and Volcanism
Division: Solid Earth Physics and Disaster Research
GeoForschungsZentrum Potsdam
Telegrafenberg
D–14473 Potsdam
Germany
Tel: +49–331–288–1210
Fax: +49–331–288–1203
E–mail: roth@gfz-potsdam.de

3.7.1 Subpart 7A: Ridge-fault interaction in Iceland employing crack models in heterogeneous media

3.7.1.1 Task 1: Magma upwelling as driving mechanism for the stress build-up in the elastic lithosphere

Tensile cracks are often employed to model magma migration in rift zones or within volcanic edifices, through lateral or feeding dykes. In a crack model, the overpressure of magma Δp with respect to the horizontal stress in the host rock, is assumed to be responsible for dyke opening and propagation. Most crack models of dykes have been developed so far in homogeneous media. The most simple heterogeneous medium has been considered, made up of two welded half-spaces, characterized by different elastic parameters. The analytical solutions available for the elementary dislocation problem in such a medium (Bonafede and Rivalta 1999) have been employed to set up an integral equation with generalized Cauchy kernel, representing the condition for static equilibrium. The unknown in such a problem is the dislocation density distribution, whose singular behaviour has been studied near the crack tips and near the intersection with the interface between the two media. When the crack is in half-space 1 but touches the interface, the order of singularity of the dislocation density distribution at the interface changes from the classical behaviour $\sim r^{-1/2}$ to $\sim r^{-b}$

(where r is the distance from the interface) and the order of infinity b is obtained solving a trascendental compatibility equation; some results are shown in Table 6.

$m = \mu_1/\mu_2$	∞	10	5	2	1	0.5	0.2	10^{-1}
b	0.255	0.312	0.352	0.430	0.500	0.576	0.678	0.752

Table 6. *Crack touching the interface.*

A crack crossing the interface $z = 0$ between the two half-spaces with rigidities μ_1 (in $z > 0$) and μ_2 (in $z < 0$) has been considered in detail. A system of generalized Cauchy equations is obtained, which is solved for the dislocation density distributions of each crack section. An internal singularity in the dislocation density distribution appears at the intersection between the crack plane and the interface. This singularity is again of the type r^{-b} on both sides of the interface and its order b depends only upon the elastic parameters of the media in welded contact and the ratio between the crack lengths in the two half-spaces (see Table 7). More specifically, the order of singularity b does not depend on the stress drop.

$m = \mu_2/\mu_1$	1	0.5	0.1	0.05	0.001
b	0	0.030	0.170	0.208	0.245

Table 7. *Crack crossing the interface.*

The horizontal stress component induced by crack opening is plotted in Figure 45, assuming 5 MPa overpressure within the crack. From a comparison with solutions pertinent to a homogeneous medium, it appears that layering can be responsible of stress changes, localized along the the interface, which may be considerably higher than the overpressure within the dyke. These results provide useful hints for the interpretation of induced seismicity in rift zones and in volcanic areas. The detailed results of this research are reported in Bonafede and Rivalta (1999).

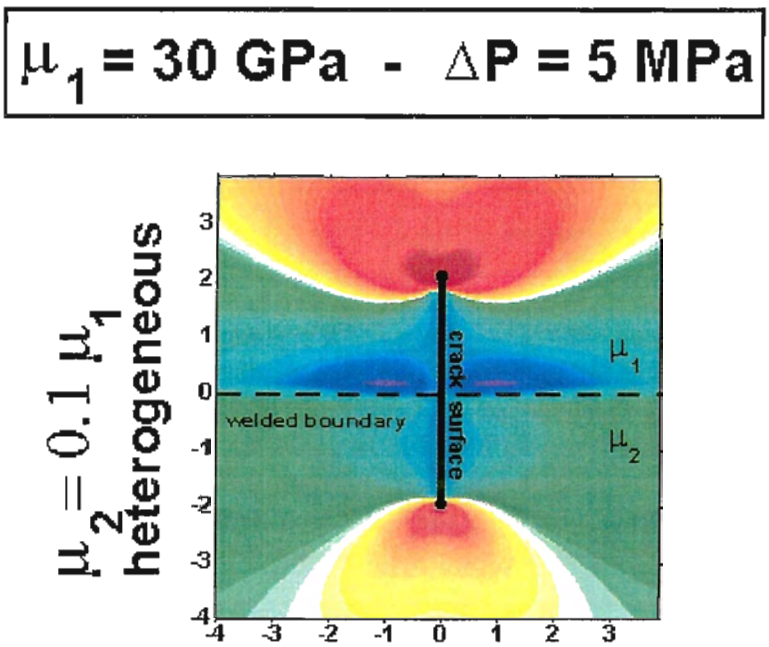

Figure 45. *Horizontal normal stress induced by rifting in proximity of a structural discontinuity (horizontal dashed line). The harder side of the interface is affected by strong compressive stresses. Other stress components (not shown) are also affected by layering, but to a lesser extent. Rifting is modelled as a tensile crack with overpressure* Δp.

3.7.1.2 Task 2: Space-time evolution of the stress field following earthquakes and episodes of magma upwelling

Mechanical effects left by an earthquake on its fault plane, in the post-seismic phase, were investigated employing the "displacement discontinuity method" and imposing the release of a constant, uni-directional shear traction. Due to unsymmetric interaction between the fault plane and the free surface, significant normal stress components are left over the shallow portion of the fault surface after the earthquake (Figure 46): these are compressive for normal faults, tensile for thrust faults, and are typically comparable to the stress drop. In Figure 46 the s-axis is along the strike of the fault, the d-axis is along the dip (positive upwards). Several observations can be explained from the present model: low-dip thrust faults and high-dip normal faults are found to be favoured, according to the Coulomb failure criterion, in repetitive earthquake cycles; the shape of dip-slip faults near the surface is predicted to be upward-concave; the shallow aftershock activity commonly observed in the hanging block of a thrust event is easily explained. The detailed results of this research are reported in Bonafede and Neri (2000).

The study of the effects induced by structural inhomogeneities on the stress and displacement fields around strike-slip faults has been recently completed. An elastic medium is considered, made up of an upper layer bounded by a free surface and welded to a lower

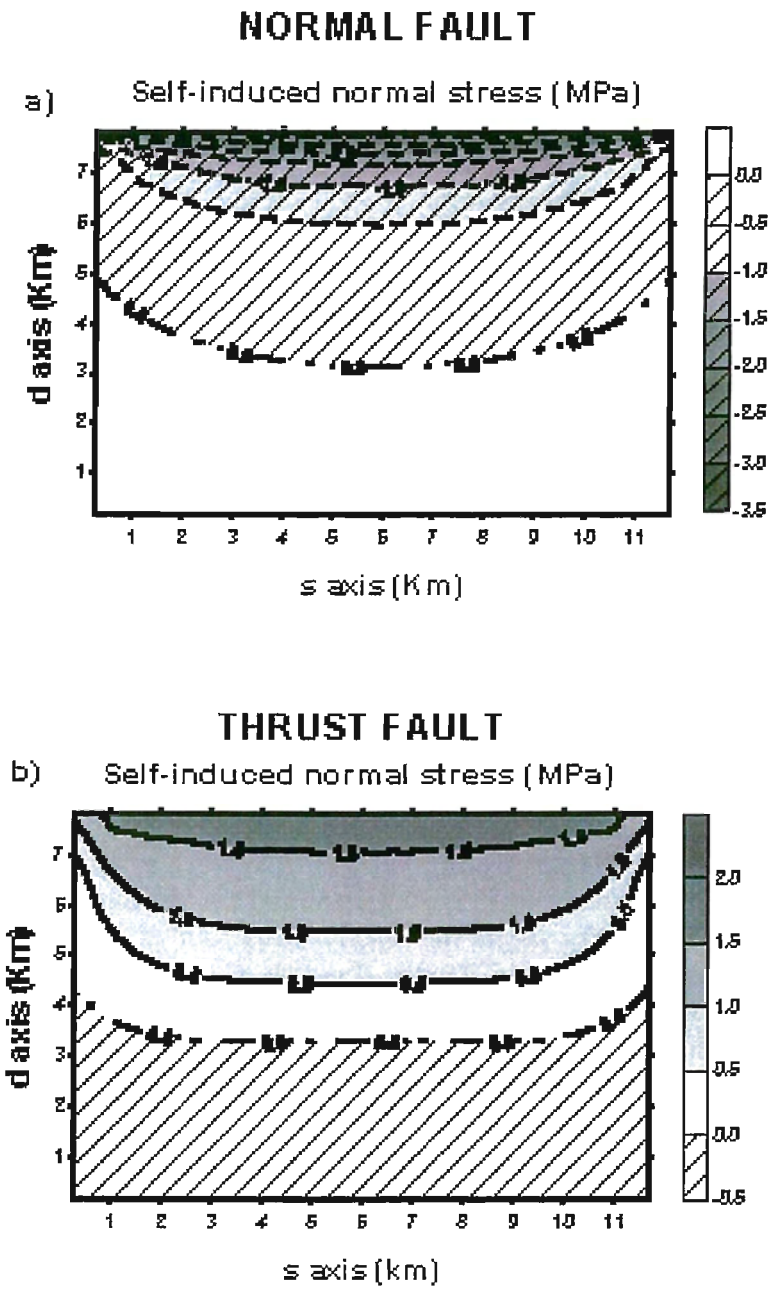

Figure 46. *Normal stress induced by uniform stress drop over a high-dip normal fault and a low-dip thrust fault. The near-surface part of a normal fault is affected by compressive stress, while tensile stresses act there for a thrust fault.*

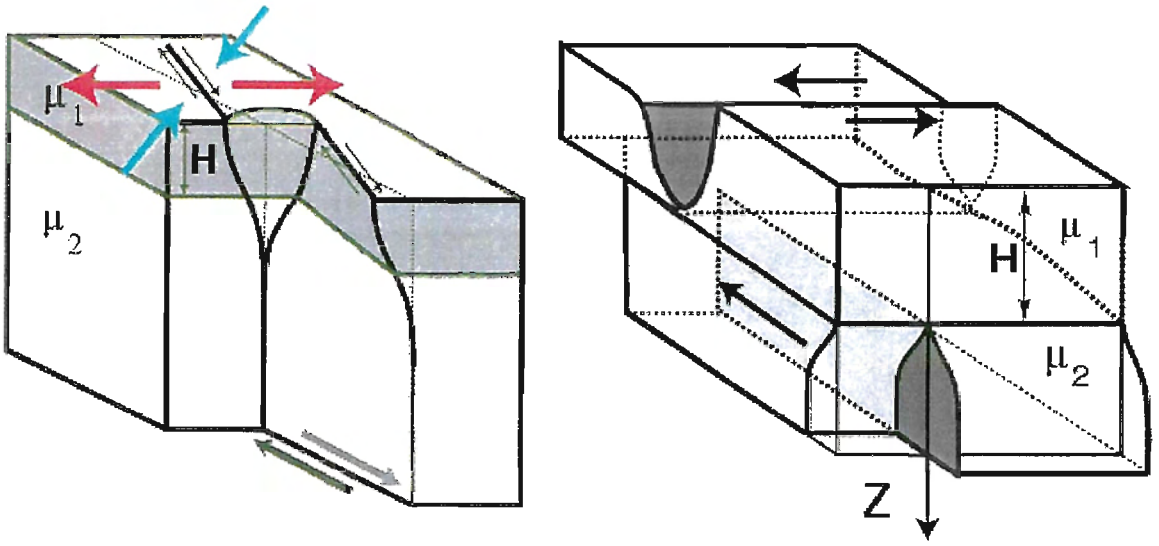

Figure 47. *According to the stress-drop-discontinuity condition, en-echelon fault segments, rotated in the direction of the tensile principal stress axis, must accompany brittle faulting at depth (left). On the contrary, anelastic deformation at depth is preferably accompanied by antithetic faulting in brittle surface layers (right).*

half-space characterized by different elastic parameters. Shear cracks with assigned stress drop are employed as mathematical models of strike-slip faults which are considered as vertical and planar. If the crack is entirely embedded within the lower medium (case A), a Cauchy-kernel integral equation is obtained, which is solved by employing an expansion of the dislocation density in Chebyshev polynomials. If the crack is within the lower medium but it terminates at the interface (case B), a generalized Cauchy singularity appears in the integral kernel. This singularity affects the singular behaviour of the dislocation density at the crack tip touching the interface. Finally, the case of a crack crossing the interface is considered (case C). The crack is split into two interacting sections, each placed in a homogeneous medium and both open at the interface. Two coupled generalized Cauchy equations are obtained and solved for the dislocation density distribution of each crack section. An asymptotic study near the intersection between the crack and the interface shows that the dislocation densities for each crack section are bounded at the interface, where a jump discontinuity appears. As a corollary, the stress drop must be discontinuous at the interface, with a jump proportional to the rigidity contrast between the adjoining media. This finding is shown to have important implications for the development of geometrical complexities within transform fault zones: planar strike-slip faults cutting across layer discontinuities with arbitrary stress drop values are shown to be admissible only if the interface between different layers becomes unwelded during the earthquake. Planar strike-slip faulting may also take place in mature transform zones, where a repetitive earthquake cycle has already developed. Otherwise, the fault cannot be planar: we infer that strike-slip faulting at depth is plausibly accompanied by en-echelon surface breaks (Figure 47) in a shallow sedimentary layer (where the stress drop is lower than prescribed by the discontinuity condition), while

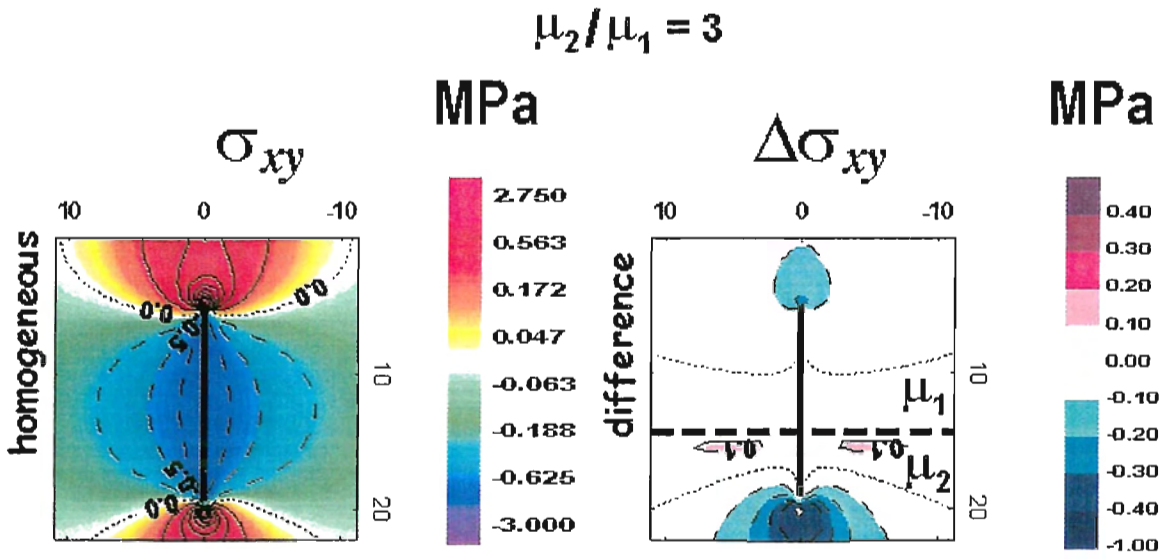

Figure 48. *Stress concentration induced by strike-slip faulting across layer interfaces. The panel on the right shows the incremental stress present in the layered model compared to the homogeneous half-space model (on the right). Accurate re-location of aftershocks in several areas of the world actually show a sharp concentration of events along bedding planes.*

ductile deformation (or steady sliding) at depth is preferably accommodated by antithetic faulting in the upper brittle layer (endowed with lower rigidity but higher stress), giving rise to bookshelf faulting (Figure 47). Results of this research were presented at several international conferences. A paper has been submitted for publication (Bonafede et al. 2000). The South Iceland seismic zone provides several instances of application of both types of complexities.

3.7.1.3 Task 3: Secondary earthquake fractures generated by a strike-slip fault in the South Iceland seismic zone

Most earthquakes in the South Iceland seismic zone occur on N-S trending dextral strike-slip faults. The resulting rupture zones display complex en-echelon patterns of secondary structures including NNE-trending arrays of (mostly) NE-trending open fractures (O.F.) and hillocks.

Three spatial scales characterize the surface faulting pattern: the length of the main fault (M.F. 104 m), the arrays here interpreted as surface evidence of secondary faults (102 m) and the individual O.F. (10 m). In order to improve our understanding of the genetic relationship between the O.F. and the M.F. we computed the stress field induced by slip on a buried M.F. using a dislocation model in a layered half-space: the fault surface is assumed to be embedded in the basement rock, topped by a softer near-surface layer. The O.F. were preliminarily considered as pure mode-I cracks opening in the near surface layer in the direction of the maximum (tensile) principal stress. Alternatively, secondary fractures were interpreted, as

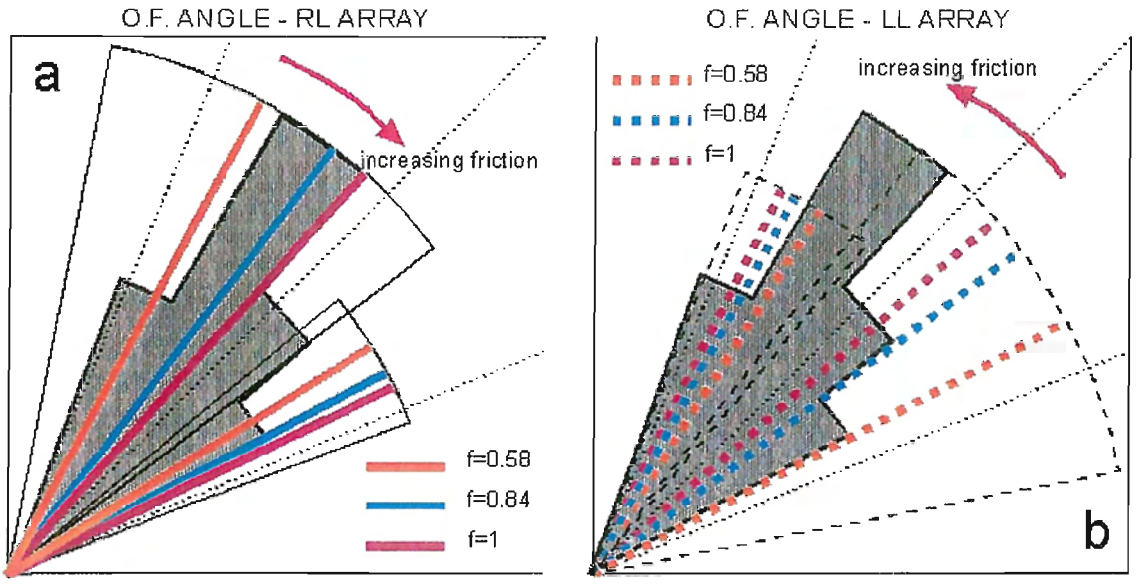

Figure 49. *Open fractures (O.F.) angles predicted from the combined effect of the main fault rupture and secondary fault (S.F.) rupture along the strike direction. The observed range and relative frequency of O.F. angles is shown shaded (from Bjarnason et al. 1993). If the friction coefficient f varies between 0.2 and 1.5 predicted O.F. angles vary within the circular sectors contoured in black. Solid lines in panel (a) represent the angle expected for O.F. belonging to dextral arrays. Dashed lines in panel (b) represents the angle expected for O.F. belonging to sinistral arrays. In both panels, longer lines indicate the predicted mixed-mode O.F. trends, while shorter lines indicate pure tensile trends. Mixed-mode O.F. are assumed to share the same style of faulting (sinistral or dextral) with the array to which they belong. The dotted lines indicate 22.5°, 45° and 67.5° directions (for reference). Coloured lines refer to particular friction values (indicated). Friction increases as indicated by the red arrow.*

mixed-mode cracks, slipping at depth as shear cracks and opening near the surface due to low confining pressure. The Coulomb failure function after the earthquake (obtained summing the M.F. stress change and the lithostatic stress) suggests that secondary faulting (S.F.) can be expected to occur in response to the main rupture below the upper soft layer down to few hundreds of meter depth. The total stress change induced by the M.F. and the S.F. (of smaller scale) is shown to yield quantitative explanations of the complex geometry observed in the fault region in terms of simple frictional laws and friction coefficients very close to those measured in the lab (Figure 48).

3.7.1.4 Meetings and conferences

XXIII EGS General Assembly, Nice, France, April 20-24, 1998.
LXXXIV Congresso Nazionale Societa Italiana di Fisica, Salerno, Italy, September 28 - October 2, 1998.
The third PRENLAB-2 workshop, Strasbourg, France, March 31, 1999.
XXIV EGS General Assembly, The Hague, The Netherlands, April 19-23, 1999.
XXV EGS General Assembly, Nice, France, April 25-29, 2000.
The fifth PRENLAB-2 workshop, Nice, France, April 27, 2000.
International School of Solid Earth Geophysics, Erice, Italy, June 17-23, 2000. 17^{th} course: Fault interaction by stress transfer: new horizons for understanding earthquake occurrence.

3.7.2 Subpart 7B: Modelling of the earthquake related space–time behaviour of the stress field in the fault system of southern Iceland

In the framework of the PRENLAB-2 project a model study which started during the PRENLAB project was continued to obtain forward models of the stress field and stress changes in the South Iceland seismic zone (SISZ).

This proposal has the target to model the space–time development of the stress field using data on strain and stress changes from the other experiments and from databases.

Two models were prepared during PRENLAB-1 and PRENLAB-2:

- a model of the South Iceland seismic zone and the adjacent part of the eastern volcanic zone.
- a scheme comprising the main ridge parts on Iceland and the North Atlantic ridge to the North and to the South of the island, including both the faults and the load due to Katla and Hekla volcanoes.

It was modelled:

- the changes in crustal strain and stress due to earthquakes and aseismic movement in the fault system of the South Iceland seismic zone.
- the interaction of faults.
- the mutual influence between volcanic and earthquake activity, e.g. magmatic upwelling and shearing at fault zones.

3.7.2.1 The model for the earthquake sequence at the SISZ

During PRENLAB-2, this model was further improved. The main features of this model are given again to ease comparison with the new results.

The method

The forward modelling of stress fields is done by applying static dislocation theory to geodetic data and data obtained through the seismic moments from seismograms. It allows to calculate displacements, strain and stresses due to double-couple and extensional sources in layered elastic and inelastic earth structures. Besides the change in displacement during the event, the changes caused by the movement of plates are included (for further details see e.g. Roth 1989).

Usually, for earthquake hazard estimation, the location, the magnitude and the statistically estimated recurrence period of former events is used. To improve this, here the rupture length and width as well as the tectonic setting and the crustal deformation rates are considered while calculating the space time development of the stress field.

The targets

In general, with these models, Subpart 7B aims:

- to achieve a better understanding of the distribution of seismicity in space and time, its clustering and migration in Iceland.

- to provide models for the joint interpretation of the data gathered in the whole research programme, of which this is one part.
- to compare models of stress fields at SISZ to those for stress fields in other regions, e.g. the North Anatolian fault zone.
- to make a contribution to the intermediate-term earthquake prediction in this populated and economically important region of Iceland.

The tectonic setting
The SISZ is situated between two sections of the mid-Atlantic ridge, the Reykjanes ridge (RR) and the eastern volcanic zone (EVZ). Even though the angle between the SISZ and the neighbouring ridges is far from 90°, it is considered as a transform fault. Following the transform fault hypothesis, left-lateral shear stress is expected along the E-W striking zone. This is equivalent to right-lateral shear stress on N-S oriented rupture planes. In fact, earthquakes seem to occur on N-S trending en-echelon faults (cf. Einarsson et al. 1981; Hackman et al. 1990), They are located side by side between the Hengill-Ölfus triple junction, where the RR meets the low activity western volcanic zone (WVZ) and Hekla volcano, in the EVZ (cf. Einarsson et al. 1981) (Figure 50). As we further know from Subprojects 4 and 5, the orientation of the larger horizontal principal stress is NE–SW, i.e. fits to an active N-S or E-W trending fault, which is (at least for the period of those investigations) not a weak fault like the San Andreas fault (cf. Zoback et al. 1987). Moreover, the stress orientation seems to have been constant since Pliocene time.

In detail, the questions to be solved are:

- Do these events, placed on parallel faults, release all the energy stored in the 3-D volume of the SISZ?
- Do the earthquakes always take place in areas of high stress?
- What is the critical stress level? How large is its variability?
- Where are the highest stresses nowadays?

The area investigated extends from 18° to 24°W and from 63° to 65°N. The origin is set to 24°W, 64°N (cf. Figure 51) it includes the SISZ, ±1° north and south of 64°N, the SW edge of the EVZ, and the northeasternmost part of the RR.

The initial stress field
The initial stress field is determined as follows: A tensional stress acting N103°E (nearly parallel to the SISZ; cf. DeMets et al. 1990) is assumed, due to the opening of the mid-Atlantic ridge in the region adjacent to the transform fault. While this rifting induces mainly shear stresses in the SISZ with a small opening component, the rift segments (RR and EVZ) are modelled with tensional stress and a small shear stress contribution. Tensional stresses at both ridges are modelled as constantly being released to end up with zero values at the rifts. This induces additional stress in the transform zone. The stress magnitude, which is unknown, is set to a value that produces left-lateral shear stresses in E-W direction as

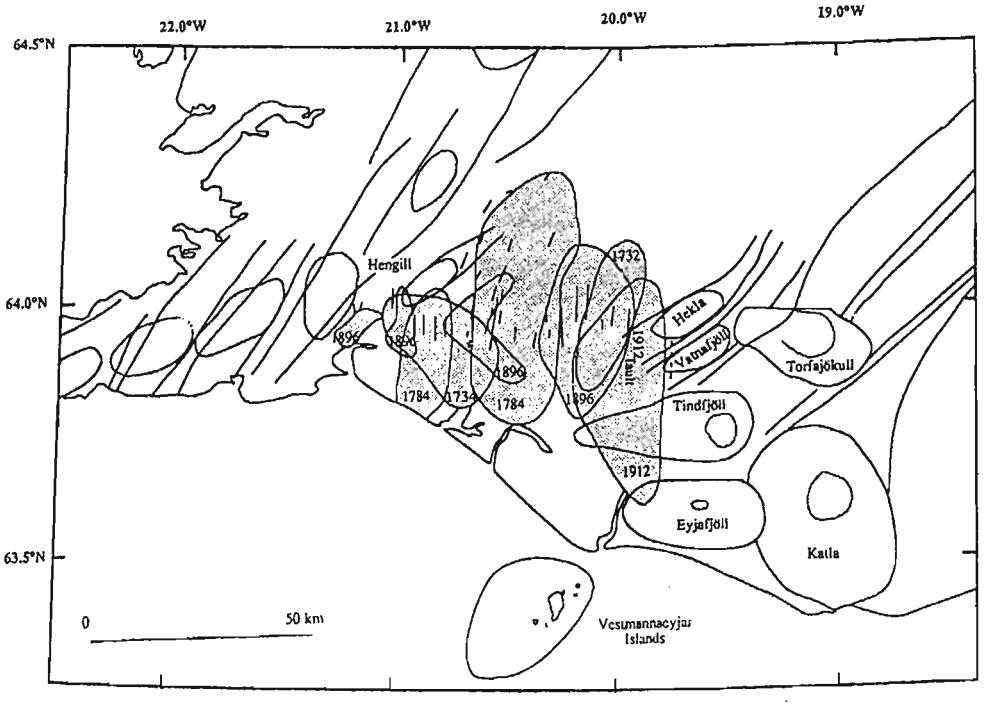

Figure 50. *The South Iceland seismic zone showing mapped surface breaks and regions in which over half of the buildings were destroyed in historic seismic events (after Einarsson et al. 1981). The north-south dashed line near Vatnafjöll indicates the estimated location of the fault on which the May 25, 1987, earthquake occurred (after Bjarnason and Einarsson 1991). The structural features and the coastline are after Einarsson and Sæmundsson (1987).*

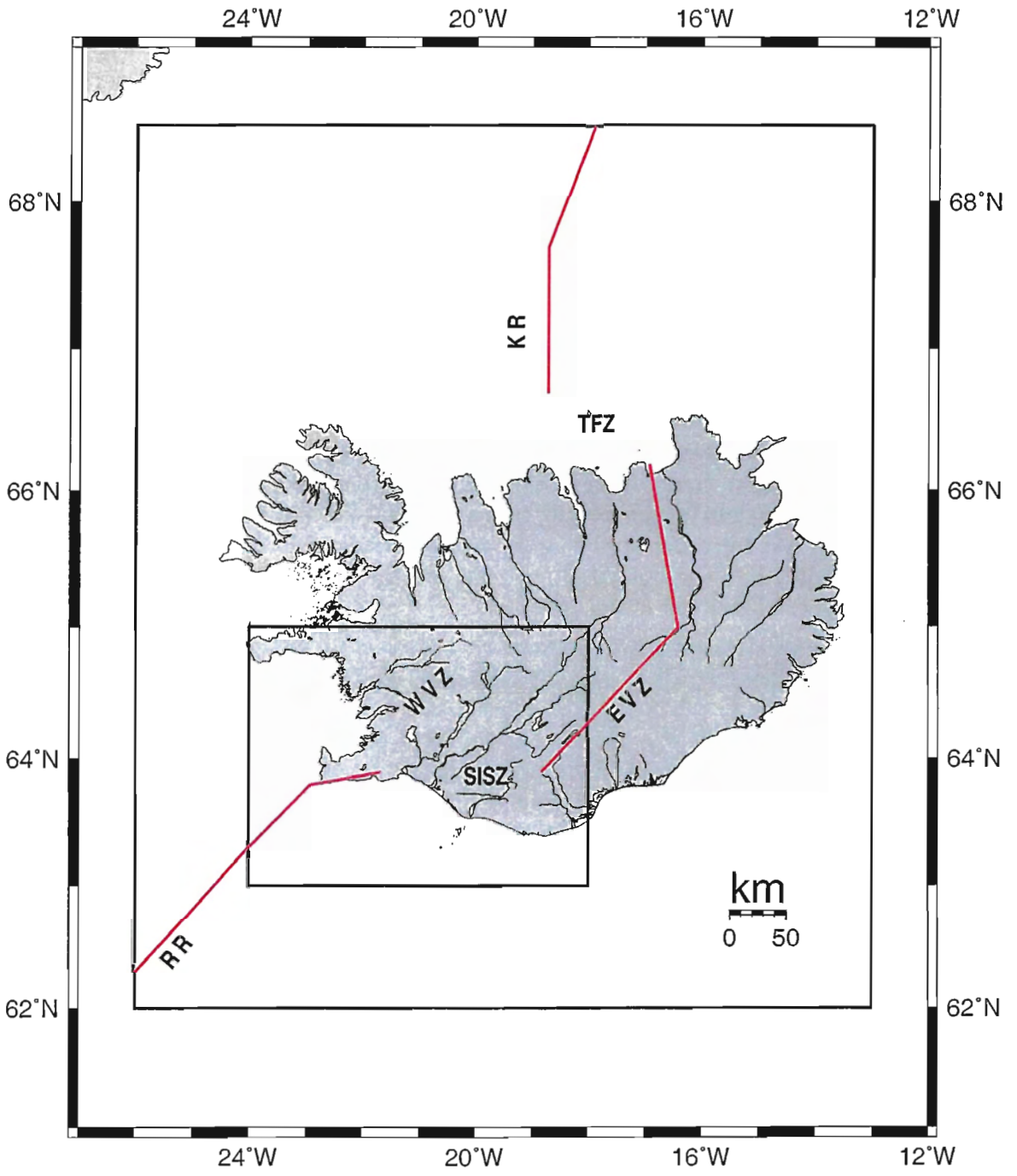

Figure 51. *Map of Iceland and surrounding area. Thick red lines indicate mid-Atlantic ridge segments, as used in the models. The smaller box shows the region of the model on the SISZ. The SISZ extends approximately between 21.4° W, 63.95° N to 18.8° W, 64° N. The large box gives the region for the Iceland rift model. RR: Reykjanes ridge, KR: Kolbeinsey ridge, WVZ/EVZ: western/eastern volcanic zone, SISZ: South Iceland seismic zone, TFZ: Tjörnes fracture zone.*

large as the stress drop determined for the largest event (M=7.1) in the studied earthquake sequence.

On this initial field, the stress changes due to earthquakes are iteratively superposed as well as the stress changes due to further spreading at the ridge segments. From global geodetic measurements an opening of 2 cm/year is found, e.g. in DeMets et al. (1990). This was used as a zero-th order approach but was reduced to only 1 cm/year, as discussed later. Further, as the simplest assumption, lacking other data, the spreading rate is taken to be constant during the modelled time period, even though this can be questioned as for instance the present debate on the stress increase in the New Madrid seismic zone shows (cf. Schweig and Gomberg 1999; Newman and Stein 1999) The stress field before every event is thus the sum of the initial field, the stress drop of all preceding events, and the plate tectonic stress build-up since the starting time of the model, which is set to 1706, when the first event in the series occurred.

Results were calculated for 280x220 test-points covering 280 km in E-W direction and 220 km in N-S direction. Stresses were computed for a homogeneous half-space, as a starting model. Although surface stress changes are calculated, these should be representative for crustal stresses using values for the moduli, that are typical for oceanic crust (see Dziewonski et al. 1975) and not for sedimentary layers at the surface. Moreover, as the faults are introduced vertically into the unlayered environment, the stresses do not vary much with depth, besides at the lower end of the fault.

Changes and improvements in PRENLAB-2

In the first phase of PRENLAB-2, the models developed in PRENLAB-1 were improved:

A The test-point density was increased from 56x44 (5 km distance) to 280x220 (1 km distance) to get more details of the stress field and to reduce interpolation errors.

B At the western end of the SISZ, segments with aseismic oblique slip (mainly normal faulting with a smaller component of left-lateral strike-slip) were introduced, to better fit the Reykjanes ridge (RR) between the southwest tip of the Reykjanes peninsula to Hengill-Ölfus triple junction (Figure 51).

C At the eastern and western tips of the SISZ two areas with steady stress release were introduced (see dashed lines in Figure 52). This could occur by a high rate of small events and maybe by creep. This is likely as these areas did never show strong events ($M \geq 6$) in the seismic history of Iceland, with the exception of possible events in 1546 and 1632 at the western end (about 21.3°W) and one event in 1311 (about 18.9°W) (cf. Halldórsson 1991). See under Task 2 for a discussion of this.

D To investigate the model resolution a set of different models is produced: Besides the main model, several extreme cases are assumed and the variation of the main results under these assumptions is observed.

E The stress field was extrapolated to 1999 and was now updated to the situation after the June 21, 2000, event.

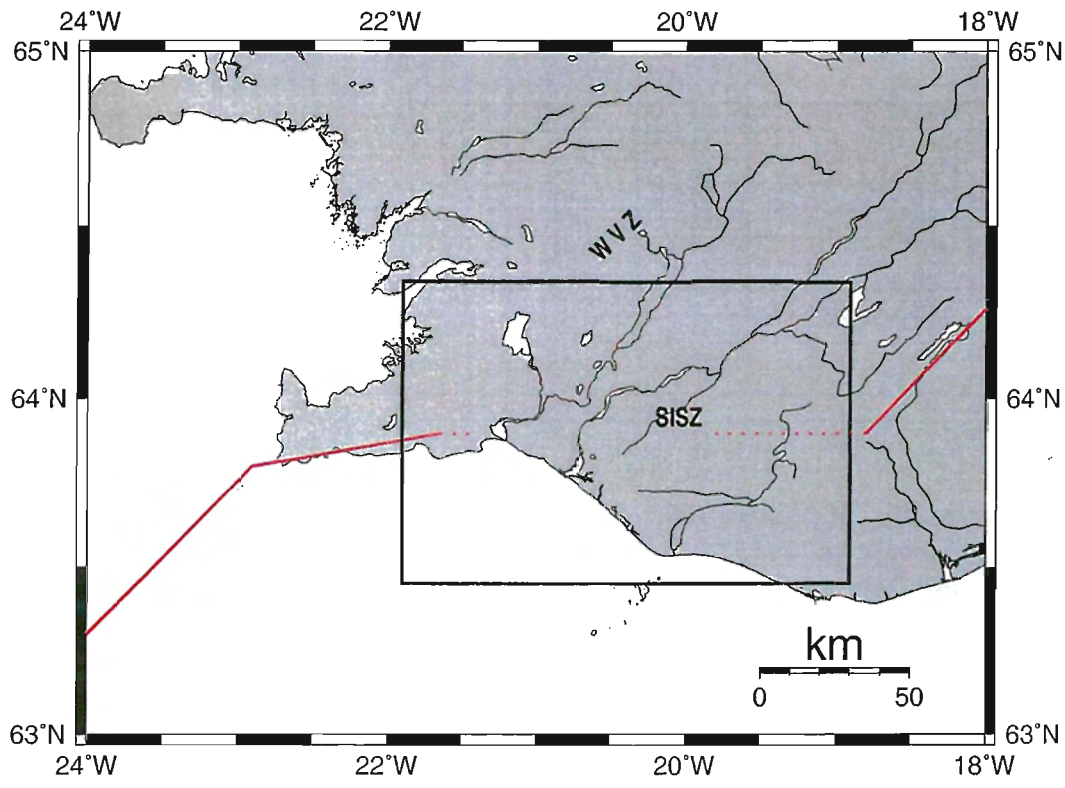

Figure 52. *The box gives the area in SW-Iceland used in the modelling as indicated with the small box in Figure 51.*

The earthquake data

All events with M $\geq$ 6 since 1706 were used (listed in Table 8., following Halldórsson et al. 1984; after Hackman et al. 1990; Stefánsson and Halldórsson 1988; and Stefánsson et al. 1993). The catalogue is supposed to be complete from 1706 for these earthquakes.

All ruptures were set to be oriented N-S, according to the isolines of damage intensity and surface ruptures shown in Figure 50. As only the events in 1912 and 2000 were instrumentally recorded, the source parameters are not very accurate – a problem to be discussed further below. The position of the epicenters and the rupture planes used in the models are given in Figure 53 and Figure 54, respectively.

Date[1]	Magnitude[1]	Epicenter[1]		South end of rupture[2]		Co-seismic slip[3]	Rupture length[4]
		Lat. °N	Long. °W	x [km]	y [km]	U_0 [m]	L [km]
1706	6.0	64.0	21.2	131	-5	0.30	10
1732	6.7	64.0	20.1	183	-11	0.77	22
1734	6.8	63.9	20.8	150	-23	0.96	25
14.08.1784	7.1	64.0	20.5	164	-18	1.9	35
16.08.1784	6.7	63.9	20.9	145	-22	0.77	22
26.08.1896	6.9	64.0	20.2	178	-14	1.2	28
27.08.1896	6.7	64.0	20.1	183	-11	0.77	22
05.09.1896	6.0	63.9	21.0	140	-16	0.30	10
05.09.1896	6.5	64.0	20.6	159	-9	0.48	18
06.09.1896	6.0	63.9	21.2	131	-16	0.30	10
06.05.1912	7.0	63.9	20.0	187	-27	1.5	32
17.06.2000	6.5	64.0	20.4	169	-12	0.9	16
21.06.2000	6.4	64.0	20.7	154	-13	1.1	18

Table 8. *Earthquakes M$\geq$6 since 1706 in the South Iceland seismic zone. 1) Data taken from Stefánsson et al. (1993); for the events in 1706, 1732, and 1734 no exact date is known. Data on the events of June 2000 are from Stefánsson, Guðmundsson and Halldórsson (pers. comm.), with magnitudes as moment magnitudes. 2) Position in the model coordinate system with origin at 64° N, 24° W. 3) Calculated via the magnitude moment relationship log M_0 [dyne cm] = 1.5M_S+(11.8 - log(σ_a/μ)) with the apparent stress σ_a = 1.5 MPa and the shear modulus μ = 39 GPa (after Kanamori and Anderson 1975), followed by using the values of μ above, the rupture length as given in the table as well as a vertical fault width of 14 km east of 21° W and 7 km between 21° W and 21.2° W. Finally, the values for all events before those in 2000 were reduced by a factor of 2, following the discussion of Hackman et al. (1990). All this does not apply to the June 17 and 21, 2000, earthquakes, for which good instrumental data are available, and e.g. a maximum rupture depth of 9 and 7 km were given, respectively. 4) Besides for the June 2000 events, calculated using log L [km] = 0.5 M - 2 (after Qian 1986) which results in slightly lower values compared to e.g. Schick (1968).*

The results

The stress fields at 20 dates were calculated: the pre- and post-seismic situation for all 13 events. The time before 6 events was too short to accumulate appreciable plate tectonic stresses since the preceding event. In these cases, the post-seismic stress field of the preceding

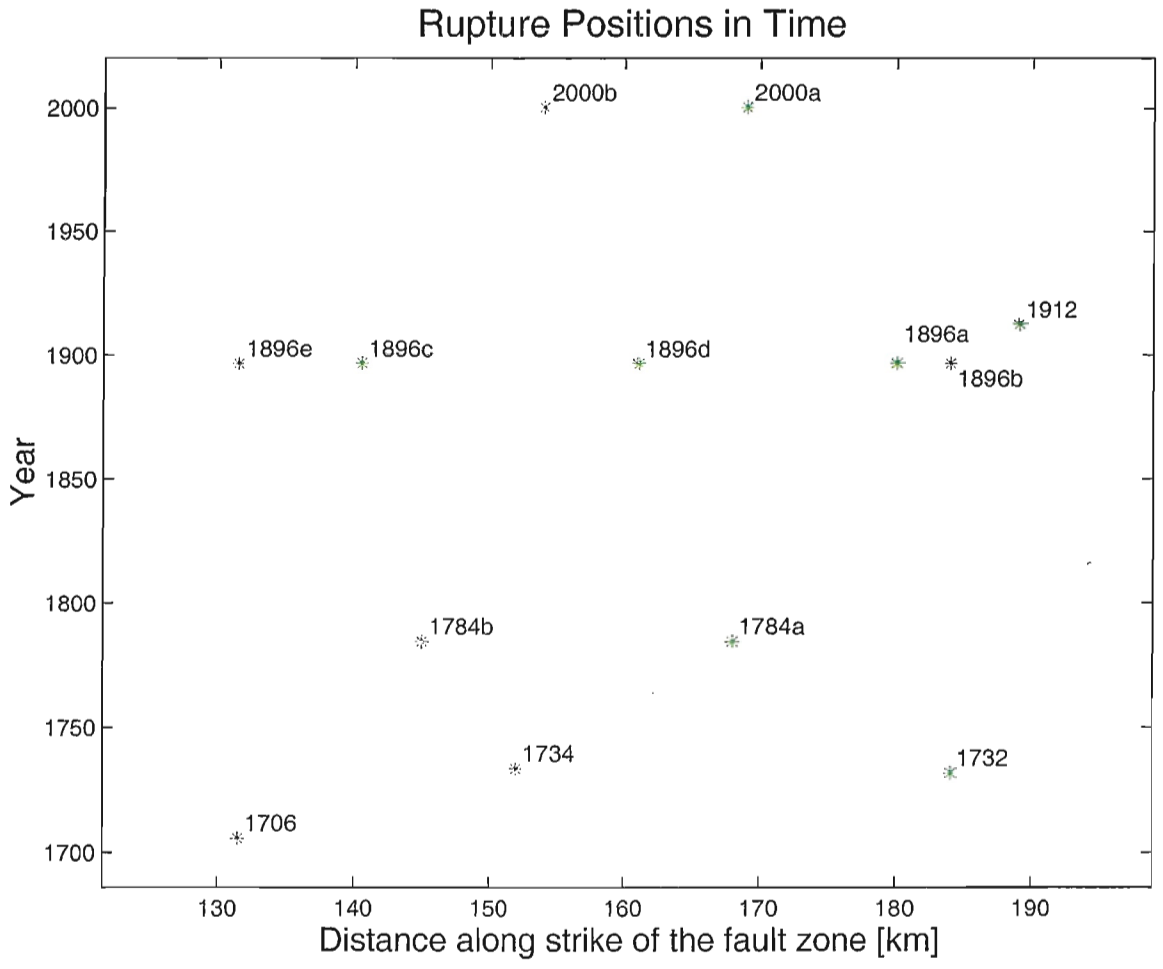

Figure 53. *Location of the earthquakes in space and time (cf. Table 8). As the events have been located on N-S trending faults in an E-W trending fault zone, their location is very accurately displayed in this graph.*

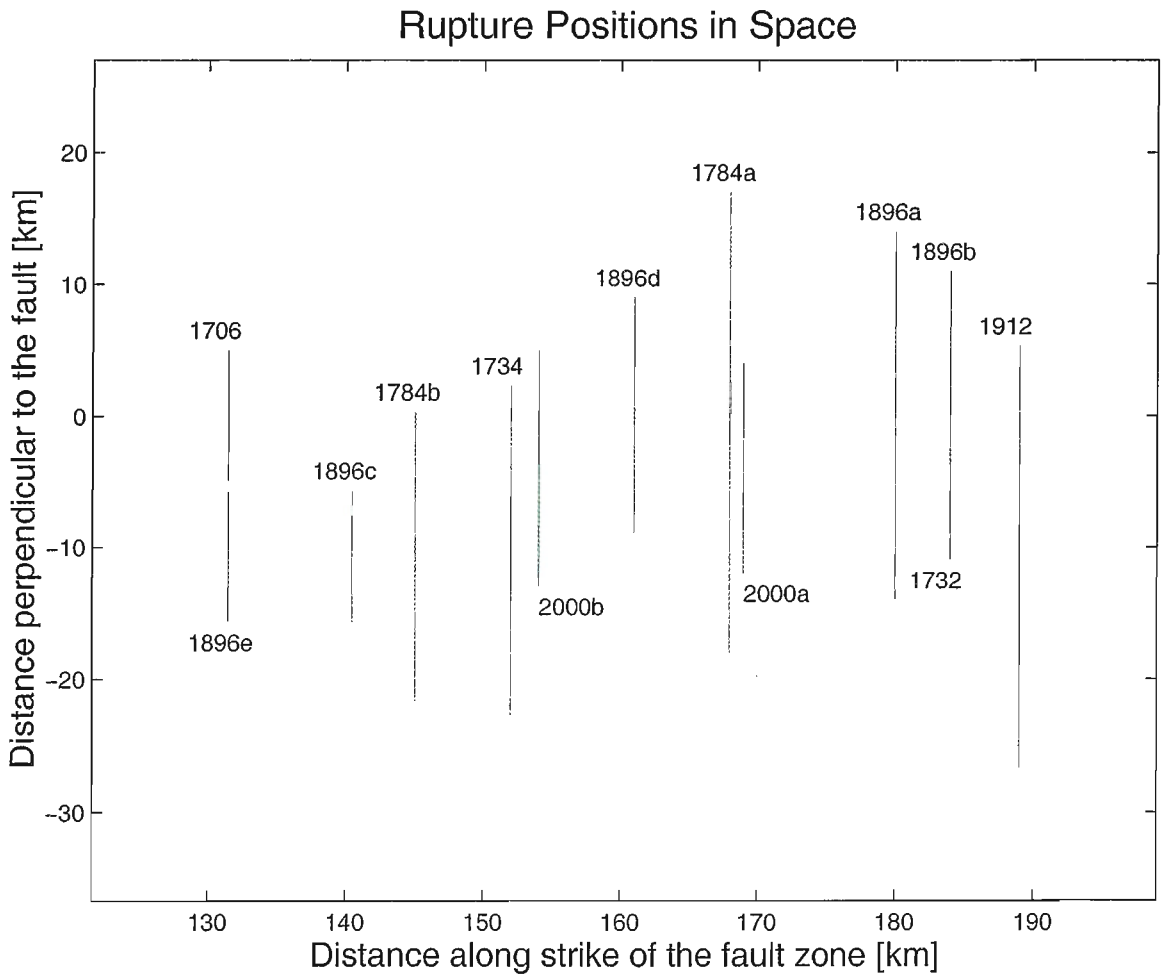

Figure 54. *The position of the rupture planes of the earthquake sequence as used in the models (cf. Table 8).*

event was set equal to the pre-seismic stress field of these earthquakes.

Originally, an extrapolation was done from the 1912 earthquake to spring 1999. After the two earthquakes happened this June, it was updated to June 17, 2000 (Figure 56) and the effect of both events were determined (see Figure 57 and Figure 58).

As a simple assumption, one might expect, that earthquakes in a certain fault zone usually occur at about the same critical shear stress level. We examine here if such an expectation matches the known facts about the earthquakes, given above, and the stress field in the SISZ from knowledge about plate motion and the modelling here. Figure 59 summarizes the mean shear stress level before each of the earthquakes at the area of the impending event. The stress level is near the average (1.8 MPa) or higher for most of the events. The highest value (for 1896e) is mainly influenced by the fact that the rupture area for the event in 1706 was located completely north of that in 1896 (cf. Figure 54). The second 1784 earthquake (two days after the first, 0.4 in magnitude smaller, 19 km away) might have been an aftershock and therefore situated in a lower stress area (1.6 MPa). The same might apply to the second of the 1896 events. The forth event in 1896 and the first shock in 2000 are both influenced by the largest event in the series, i.e. the first one in 1784. Thus, the accuracy of the source parameter of this 1784 earthquake strongly influences the whole model. Concerning the first event in June 2000, it has to be noted that it took place in a very inhomogeneous stress field, i.e. there are low stresses in the north of the rupture plane and high ones in the south (see Figure 56). Calculating an average pre-seismic stress level might be especially misleading for this event, when all the test-points around the rupture plane are considered equally.

Checking the performance of the model in a qualitative way, we examined if the earthquakes hit the high stress area and how large the high stress areas with no event were at the same time (the range in longitude with high stresses was summed when the N-S extension of the area was at least 5 km and the longitude range for the event that occurred was subtracted, usually 0.1 to 0.2 degrees in longitude). The results can be found in Table 9 and are quite satisfying with respect to the named question. Almost all events hit high stress areas and the size of high stress areas with no event was rather small after the earthquakes in the eighteenth century. Nevertheless, the problem remains, why some events did not occur earlier (at lower stress), just passing the "limit in pre-seismic stress" (i.e. here: the average pre-seismic stress).

As stated earlier, the plate velocity used in the model was set to 1 cm/year, only half of that what is measured. The reason can be seen in Figure 59 in comparison with Figure 60. The higher plate velocity leads to a steady and strong increase in the pre-seismic stress level, which is very unlikely, while the reduced rate entails an almost constant level. As the model cannot change the geodetic results, the reason for the discrepancy might be that only 50% of the stress build-up by plate tectonics is released seismically. For the rest, stable sliding or aseismic creep could be responsible.

Two problems were addressed next: (i) To see how sensitive the results depend on the model parameters, it was begun to check extreme cases and their outcome. (ii) The average stress level before some events is considerably lower than for others (cf. the discussion on Figure 59). This is, among other reasons, due to the fact that the rupture planes, used until now, extend rather far to the north and south of the SISZ. The damage areas from historical records are not gathered by scientists and are usually biased by uneven population density.

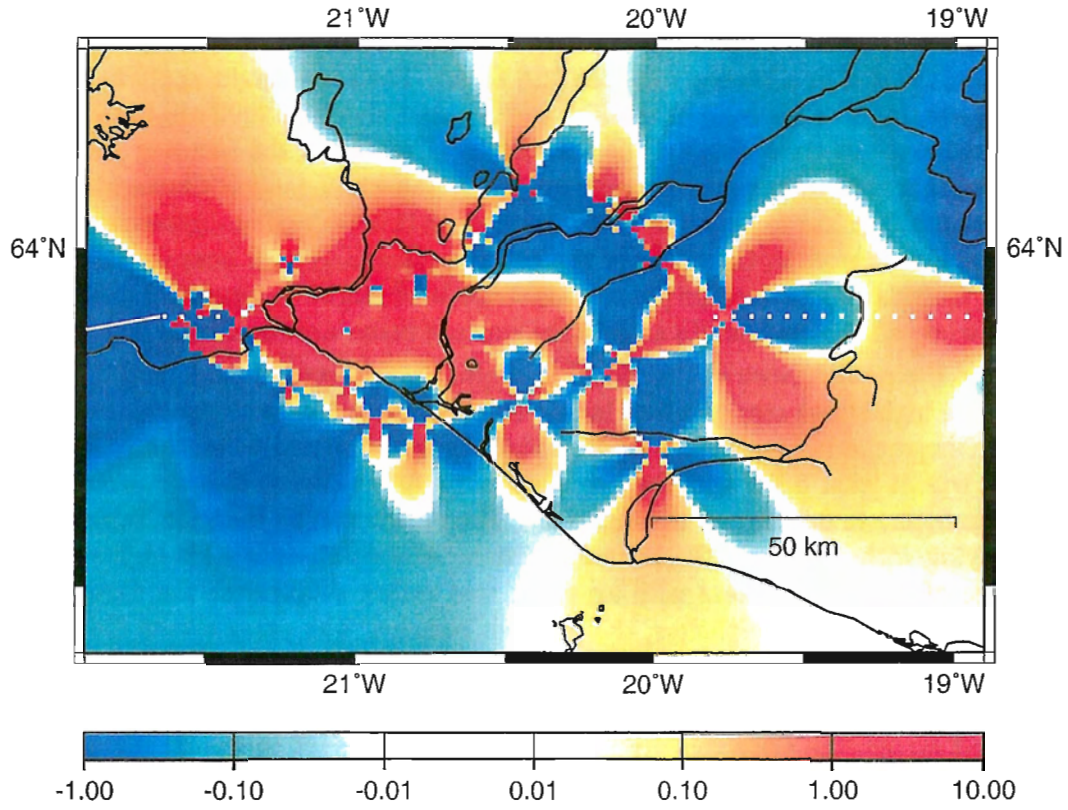

Figure 55. *The stress field after the May 6, 1912 earthquake.*

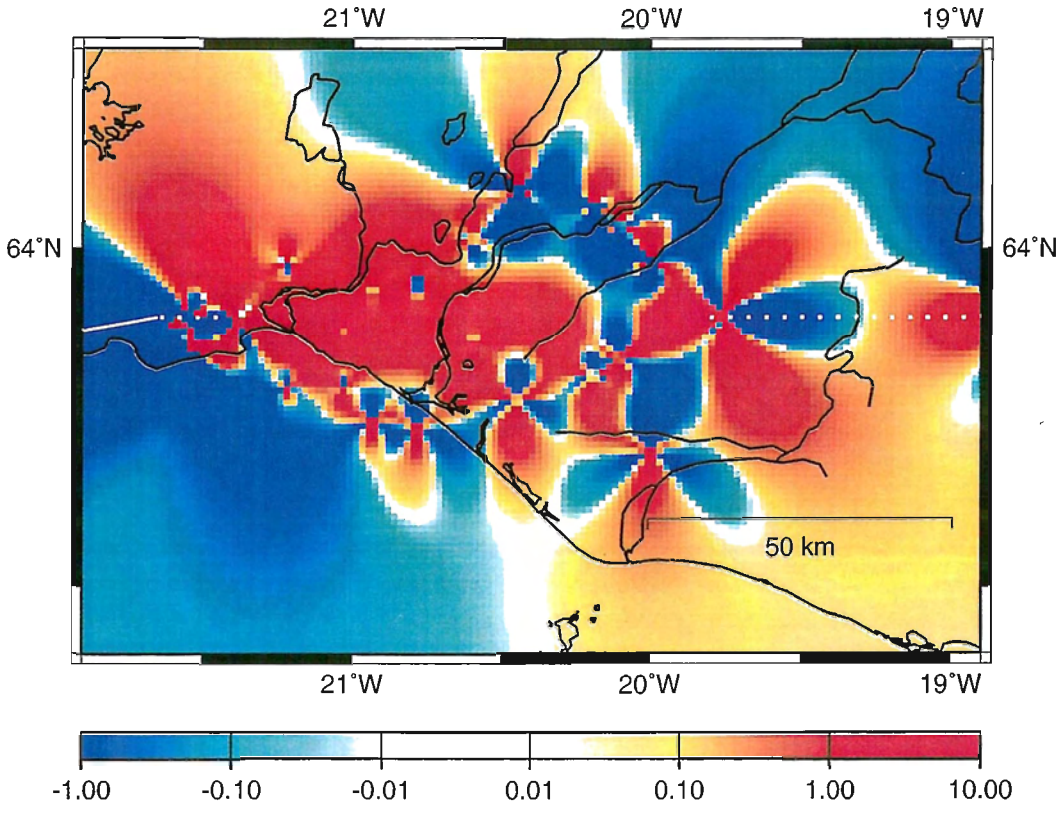

Figure 56. *The stress field before the June 17, 2000, M=6.5 earthquake occurring at 20.4° W, 64.0° N, i.e. (169, -12 — +4).*

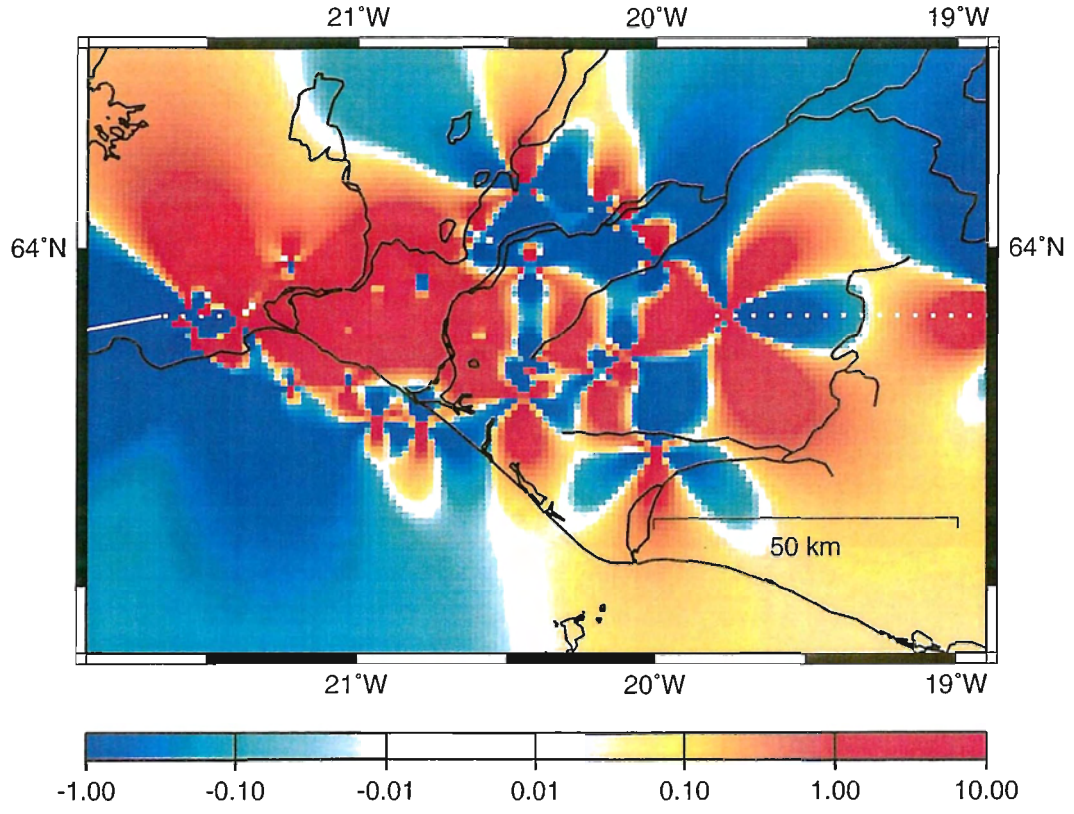

Figure 57. *The stress field after the June 17, 2000, M=6.5 earthquake occurring at 20.4° W, 64.0° N), i.e. (169, -12 — +4).*

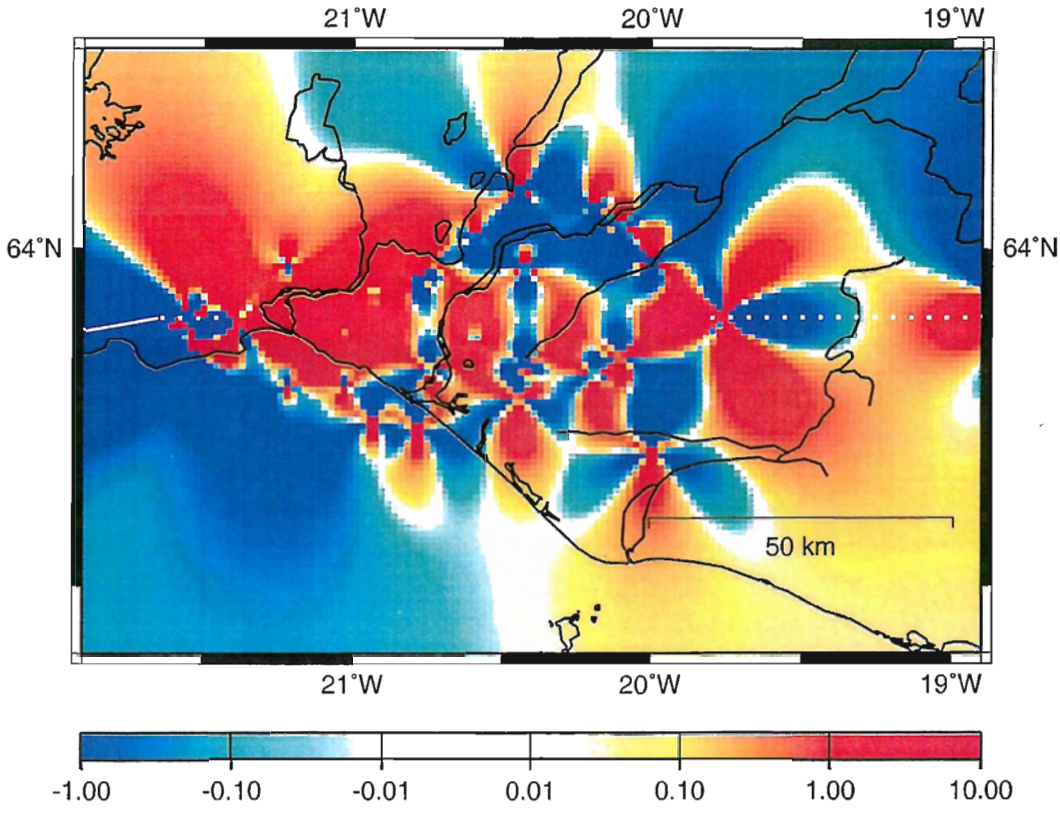

Figure 58. *The stress field after the June 21, 2000, M=6.4 earthquake occurring at 20.7° W, 64.0° N, i.e. (154, -13 — +5).*

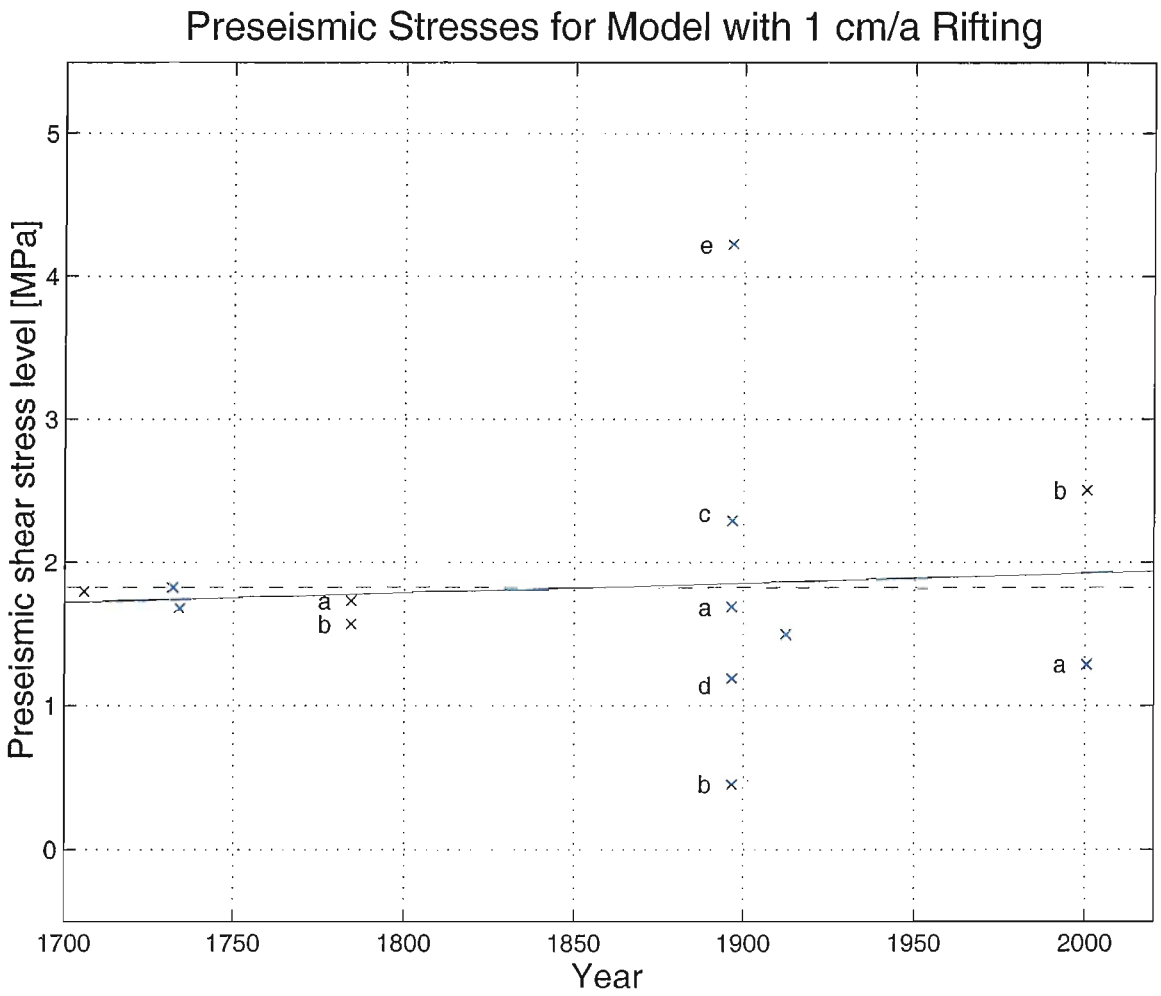

Figure 59. *Cross plot of the pre-seismic shear stress level at the site of the impending earthquakes vs. occurrence time. The stress values at 2 to 14 test-points at 0.5 km distance to the surface trace of the rupture plane were averaged. Instead of a plate velocity of 2 cm/year only 1 cm/year was used (see text). Letters "a" through "e" denote the events in one year in temporal sequence. The dashed line gives the average stress, the solid line represents the trend found by a linear least squares fit.*

Event time:	Pre-seismic stress high at °W:	Earth-quake at °W:	Hit high stress area?	Size of other areas with high stress:	Remarks:
1706	19.8 – 21.2	21.2	yes	large	tuning phase[1]
1732	19.8 – 21.1	20.1	yes	large	tuning phase
1734	19.8 – 20.0, 20.2 – 21.1	20.8	yes	large	tuning phase
1784a	19.8 – 20.0, 20.2 – 20.7, 20.8 – 21.1	20.5	yes	medium	tuning phase
1784b	19.8 – 20.0, 20.9 – 21.1	20.9	yes	small	tuning phase
1896a	19.8 – 20.3, 20.8 – 21.2	20.2	yes	medium	other high stress area hit 10 days later
1896b	19.8 – 20.0, ± 20.6, 20.8 – 21.2	20.1	no	medium	other high stress area hit 9 days later
1896c	19.8 – 20.0, ± 20.6, 20.8 – 21.2	21.0	yes	medium	other high stress area hit next day
1896d	19.8 – 20.0, ± 20.6, 20.8 – 21.2	20.6	yes	medium	other high stress area hit at the same day
1896e	19.8 – 20.0, 20.8 – 21.2	21.2	yes	small	
1912	19.8 – 20.0, 20.8 – 21.2	20.0	yes	small	
2000a	± 19.9, 20.5 – 21.2	20.4	no/ yes	small	hit short (N-S) high stress area[2]
2000b	± 19.9, 20.6 – 21.2	20.7	yes	small	

Table 9. *Qualitative evaluation of the model performance. 1) As the initial stress field is unknown, it was assumed to be homogeneous. So the first series of events that ruptures all across the fault zone is very strongly influenced by this assumption. 2) The stress field before the first earthquake in June 2000 is very inhomogeneous, i.e. there are low stresses in the north of the rupture plane and high ones in the south (see Figure 56). Looking at the development of the stress distribution, this situation is still influenced by the rupture position and magnitude of the first event in 1784 (cf. Figure 54). These historical data have some uncertainty (cf. Figure 50).*

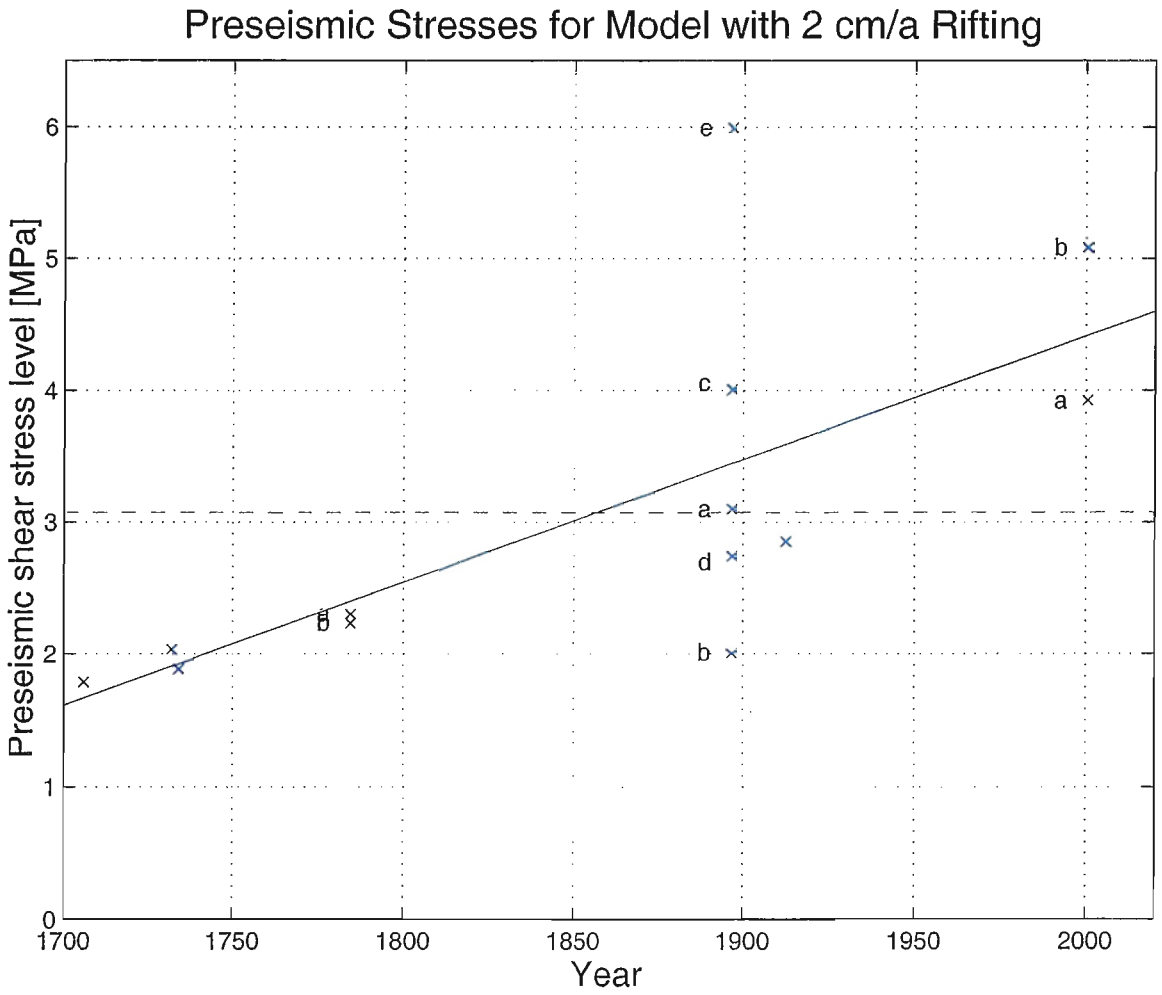

Figure 60. *Cross plot of the pre-seismic shear stress level at the site of the impending earthquakes vs. occurrence time. A plate velocity of 2 cm/year was used. For further explanations see Figure 59.*

So the magnitudes and locations are not very accurate, as stated earlier. And as mentioned in the footnotes of Table 9, there are doubts on the correct rupture size from global relations between magnitude and rupture length.

From both reasons given here, a model was calculated that uses the same seismic moment of the events, but cuts the fault length to 50% while doubling the co-seismic displacement. It will be termed "short rupture model". One side-effect of this change is an increase of the stress level, as the moment release is concentrated to a smaller area. The initial stress field amplitude was increased accordingly, because – as described above – this field is adjusted to the average stress change of the strongest event. It is important to note that the increase in stress level does not change the stress pattern of the initial stress field; as we are not looking for specific stress amplitudes but for stress concentrations, the change in level is not important. The resulting variation of the pre-seismic stress level is – as expected – smoother than before due to the concentration of stress release to high stress areas. However, this approach could only be used, once the historical events are re-evaluated with the result of shorter ruptures.

The processing of the recent earthquakes last June led to maximum rupture depth of less than ten kilometres. Even though there are smaller events located down to 13 km (cf. Stefánsson et al. 1993), the assumption that all ruptures extend to no more than a depth of 10 km seems to be reasonable. Such a model was calculated too, replacing the maximum depth of 14 km for most events (cf. Table 9) by 10 km. In this case too, the stress release by the events is higher, as it is concentrated to an area closer to the rupture plane. Moreover, the interaction of the events is lower due to this concentration in space. However, the stress level before the main events remains in a similar range as before (average now 2.1 MPa instead of 1.8 MPa), and the variation in the pre-seismic stress does not differ much (the standard deviation is 0.87 MPa instead of 0.88 MPa) from the model with deeper ruptures (cf. Figure 61).

In general, the variation of the model parameters shows that the models are stable, i.e. small changes in the parameters do not lead to totally different results. Therefore, they fulfill this important quality criterium.

3.7.2.2 Task 1: Extrapolation of the stress field for the next years

Originally, the stress field for the new models was extrapolated to spring 1999, with the additional stresses due to plate motion since 1912. This became obsolete when the earthquakes in June 2000 occurred. As presented above, the stress field before and after these events was determined. To examine if the stresses were high before the events was a good check for the model results. The present situation is essentially that after the second earthquake in June (see Figure 58). For more details see the discussion below.

3.7.2.3 Task 2: Pin-pointing of stress concentrations in space and time

At present, stresses are concentrated around 19.9°W and at 20.8–21.2°W. As there have not been earthquakes since 1912 and 1896, respectively, this is to be expected and was reproduced by the model.

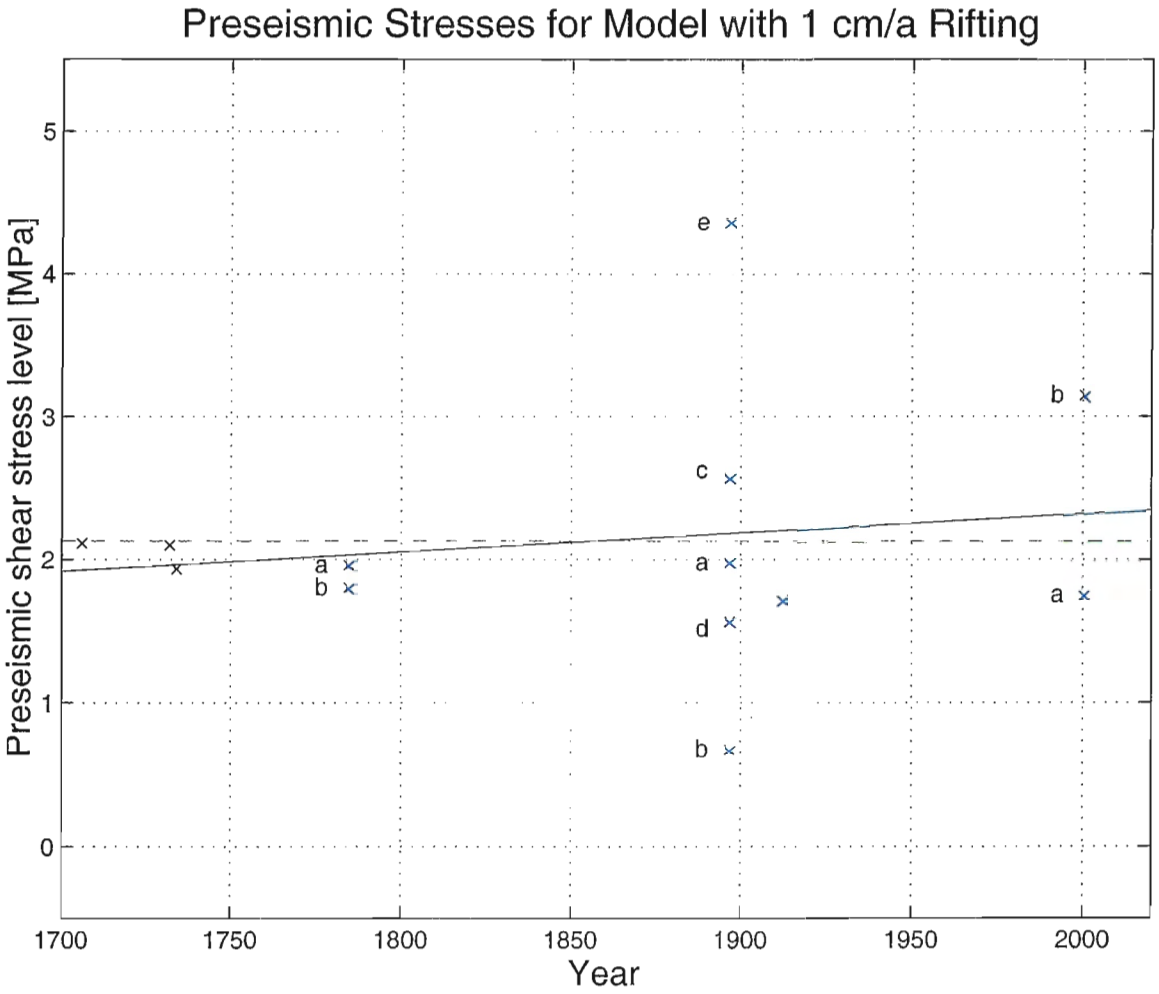

Figure 61. *Cross plot of the pre-seismic shear stress level at the site of the impending earthquakes vs. occurrence time. A maximum rupture depth of 10 km was used. For further explanations see Figure 59.*

Once more, we would like to point to the fact that, in the model, stresses are steadily released at those areas (marked with dashed lines) where the SISZ approaches the ridge segments, as noted under item "C" of the list of improvements above. It are sections of the SISZ between the high stress areas just mentioned and the rift tips.

Is this a weakness of the models or is it the real situation? Could these high stress areas be excluded from the model? The answer is essentially "no". The origin of the stress concentrations at the end of the SISZ, i.e. at the tips of the adjoining ridges, is the fact that the ridges do not extend to infinite depth, but are assumed to reach only 7 km depth and enter than an inelastic, hot region not capable of supporting stresses for time periods of years. Deeper penetration of the brittle layer there would homogenize the stress field between rift tips at some average value. Although this is not very likely, a similar effect would be produced by drag at the base of the adjacent plates. Nevertheless, such a redistribution of stress would not lead to low stresses at the ends of the SISZ.

Possibly, there might have been stronger events in 1546 and 1632 at the western end (about 21.3°W) and one event in 1311 (about 18.9°W) (cf. Halldórsson 1991). But all other evidence only shows small and medium sized events there. The main argument against high seismogenic stress release there is, that there was no large event ($M \geq 6$) since 1706. There are several indications that the stress release indeed mainly takes place in small and medium events at the ends of the SISZ. In 1987, there was a medium sized earthquake (M_S=5.8) at 63.91°N 19.78°W (198, -9) near Vatnafjöll (see Figure 50) at the east end of the SISZ. And in 1998, there were 2 similar events at the Hengill-Ölfus triple junction at the western end of the SISZ: June 4 (M=5.1) and November 13 (M=5) both accompanied by a lot of smaller events.

Therefore, we believe that the tips of the SISZ might only be the place where medium sized events take place and the stress concentrations given around 19.9°W and at 20.8–21.2°W represent those for future strong earthquakes.

As the stress build-up by plate motion is very low in these models (compare the stress field in 2000 in Figure 56 with that of 1912 in Figure 55), the uncertainty in time is very large in the occurrence time, see also the discussion below.

3.7.2.4 Task 3: Search for characteristic preseismic stress level

As a simple assumption, one might expect, that earthquakes in a certain fault zone usually occur at about the same critical shear stress level. Here, we tried to find out, if such an expectation matches the known facts about the earthquakes and the stress field in the SISZ.

In all models, the pre-seismic stress level for most main shocks is high and fairly stable. This is also true for the events at the end of the sequence, namely those of 1912, of June 20, 2000, and – with minor reservations – of June 17, 2000. It indicates that the rather simple model can already explain the main features of the behaviour of the SISZ. This is especially astonishing, when the fact is kept in mind, that most (all but one) events used are not instrumentally recorded. Before the June 2000 events the SISZ seems to have been prepared for rupturing at the specific locations. This fits very well to the findings from stress measurements in wells (see Subproject 4) that E-W left-lateral shear stress was acting on the fault zone. To improve the model further, the initial unknown stress field of 1706 could be reduced in the eastern part and the central part, where the first events did not occur before

1732 and 1734, respectively. Another improvement might be to include more basal drag as the source of plate tectonic stress increase as compared to ridge push.

Nevertheless, the problem remains, why some events, as those of September 6, 1896, or June 21, 2000, did not occur earlier (i.e. at lower stress), just passing the "threshold in pre-seismic stress" (here e.g. the average pre-seismic stress (cf. Figure 59). Only if this would be the case, a prediction of the occurrence time might be at reach.

Even though the earthquake rupture planes strike N-S, the stress changes calculated here affect the whole area of the SISZ.

A tendency with time towards higher values of pre-seismic stress was found. It is an indication that the stress increase due to rifting might have been assumed too high, i.e. not all of the stress increase due to the spreading rate of 2 cm/year (assumed to be constant between 1706 to 2000) was released by earthquakes. The assumption that only half of the accumulated stress is seismically released led to a rather constant pre-seismic stress level.

The variation in model parameters does not lead to totally different results, i.e. the model is rather stable.

In general, the models go beyond the standard earthquake moment release and hazard analysis as they include the spatial location and extension of the events, quantify the amplitudes of stress release and that of plate motion on the faults, as well as providing an extrapolation to the present stress situation. This report will be submitted for publication in an appropriate form.

3.7.2.5 Meetings and conferences

A meeting between Maurizio Bonafede and coworkers with Frank Roth took place in March 1999 in Strasbourg, France, parallel to the tenth biennal EUG meeting. Another meeting with Bonafede and Ragnar Stefánsson took place at the GeoForschungsZentrum Potsdam in June 1999.

3.7.2.6 Acknowledgements

I like to thank the staff of IMOR.DG, especially Páll Halldórsson, for great support on the seismicity of Iceland. I am also indebted to F. Lorenzo Martín and Fernando J. Lorén Blasco for assisting in the graphics and checking the text.

3.7.3 References

Bjarnason, I.Þ. & P. Einarsson 1991. Source mechanism of the 1987 Vatnafjöll earthquake in South Iceland. *J. Geophys. Res.* 96, 4313-4324.

Bjarnason, I.Þ., P. Cowie, M.H. Anders, L. Seeber & C.H. Scholz 1993. The 1912 Iceland earthquake rupture: growth and development of a nascent transform system. *Bull. Seism. Soc. Am.* 83, 416-435.

Bonafede, M. & E. Rivalta 1999. The tensile dislocation problem in a layered elastic medium. *Geophys. J. Int.* 136, 341-356.

Bonafede, M. & A. Neri 2000. Effects induced by an earthquake on its fault plane: a boundary element study. *Geophys. J. Int.* 141, 43-56.

Bonafede, M., B. Parenti & E. Rivalta 2000. Strike-slip faulting in layered media. *Geophys. J. Int.*, submitted.

DeMets, C., R.G. Gordon, D.F. Argus & S. Stein 1990. Current plate motions. *Geophys. J. Int.* 101, 425-478.

Dziewonski, A.M., A.L. Hales & E.R. Lapwood 1975. Parametrically simple earth models consistent with geophysical data. *Phys. Earth Plan. Int.* 10, 12.

Einarsson, P., S. Björnsson, G.R. Foulger, R. Stefánsson & Þ. Skaftadóttir 1981. Seismicity pattern in the South Iceland seismic zone. In: D. Simpson & P. Richards (editors), Earthquake prediction - an international review. *Maurice Ewing Series* 4. American Geophysical Union, 141-151.

Einarsson, P. & K. Sæmundsson 1987. Earthquake epicenters 1982-1985 and volcanic systems in Iceland. In: Þ.I. Sigfússon (editor), *Í hlutarins eðli.* Map accompanying the festschrift, scale 1:750000. Reykjavík, Menningarsjóður.

Hackman, M.C., G.C.P. King & R. Bilham 1990. The mechanics of the South Iceland seismic zone. *J. Geophys. Res.* 95, 17339-17351.

Halldórsson, P. 1991. Historical earthquakes in Iceland until 1700. In: K. Kozák (editor), *Proceedings of the third international symposium on historical earthquakes in Europe.* Prague, Czechoslovakia, 115-125.

Halldórsson, P., R. Stefánsson, P. Einarsson & S. Björnsson 1984. *Mat á jarðskjálftahættu: Dysnes, Geldinganes, Helguvík, Vatnsleysuvík, Vogastapi og Þorlákshöfn.* Veðurstofa Íslands, Raunvísindastofnun Háskólans, Reykjavík.

Kanamori, H. & D.L. Andersson 1975. Theoretical basis of some empirical relations in seismology. *Bull. Seism. Soc. Am.* 65, 1073-1096.

Newman, A. & Stein 1999. Reply: New results justify open discussion of alternative models. *EOS, Trans. Am. Geophys. Un.* 80, 197 and 199.

Qian, H. 1986. Recent displacements along Xianshuihe fault belt and its relation with seismic activities. *J. Seism. Res.* 9, 601-614.

Roth, F. 1989. A model for the present stress field along the Xian-shui-he fault belt, NW Sichuan, China. In: M.J. Berry (editor), Earthquake hazard assessment and prediction. *Tectonophysics* 167, 103-115.

Schick, R. 1968. A method for determining source parameters of small magnitude earth-

quakes. *Zeitschr. f. Geophys.* 36, 205-224.

Schweig, E.S. & J.S. Gomberg 1999. Comment: Caution urged in revising earthquake hazards estimates in New Madrid seismic zone. *EOS, Trans. Am. Geophys. Un.* 80, 197.

Stefánsson, R. & P. Halldórsson 1988. Strain release and strain build-up in the South Iceland seismic zone. *Tectonophysics* 152, 267-276.

Stefánsson, R., R. Böðvarsson, R. Slunga, P. Einarsson, S.S. Jakobsdóttir, H. Bungum, S. Gregersen, J. Havskov, J. Hjelme & H. Korhonen 1993. Earthquake prediction research in the South Iceland seismic zone and the SIL project. *Bull. Seism. Soc. Am.* 83, 696-716.

Zoback, M.D., M.L. Zoback, V.S. Mount, J. Suppe, J. Eaton, J.H. Healy, D. Oppenheimer, P. Reasenberg, L. Jones, C.B. Raleigh, I.G. Wong, O. Scotti & C. Wentworth 1987. New evidence on the state of stress on the San Andreas fault system. *Science 238*, 1105-1111.

Chapter 4

Publications

Papers directly associated with PRENLAB–2

Subproject 1

Ágústsson, K. 1998. Jarðskjálftahrina á Hellisheiði og í Hengli í maí–júlí 1998. *Greinargerð Veðurstofu Íslands* VÍ–G98040–JA06. Report, Icelandic Meteorological Office, Reykjavík, 35 pp.

Ágústsson, K., A.T. Linde, R. Stefánsson & S. Sacks 1998. Strain changes for the 1987 Vatnafjöll earthquake in South Iceland and possible magmatic triggering. *J. Geophys. Res.* 104, 1151–1161.

Ágústsson, K., S.Th. Rögnvaldsson, B.H. Bergsson & R. Stefánsson 1998. Jarðskjálftamælanet Veðurstofu Íslands og Hitaveitu Suðurnesja – lýsing á mælaneti og fyrstu niðurstöður. *Rit Veðurstofu Íslands* VÍ–R98002–JA02. Research report, Icelandic Meteorological Office, Reykjavík, 17 pp.

Árnadóttir, Þ. & K.B. Olsen 2000. Simulation of long–period ground motion and stress changes for the Ms=7.1, 1784 earthquake, Iceland. *Rit Veðurstofu Íslands* VÍ–R00003–JA03. Research report, Icelandic Meteorological Office, Reykjavík, 31 pp.

Bergerat, F., Á. Guðmundsson, J. Angelier & S.Th. Rögnvaldsson 1998. Seismotectonics of the central part of the South Iceland seismic zone. *Tectonophysics* 298, 319–335.

Böðvarsson, R., S.Th. Rögnvaldsson, R. Slunga & E. Kjartansson 1998. The SIL data acquisition system – at present and beyond the year 2000. *Rit Veðurstofu Íslands* VÍ–R98005–JA04. Research report, Icelandic Meteorological Office, Reykjavík, 22 pp.

Böðvarsson, R., S.Th. Rögnvaldsson, R. Slunga & E. Kjartansson 1999. The SIL data acquisition system – at present and beyond year 2000. *Phys. Earth Planet. Inter.* 113, 89–101.

Crampin, S., T. Volti & R. Stefánsson 1999. A successfully stress–forecast earthquake. *Geophys. J. Int.* 138, F1-F5.

Halldórsson, P., R. Stefánsson, B. Þorbjarnardóttir & I. Jónsdóttir 2000. Bráðaviðvaranir um jarðvá - áfangaskýrsla. *Greinargerð Veðurstofu Íslands* VÍ–G00005–JA02. Report, Icelandic Meteorological Office, Reykjavík, 16 pp.

Rögnvaldsson, S.Th. 1999. Frammistaða SIL kerfisins frá ágúst 1998 til mars 1999. *Greinargerð Veðurstofu Íslands* VÍ–G99004–JA01. Report, Icelandic Meteorological Office, Reykjavík, 14 pp.

Rögnvaldsson, S.Th. 2000. Kortlagning virkra misgengja með smáskjálftamælingum - yfirlit. *Rit Veðurstofu Íslands* VÍ–R00001–JA01. Research report, Icelandic Meteorological Office, Reykjavík, 15 pp.

Rögnvaldsson, S.Th., K. Ágústsson, B.H. Bergsson & G. Björnsson 1998. Jarðskjálftamælanet í nágrenni Reykjavíkur - lýsing á mælaneti og fyrstu niðurstöður. *Rit Veðurstofu Íslands* VÍ–R98001–JA01. Research report, Icelandic Meteorological Office, Reykjavík, 15 pp.

Rögnvaldsson, S.Th., Þ. Árnadóttir, K. Ágústsson, Þ. Skaftadóttir, G.B. Guðmundsson, G. Björnsson, K.S. Vogfjörð, R. Stefánsson, R. Böðvarsson, R. Slunga, S.S. Jakobsdóttir, B.S. Þorbjarnardóttir, P. Erlendsson, B.H. Bergsson, S. Ragnarsson, P. Halldórsson, B. Þorkelsson & M. Ásgeirsdóttir 1998. Skjálftahrina í Ölfusi í nóvember 1998. *Greinargerð Veðurstofu Íslands* VÍ–G98046–JA09. Report, Icelandic Meteorological Office, Reykjavík, 19 pp.

Rögnvaldsson, S.Th., Á. Guðmundsson & R. Slunga 1998a. Seismotectonic analysis of the Tjörnes fracture zone, an active transform fault in North Iceland. *J. Geophys. Res.* 103, 30117–30129.

Rögnvaldsson, S.Th., Á. Guðmundsson & R. Slunga 1998b. Seismotectonic analysis of the Tjörnes fracture zone, an active transform fault in North Iceland. *Rit Veðurstofu Íslands* VÍ–R98004–JA03. Research report, Icelandic Meteorological Office, Reykjavík, 23 pp.

Rögnvaldsson, S.Th., G.B. Guðmundsson, K. Ágústsson, S.S. Jakobsdóttir, R. Slunga & R. Stefánsson 1998. Overview of the 1993–1996 seismicity near Hengill. *Rit Veðurstofu Íslands* VÍ–R98006–JA05. Research report, Icelandic Meterological Office, Reykjavík, 16 pp.

Rögnvaldsson, S.Th., K.S. Vogfjörð & R. Slunga 1999. Kortlagning brotflata á Hengilssvæði með smáskjálftum. *Rit Veðurstofu Íslands* VÍ–R99002–JA01. Research report, Icelandic Meterological Office, Reykjavík, 22 pp.

Stefánsson, R. 1998. Earthquake–prediction research in a natural laboratory – PRENLAB. In: C.P. Providakis & M. Yeroyanni (editors), *Earthquake strong ground motion evaluation.* Proceedings of the EU–Japan workshop on seismic risk, Chania, Crete, Greece, March 24–26, 1998. European Commission, 113–122.

Stefánsson, R. 1999. A tentative model for the stress build–up and stress release in and around the SISZ.
URL: http://hraun.vedur.is/ja/prenlab/symp-mar-1999/ragnar/index2.html. Last modified March 31, 1999.

Stefánsson, R. 2000. Information and warnings to authorities and to the public about seismic and volcanic hazards in Iceland. To appear in a book of papers presented at the Early Warning Conference (EWC98), Potsdam, Germany, September 7-11, 1998, 11 pp.

Stefánsson, R., S.Th. Rögnvaldsson, P. Halldórsson & G.B. Guðmundsson 1998. PRENLAB workshop on the Húsavík earthquake, July 30, 1998. *Greinargerð Veðurstofu Íslands* VÍ–G98032–JA04. Report, Icelandic Meteorological Office, Reykjavík, 5 pp.

Stefánsson, R., F. Bergerat, M. Bonafede, R. Böðvarsson, S. Crampin, P. Einarsson, K.L. Feigl, Á. Guðmundsson, F. Roth & F. Sigmundsson 1999. Earthquake–prediction research in a natural laboratory – PRENLAB. In: M. Yeroyanni (editor), *Seismic risk in the European Union II.* Proceedings of the review meeting, Brussels, Belgium, Novem-

ber 27–28, 1997, European Commission, 1–39.

Stefánsson, R., G.B. Guðmundsson & P. Halldórsson 2000a. The two large earthquakes in the South Iceland seismic zone on June 17 and 21, 2000. *Greinargerð Veðurstofu Íslands* VÍ-G00010-JA04. Report, Icelandic Meteorological Office, Reykjavík, 8 pp.

Stefánsson, R., G.B. Guðmundsson & P. Halldórsson 2000b. Jarðskjálftarnir miklu á Suðurlandi 17. og 21. júní, 2000. *Greinargerð Veðurstofu Íslands* VÍ–G00011–JA05. Report, Icelandic Meteorological Office, Reykjavík, 8 pp.

Stefánsson, R., G.B. Guðmundsson & R. Slunga 2000. The PRENLAB-2 project, premonitory activity and earthquake nucleation in Iceland. In: B. Þorkelsson & M. Yeroyanni (editors), *Destructive earthquakes: Understanding crustal processes leading to destructive earthquakes.* Proceedings of the second EU-Japan workshop on seismic risk, Reykjavík, Iceland, June 23–27, 1999. European Commission, 161–172.

Stefánsson, R., Þ. Árnadóttir, G.B. Guðmundsson, P. Halldórsson & G. Björnsson 2001. Two recent M=6.6 earthquakes in the South Iceland seismic zone. A challenge for earthquake prediction research. *Rit Veðurstofu Íslands* VÍ-R01001-JA01. Research report, Icelandic Meteorological Office, Reykjavík, in press.

Tryggvason, A., S.Th. Rögnvaldsson & Ó.G. Flóvenz 2000. Three–dimensional imaging of the P- and S-wave velocity structure and earthquake locations beneath Southwest Iceland. *J. Geophys. Res.*, submitted.

Vogfjörð, K.S & S.Th. Rögnvaldsson 2000. Identification and modelling of secondary phases in short–period seismograms from local earthquakes in the South Iceland seismic zone. *Geophys. J. Int.*, accepted.

Subproject 2

Böðvarsson, R., S.Th. Rögnvaldsson, R. Slunga & E. Kjartansson 1998. The SIL data acquition system – at present and beyond year 2000. *Rit Veðurstofu Íslands* VÍ–R98005–JA04. Research report, Icelandic Meteorological Office, Reykjavík, 22 pp.

Böðvarsson, R., S.Th. Rögnvaldsson, R. Slunga & E. Kjartansson 1999. The SIL data acquisition system – at present and beyond year 2000. *Phys. Earth Planet. Inter.* 113, 89–101.

Lund, B. & R. Slunga 1999. Stress tensor inversion using detailed microearthquake information and stability constraints: application to Ölfus in southwest Iceland. *J. Geophys. Res.* 104, 14947–14964.

Lund, B. & R. Böðvarsson 2000. Correlation of microearthquake body–wave spectral amplitudes. *Bull. Seism. Soc. Am.*, accepted.

Shomali, Z.H. & R. Slunga 2000. Body wave moment tensor inversion of local earthquakes: an application to the South Iceland seismic zone. *Geophys. J. Int.*, 63–70.

Slunga, R. 2001. Foreshock activity, fault radius and silence - earthquake warnings based on microearthquakes. *Greinagerð Veðurstofu Íslands* VÍ-01003-JA03. Report, Icelandic Meteorological Office, Reykjavík, in press.

Slunga, R., R. Böðvarsson, G.B. Guðmundsson, S.S Jakobsdóttir, B. Lund & R. Stefánsson

2000. A simple earthquake warning algorithm based on microearthquake observations - retrospective applications on Iceland. Submitted.

Subproject 3

Crampin, S. 1998a. Stress–forecasting: a viable alternative to earthquake prediction in a dynamic Earth. *Trans. R. Soc. Edin. Earth Sci.* 89, 121–133.

Crampin, S. 1998b. Shear–wave splitting in a critical crust: the next step. In: P. Rasolofosaon (editor), *Rev. Inst. Franc. Pet.* 53. Proceedings of Eighth International Workshop on Seismic Anisotropy, Boussens, France, 749–763.

Crampin, S. 1999a. A successful stress–forecast: an addendum to "Stress–forecasting: a viable alternative to earthquake prediction in a dynamic Earth". *Trans. R. Soc. Edin. Earth Sci.* 89, 231.

Crampin, S. 1999b. Calculable fluid–rock interactions. *J. Geol. Soc.* 156, 501–514.

Crampin, S. 2000a. The "New Geophysics": a critical, compliant, calculable, and controllable reservoir. In: Extended abstracts from the 62nd EAGE meeting, Glasgow, United Kingdom.

Crampin, S. 2000b. The potential of shear–wave splitting in a stress–sensitive compliant crust: a new understanding of pre–fracturing deformation from time–lapse studies. In: Expanded abstracts from the 70th Annual International SEG Meeting, Calgary, Alberta, Canada, 1520–1523.

Crampin, S. 2000c. Shear–wave splitting in a critical self–organized crust: the New Geophysics. Expanded abstracts from the 70th Annual International SEG Meeting, Calgary, Alberta, Canada, 1544–1547.

Crampin, S. 2000d. Stress–monitoring sites (SMSs) for stress–forecasting the times and magnitudes of future earthquakes. *Tectonophysics*, in press.

Crampin, S., T. Volti & R. Stefánsson 1999. A successfully stress–forecast earthquake. *Geophys. J. Int.* 138, F1–F5.

Crampin, S. & S. Chastin 2000. Shear–wave splitting in a critical crust: II - compliant, calculable, controllable fluid–rock interactions. In: L. Ikelle (editor), *Proceedings of the Ninth International Workshop on Seismic Anisotropy*, Cape Allen, Houston, Texas, USA, 2000, submitted.

Crampin, S., T. Volti & P. Jackson 2000. Developing a stress–monitoring site (SMS) near Húsavík for stress–forecasting the times and magnitudes of future large earthquakes. In: B. Þorkelsson & M. Yeroyanni (editors), *Destructive earthquakes: Understanding crustal processes leading to destructive earthquakes.* Proceedings of the second EU–Japan workshop on seismic risk, Reykjavík, Iceland, June 23–27, 1999, 136–149.

Gao, Y., P. Wang, S. Zheng, M. Wang & Y.-T. Chen 1998. Temporal changes in shear–wave splitting at an isolated swarm of small earthquakes in 1992 near Dongfang, Hainan Island, Southern China. *Geophys. J. Int.* 135, 102–112.

Volti, T. & S. Crampin 2000. Shear–wave splitting in Iceland: four years monitoring stress changes before earthquakes and volcanic eruptions. *Geophys. J. Int.*, submitted.

Subproject 4

Henneberg, K., F. Roth, H. Sigvaldason, S.Þ Guðlaugsson & V. Stefánsson 1998. Ergebnisse von Bohrlochmessungen in der Südisländischen Seismizitätszone in den Jahren 1996 und 1997. Paper presented at the third meeting of the FKPE working group on Borehole Geophysics and Rock Physics, Hannover, Germany, 1998.

Roth, F. 1999a. Erforschung von Erdbeben auf Island. Invited talk at the Faculty of Geosciences, University of Hamburg, Germany, 1999.

Roth, F. 1999b. Bohrlochmessungen zum Spannungsfeld und zu Aquifären. Invited talk at the Faculty of Geosciences, Geotechniques and Mining, Technische Universität Bergakademie Freiberg, 1999.

Roth, F. & P. Fleckenstein 1999a. Report on repeated logging in the framework of PRENLAB–2. PRENLAB–2 workshop, Strasbourg, France, March 31, 1999.

Roth, F. & P. Fleckenstein 1999b. Ergebnisse von Bohrloch–Spannungsmessungen in der Südisländischen Seismizitätszone. Paper presented at the fifth meeting of the FKPE working group on Borehole Geophysics and Rock Physics, Hannover, Germany, 1999.

Roth, F., K. Henneberg, P. Fleckenstein, J. Palmer, V. Stefánsson & S.Þ. Guðlaugsson 2000. Ergebnisse von Bohrloch–Spannungsmessungen in der Südisländischen Seismizitätszone. In: *Trans. Dt. Geophys. Ges.* III. Extended abstracts from the fifth meeting of the FKPE working group on Borehole Geophysics and Rock Physics, Hannover, Germany, 1999, 49–50.

Subproject 5

Clifton, A. 2000. Surface deformation related to volcanic uplift and seismicity in SW–Iceland. Poster presented at the Nordvulk–Ridge summer school, Iceland, August 20–30, 2000.

Clifton, A. & F. Sigmundsson 2000. Faulting and deformation resulting from magma accumulation at the Hengill triple junction, SW–Iceland. Abstract submitted the AGU fall meeting, San Francisco, California, USA, December 15–19, 2000.

Feigl, K.L., J. Gasperi, F. Sigmundsson & A. Rigo 2000. Crustal deformation near Hengill volcano, Iceland 1993–1998: coupling between magmatic activity and faulting inferred from elastic modeling of satellite radar interferograms. *J. Geophys. Res.* 105, 25655–25670.

Guðmundsson, S., F. Sigmundsson & J.M. Carstensen 2000. Three–dimensional surface motion maps estimated from combined InSAR and GPS data. *J. Geophys. Res.*, submitted.

Hreinsdóttir, S., P. Einarsson & F. Sigmundsson 2000. Crustal deformation at the oblique spreading Reykjanes peninsula, SW–Iceland: GPS measurements from 1993 to 1998. *J. Geophys. Res.*, submitted.

Johnson, D.J., F. Sigmundsson & P.T. Delaney 2000. Comment of "Volume of magma accumulation or withdrawal estimated from surface uplift or subsidence, with application to the 1960 collapse of Kilauea volcano" by P.T. Delaney and D.F. McTigue. *Bull.*

Volc. 61, 491–493.

Vadon, H. & F. Sigmundsson 1997. Crustal deformation from 1992 to 1995 at the mid-Atlantic ridge, Southwest Iceland, mapped by satellite radar interferometry. *Science* 257, 194–197.

Subproject 6

Acocella, V., Á. Guðmundsson & R. Funiciello 1999. The interaction between extensional segments at the Icelandic mid-oceanic ridge. In: Abstracts from the tenth biennial EUG meeting, Strasbourg, France, March 28 - April 1, 1999.

Acocella, V., Á. Guðmundsson & R. Funiciello 2000. Interaction and linkage of extension fractures and normal faults: examples from the rift zone of Iceland. *Journal of Structural Geology* 22, 1233–1246.

Angelier, J. 1998. A new direct inversion of earthquake focal mechanisms to reconstruct the stress tensor. In: *Annales Geophysicae.* Abstracts from the XXIII EGS General Assembly, Nice, France, April 20–24, 1998.

Angelier, J. & F. Bergerat 1998. Stress fields and mechanisms of seismogenic faults: the South Iceland seismic zone as a case example. In: Abstracts from the international workshop on the Resolution of geological analysis and models for earthquake faulting studies, Camerino, Italy, June 3–6, 1998.

Angelier, J., F. Bergerat & S.Th. Rögnvaldsson 1998. Seismogenic stress field in the South Iceland seismic zone. In: *Annales Geophysicae.* Abstracts from the XXIII EGS General Assembly, Nice, France, April 20–24, 1998.

Angelier, J., F. Bergerat , H.-T. Chu, Á. Guðmundsson, C. Homberg, J.-C. Hu, H. Kao, J.-C. Lee & S.Th. Rögnvaldsson 1999. Active faulting, earthquakes and deformation-stress fields: from the mid–Atlantic ridge (Iceland) to a collision boundary of Southeast Asia (Taiwan). Abstracts from the second EU–Japan workshop on seismic risk, Reykjavík, Iceland, June 23–27, 1999.

Angelier, J., F. Bergerat & C. Homberg 1999. Variations in mechanical coupling as a source of apparent polyphase tectonism: the case of the Tjörnes transform zone, North Iceland. In: *Annales Geophysicae.* Abstracts from the XXIV EGS General Assembly, The Hague, The Netherlands, April 19–23, 1999.

Angelier, J., F. Bergerat & S.Th. Rögnvaldsson 1999a. Using inversion of large population of earthquake focal mechanisms to derive the regional seismotectonic field: Iceland. In: Abstracts from the tenth biennial EUG meeting, Strasbourg, France, March 28 - April 1, 1999.

Angelier, J., F. Bergerat & S.Th. Rögnvaldsson 1999b. Perturbation of late–scale extension across oceanic rift and transform faults revealed by inversion of earthquake focal mechanisms in Iceland. In: *Annales Geophysicae.* Abstracts from the XXIV EGS General Assembly, The Hague, The Netherlands, April 19–23, 1999.

Angelier, J., F. Bergerat, H.-T. Chu, Á. Guðmundsson, J.-C. Hu, J.-C. Lee, C. Homberg, H. Kao & S.Th. Rögnvaldsson 2000. Active faulting, earthquakes and deformation–stress fields: from mid–Atlantic ridge spreading (Iceland) to collision in Southeast

Asia (Taiwan). In: B. Þorkelsson & M. Yeroyanni (editors), *Destructive earthquakes: Understanding crustal processes leading to destructive earthquakes.* Proceedings of the second EU–Japan workshop on seismic risk, Reykjavík, Iceland, June 23–27, 1999. European Commission, 48–61.

Angelier, J., F. Bergerat & C. Homberg 2000. Variable coupling explains complex tectonic regimes near oceanic transform fault: Flateyjarskagi, Iceland. *Terra Nova*, in press.

Belardinelli, M.E., M. Bonafede & Á. Guðmundsson 1999. Multiscale surface faulting generated by strike–slip earthquakes in Iceland. In: *Annales Geophysicae.* Abstracts from the XXIV EGS General Assembly, The Hague, The Netherlands, April 19–23, 1999.

Belardinelli, M.E., M. Bonafede & Á. Guðmundsson 2000. Secondary earthquake fractures generated by a strike–slip fault in the South Iceland seismic zone. *J. Geophys. Res.* 105, 13613–13629.

Bergerat, F. & J. Angelier 1998. Neotectonic evidences from field studies of recent faulting in the South Iceland seismic zone (SISZ). In: *Annales Geophysicae.* Abstracts from the XXIII EGS General Assembly, Nice, France, April 20–24, 1998.

Bergerat, F., Á. Guðmundsson, J. Angelier & S.Th. Rögnvaldsson 1998. Seismotectonics of the central part of the South Iceland seismic zone. *Tectonophysics* 298, 319–335.

Bergerat, F. & J. Angelier 1999a. Géométrie des failles et régimes de contraintes à différents stades de développement des zones transformantes océaniques: exemple de la Zone Sismique Sud–Islandaise et de la Zone de Fracture de Tjörnes (Islande). *Sciences de la terre et des planètes* 329. C. R. Acad. Sc. Paris, 653–659.

Bergerat, F. & J. Angelier 1999b. Fault and stress patterns at different stages of development of oceanic transform zones: examples in Iceland. In: *Annales Geophysicae.* Abstracts from the XXIV EGS General Assembly, The Hague, The Netherlands, April 19–23, 1999.

Bergerat, F., J. Angelier & C. Homberg 1999. Field studies of recent faulting along the Húsavík–Flatey fault (Tjörnes transform zone, northern Iceland): complex tectonic regimes and variable coupling. In: Abstracts from the tenth biennial EUG meeting, Strasbourg, France, March 28 - April 1, 1999.

Bergerat, F., J. Angelier & S. Verrier 1999. Tectonic stress regimes, rift extension and transform motion: the South Iceland seismic zone. *Geodin. Acta* 12(5), 303–319.

Bergerat, F. & J. Angelier 2000. The South Iceland seismic zone: tectonic and seismotectonic analyses revealing the evolution from rifting to transform motion. *Journ. Geodynamics* 29(3–5), 211–231.

Bergerat, F., J. Angelier & C. Homberg 2000. Tectonic analysis of the Húsavík–Flatey fault (northern Iceland) and mechanisms of an oceanic transform zone, the Tjörnes fracture zone. *Tectonics*, in press.

Bergerat, F., J. Angelier & Á. Guðmundsson 2000. The Leirubakki fault, a large earthquake rupture of the South Iceland seismic zone. In: *Annales Geophysicae.* Abstracts from the XXV EGS General Assembly, Nice, France, April 25–29, 2000.

Bergerat, F., J. Angelier & Á. Guðmundsson. The Leirubakki earthquake rupture: a large fault of the South Iceland seismic zone. In preparation.

Dauteuil, O., J. Angelier, F. Bergerat, S. Verrier & T. Villemin 2000. Deformation partitioning inside a fissure swarm of the northern Icelandic rift. *Journal of Structural Geology*, accepted, in revision.

Garcia, S. 1999. *De sismotectonique d'un segment transformant en domaine océanique: la Zone de Fracture de Tjörnes, Islande.* Unpublished master thesis. Universite Pierre & Marie Curie, Paris.

Garcia, S., J. Angelier, F. Bergerat & C. Homberg 2000. Etude sismotectonique d'un segment transformant: la Zone de Fracture de Tjörnes, Islande. $18^{ème}$ RST, Paris, France, April 2000.

Garcia, S., J. Angelier, F. Bergerat & C. Homberg. Tectonic behaviour of an oceanic transform fault zone from fault–slip data and focal mechanisms of earthquakes analyses: the Tjörnes fracture zone, Iceland. In preparation.

Guðmundsson, Á. 1998a. Development of permeability in fault zones. In: *Annales Geophysicae* Abstracts from the XXIII EGS General Assembly, Nice, France, April 20–24, 1998.

Guðmundsson, Á. 1998b. Rift–zone and off–rift earthquakes in Iceland. In: *Annales Geophysicae.* Abstracts from the XXIII EGS General Assembly, Nice, France, April 20–24, 1998.

Guðmundsson, Á. 1999a. Fluid pressure and stress drop in fault zones. *Geophys. Res. Lett.* 25, 115–118.

Guðmundsson, Á. 1999b. Fluid flow in fractured rocks: application to the hydrogeology of Norway. In: Abstracts from the General Meeting of the Geological Society of Norway, Stavanger, Norway.

Guðmundsson, Á. 1999c. Extensional veins used to estimate overpressure and depth of origin of fluids in fault zones. In: Abstracts from the tenth biennial EUG meeting, Strasbourg, France, March 28 - April 1, 1999.

Guðmundsson, Á. 1999d. Fluid pressure and stress for large earthquakes. In: *Annales Geophysicae.* Abstracts from the XXIV EGS General Assembly, The Hague, The Netherlands, April 19–23, 1999.

Guðmundsson, Á. 1999e. Injection and arrest of water–filled fractures. In: *Annales Geophysicae.* Abstracts from the XXIV EGS General Assembly, The Hague, The Netherlands, April 19–23, 1999.

Guðmundsson, Á. 1999f. Flow of groundwater into and along fault zones. In: *Annales Geophysicae.* Abstracts from the XXIV EGS General Assembly, The Hague, The Netherlands, April 19–23, 1999.

Guðmundsson, Á. 1999g. Similarities in the structural evolution of rift basins and rift–zone grabens. In: Abstracts from the Norwegian Petroleum Society Meeting on Sedimentary Environments Offshore Norway, Bergen, Norway.

Guðmundsson, Á. 1999h. Fluid overpressure and flow in fault zones: field measurements and models. Workshop on Fluids and Fractures in the Lithosphere, Nancy, France. Tectonic Study Group of Nancy, Geological Society of France.

Guðmundsson, Á. 2000a. Active fault zones and groundwater flow. *Geophys. Res. Lett.*,

in press.

Guðmundsson, Á. 2000b. Fluid overpressure and flow in fault zones: field measurements and models. *Tectonophysics*, in press.

Guðmundsson, Á. 2000c. Fracture dimensions, displacements and fluid transport. *Journal of Structural Geology* 22, 1221–1231.

Guðmundsson, Á. 2000d. Dynamics of volcanic systems in Iceland: Example of tectonism and volcanism at juxtaposed hot spot and mid–ocean ridge system. *Annual Review of Earth and Planetary Sciences* 28, 107–140.

Guðmundsson, Á. 2000e. Fault slip and groundwater transport. In: Abstracts from the XXIV Nordic Geological Winter Meeting, Trondheim, Norway.

Guðmundsson, Á. 2000f. Propagation of hydrofractures in a layered rock mass. In: Abstracts from a Meeting on Hydrogeology and Environmental Geochemistry, Trondheim, Norway. The Geological Survey of Norway.

Guðmundsson, Á. 2000g. Effect of fault slip on the flow of crustal fluids. In: *Annales Geophysicae*. Abstracts from the XXV EGS General Assembly, Nice, France, April 25–29, 2000.

Guðmundsson, Á. 2000h. Magma flow beneath the volcanic zones of Iceland. In: *Annales Geophysicae*. Abstracts from the XXV EGS General Assembly, Nice, France, April 25–29, 2000.

Guðmundsson, Á. Displacement and stresses of arrested hydrofractures. *Tectonophysics*, in preparation.

Guðmundsson, Á. & C. Homberg 1999. Evolution of stress fields and faulting in seismic zones. *Pure and Applied Geophysics* 154, 257–280.

Guðmundsson, Á., S.S. Berg, K.B. Lyslo & E. Skurtveit 2000. Fracture networks and fluid transport in active fault zones. *Journal of Structural Geology*, in press.

Henriot, O., T. Villemin & F. Jouanne 1998a. Surface deformation at the Tjörnes rift–transform junction (North Iceland) computed from SAR images. In: *Annales Geophysicae*. Abstracts from the XXIII EGS General Assembly, Nice, France, April 20–24, 1998.

Henriot, O., T. Villemin & F. Jouanne 1998b. Cartographie de la déformation de surface par interférométrie radar: l'exemple de la jonction rift transformante de Tjörnes. Colloque Mouvements Actuels de la Surface Terrestre, October 5–6, 1998. Ecole de Physique des Houches.

Henriot, O., T. Villemin & F. Jouanne 1999a. Seismic risk in northern Iceland: (2) deformation maps of the Tjörnes peninsula computed from INSAR. In: Abstracts from the tenth biennial EUG meeting, Strasbourg, France, March 28 - April 1, 1999.

Henriot, O., T. Villemin & F. Jouanne 1999b. Seismic risk in northern Iceland: Deformation maps of Tjörnes computed from INSAR. Fringe'99, Liège, Belgium, November 10–12, 1999.

Henriot, O., T. Villemin & F. Jouanne 2000. Long period interferograms reveal 1992–1998 steady rate of deformation at Krafla volcano (North Iceland). *Geophys. Res. Lett.*, in

press.

Henriot, O. & T. Villemin. The Krafla fissure swarm, northern Iceland: the end of the subsidence due to the postrifting cooling of magma? In preparation.

Jouanne, F., T. Villemin, V. Ferber, C. Maveyraud, J. Ammann, O. Henriot & J.-L. Got 1999. Seismic risk at the rift–transform junction in North Iceland. *Geophys. Res. Lett.* 26(24), 3689.

Lyslo, K.B. & Á. Guðmundsson 2000. Permeability and stress concentration around active faults. In: Abstracts from a Meeting on Hydrogeology and Environmental Geochemistry, Trondheim, Norway. The Geological Survey of Norway.

Skurtveit, E. & Á. Guðmundsson 1999. Hydromechanical infrastructure of a major fault zone in Iceland. In: Abstracts from a Meeting on Hydrogeology and Environmental Geochemistry, Trondheim, Norway. The Geological Survey of Norway.

Villemin, T., F. Jouanne & GPS–TFZ Team 1998. 1995–1997 surface deformation along the Húsavík–Flatey transform fault and around its junction with the northern volcanic zone in Iceland. In: *Annales Geophysicae.* Abstracts from the XXIII EGS General Assembly, Nice, France, April 20–24, 1998.

Villemin, T., F. Jouanne & O. Henriot 1999. Seismic risk in northern Iceland: (1) locking of the Húsavík fault deduced from GPS. In: Abstracts from the tenth biennial EUG meeting, Strasbourg, France, March 28 - April 1, 1999.

Villemin, T. & O. Henriot. Active faulting in the Theistareykir fissure swarm, northern Iceland. In preparation.

Villemin, T. & F. Jouanne. Active deformation in northern Iceland at the rift transform junction: a dynamic system in rapid evolution. In preparation.

Villemin, T., G. Ouillon & V. Ferber 2000. Processes of fractures pattern evolution deduced from field data: the Krafla fissure swarm and the last rifting episode in North Iceland. *J. Geophys. Res.*, submitted.

Subproject 7

Belardinelli, M.E., M. Bonafede & Á. Guðmundsson 2000. Secondary earthquake fractures generated by a strike–slip fault in the South Iceland seismic zone. *J. Geophys. Res.* 105, 13613–13630.

Bonafede, M. & N. Cenni 1998. A porous flow model of magma migration within Mt. Etna: the influence of extended sources and permeability anisotrophy. *J. Volcanol. Geotherm. Res.* 81, 51–68.

Bonafede, M. & M. Mazzanti 1998. Modelling gravity variations consistent with ground deformation in the Campi Flegrei caldera. *J. Volcanol. Geotherm. Res.* 81, 137–157.

Bonafede, M. & E. Rivalta 1999a. The tensile dislocation problem in a layered elastic medium. *Geophys. J. Int.* 136, 341–356.

Bonafede, M. & E. Rivalta 1999b. On tensile cracks close to and across the interface between two welded elastic half–spaces. *Geophys. J. Int.* 138, 410–434.

Bonafede, M. & A. Neri 2000. Effects induced by an earthquake on its fault plane: a

boundary element study. *Geophys. J. Int.* 141, 43–56.

Bonafede, M., B. Parenti & E. Rivalta 2000. Strike–slip faulting in layered media. *Geophys. J. Int.*, submitted.

Bonafede, M. & E. Rivalta. The stress–drop discontinuity condition: implications for fault complexities in transform boundaries. In preparation.

Bonafede, M. & E. Rivalta. Dip–slip faulting in layered media. In preparation.

Roth, F. 1998. Modellrechnungen zu den plattentektonischen, insbesondere seismotektonischen Spannungen auf Island (model calculations on plate tectonic and especially seismotectonic stresses on Iceland). Paper presented at the 4th workshop of the FKPE working group on Borehole Geophysics and Rock Physics, Hannover, Germany.

Roth, F. 1999a. Stress changes in space and time at the South Iceland seismic zone - model calculations. Poster on the Workshop on Recurrence of Great Interplate Earthquakes and its Mechanism, Kochi, Shikoku, Japan, January 20–22, 1999. Japan Science and Technology Agency.

Roth, F. 1999b. Entwicklung des tektonischen Spannungsfeldes im Süden Islands - Modellierung einer Erdbebenserie (development of the tectonic stress field in the south of Iceland - modelling of an earthquake series). In: *Proceedings of the 59th Annual Meeting of the German Geophysical Society*, Braunschweig, Germany.

Roth, F. 1999c. Stress changes in space and time at the South Iceland seismic zone - model calculations. In: Abstracts from the tenth biennial EUG meeting, Strasbourg, France, March 28 - April 1, 1999.

Roth, F. 1999d. Erforschung von Erdbeben auf Island (research about earthquakes on Iceland). Paper presented at the Institute of Geophysics, University of Hamburg, Germany.

Roth, F. 1999e. Stress changes in space and time at the South Iceland seismic zone - model calculations. In: *Proceedings of the Workshop on Recurrence of Great Interplate Earthquakes and its Mechanism*, Kochi, Shikoku, Japan, January 20–22, 1999. Japan Science and Technology Agency, 22–32.

Roth, F. 1999f. Stress changes at the South Iceland seismic zone - a model from 1706 up to the present for better hazard estimation. In: Abstracts from the XXII IUGG General Assembly, Birmingham, United Kingdom, July 18–30, 1999.

Roth, F. 2000. Stress changes in the South Iceland transform zone due to strong earthquakes and forcing from the adjacent rifts. In: Abstracts from the XXVII ESC General Assembly, Lisbon, Portugal, September 10–15, 2000.